



Extending service life of hall thrusters: recent progress and future challenges

Yongjie Ding^{1,2} · Haotian Fan¹ · Dong Ma¹ · Lei Wang¹ · Boyang Jia¹ · Hezhi Sun¹ · Weifeng Xu¹ · Hongbo Su¹ · Liqiu Wei^{1,2} · Hong Li^{1,2} · Daren Yu^{1,2}

Received: 26 December 2018 / Accepted: 23 October 2019 / Published online: 14 November 2019

© Division of Plasma Physics, Association of Asia Pacific Physical Societies 2019

Abstract

Hall thrusters are widely applied to space propulsion missions because of characteristics such as high specific impulse, great thrust-to-power ratio, high efficiency, and simple structure. Because the scope of space missions using Hall thrusters has expanded, a higher total impulse is required to extend a north–south station-keeping mission to an orbit transfer mission, requiring Hall thrusters with improved lifetimes. Existing research shows that improving the anti-sputtering capacity of the discharge channel and significantly reducing the ion energy and flux bombardment on the wall of the discharge channel are the best measures to improve the lifetime of Hall thrusters. This study summarizes the lifetime restraining factors of Hall thrusters and analyzes the magnetic shielding technology, wall-less technology, aft-magnetic technology, and cylindrical Hall thruster technology to reduce ion energy and flux bombardment on the discharge-channel wall, adopting low-sputtering yield materials to reduce the wall erosion rate, which can improve the lifetime of Hall thrusters. This paper also identifies the limitations of each technology, such as the erosion of magnetic poles (MS) and ceramic cover plates (CHT), larger plume divergence angle (wall-less), hard-to-select aft-magnetic degree (aft-magnetic technology), low compactness, and great porosity (graphite material), providing a reference for further research.

Keywords Space propulsion · Hall thruster · Long-life technology

✉ Yongjie Ding
dingyongjie@hit.edu.cn

¹ School of Energy Science and Engineering, Harbin Institute of Technology, Heilongjiang, People's Republic of China

² Electric Drive and Propulsion Technology Lab, Harbin Institute of Technology, Harbin 150001, People's Republic of China

1 Introduction

Remarkable achievements have been made in the field of space science and technology, and the quality of people's lives has been significantly improved (Zypries 2017; Kishi 2017). With the proposal of plans for the colonization of the Moon and Mars (Szocik et al. 2016; Levchenko et al. 2018a), the scope of space missions has expanded further. The intensity of space launches has also drastically increased over the past few years (Oluwafemi et al. 2018). This, in turn, has led to higher demands on the functions and performance of spacecraft (Levchenko et al. 2018b), and their structure (Behroozfar et al. 2017), material (Levchenko et al. 2018c; Potrivityt et al. 2018; Levchenko et al. 2016; Agrawal et al. 2013; Baranov et al. 2017), and control technology (Mazouffre 2016), which need to be further optimized and improved. Simultaneously, the demands on propulsion technology have also been growing (Choueiri 2004), and new and more efficient, long-serving thrusters are urgently and critically needed. Mature propulsion modes applied to space aircraft can be classified into two modes of propulsion: chemical and electric. Chemical propulsion generates thrust via the chemical combustion of a propellant, which expands in the nozzle. Electrical propulsion is used to convert electrical energy into kinetic energy through different methods to generate thrust (Levchenko et al. 2018d; Baranov et al. 2017). Electrical propulsion has many advantages in earth-orbit flight missions, and it is gradually replacing chemical propulsion (Martinez-Sanchez and Pollard 1998; Chiu et al. 2006; Levchenko et al. 2018e). Typical flight-mission activities include orbit transfer, attitude control, orbit maintenance, and descent (Levchenko et al. 2018f).

The Hall thruster is an electric propulsion device that has been widely applied to flight missions. The device ionizes propellant into plasma and accelerates ions during discharge through a channel to generate thrust (Ding et al. 2018a). Because of high specific impulse, high efficiency, high thrust-to-power ratio, simple structure, and other characteristics, it has been used in various satellites. The structure and operating principle of the Hall thruster are shown in Fig. 1; the photograph of an actual thruster is shown in Fig. 2 (Nakles et al. 2012). The basic structure includes an anode, cathode, gas distributor, discharge channel, and magnetic circuit system. Under the radial magnetic field, the electron axial conduction is inhibited and a closed electron current is formed along the azimuthal direction, which is favorable for the sufficient ionization of the propellant gas entering the channel from the upstream gas distributor. The azimuthal closure of the electron current also results in a strong electric field in the axial direction, to accelerate the ions through the channel outlet and generate thrust. Simultaneously, electrons reach the anode via various conduction mechanisms, achieving a stable plasma discharge process and providing sustained and stable thrust (Zhurin et al. 1999).

Presently, the application scope of a mature BPT-4000 Hall thruster has begun to shift from traditional north-south station-keeping to orbital transfer and other applications (King et al. 1998; Welander et al. 2006; Petro and Sedwick 2017). Hall thrusters performing orbital transfer missions have a more complex operation environment, longer operation cycle, and higher requirements of

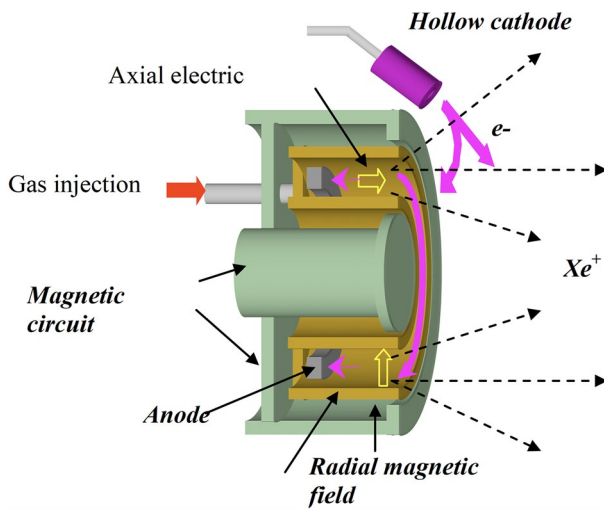


Fig. 1 View of Hall thruster (Dudeck et al. 2012)

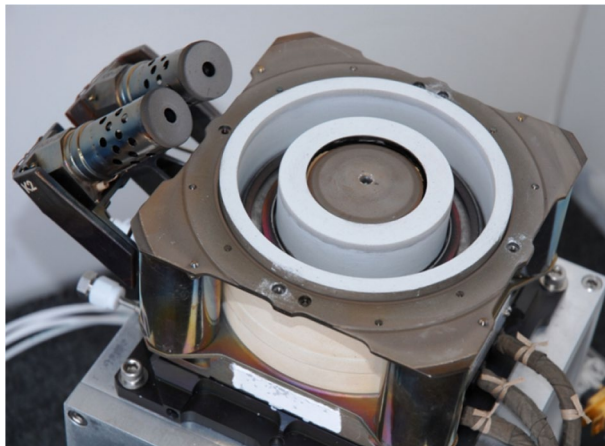
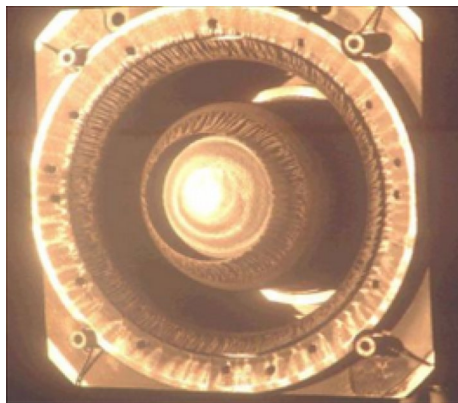


Fig. 2 Photograph of an SPT-100 Hall thruster (Nakles et al. 2012)

total impulse. Owing to these complex operations and new operational requirements, the Hall thruster needs a longer lifetime. This has become a key research direction in this field. The US, Europe, Russia, China, and other countries have studied the Hall thruster to improve its lifetime. The National Aeronautics and Space Administration (NASA) and Aerojet have already improved the BPT-4000, achieving a lifetime of more than 10,000 h (Hofer et al. 2007, 2010). However, high-power Hall thrusters required for deep-space exploration and interplanetary applications must have even longer lifetimes to complete in-orbit missions (Jacobson and Manzella 2003; Brandhorst et al. 2002; Dudeck et al. 2012). With

Fig. 3 Sputtering erosion on the walls of a Hall thruster (Dudeck et al. 2012)



the development of spacecrafts with longer service lives and thrusters with higher power, the Hall thruster has more stringent requirements. This is a key issue in the development of Hall propulsion technology and practicality.

Owing to the divergence of the ion beam, some ions in the channel collide with the channel wall. During the collision process, ions transfer their kinetic energy to the channel wall, resulting in sputtering erosion, as shown in Fig. 3. This is the gravest issue for sustaining a Hall thruster (Kim 1998; Mazouffre et al. 2003; Becatti et al. 2018). Wall erosion not only causes a loss of mass from the wall, but it also poses a grave threat to the conditions required for normal operation of the magnetic pole (Peterson et al. 2001; Morozov and Savelyev 2001). Furthermore, the plasma-discharge characteristics can be affected by the interaction between the plasma and the eroded wall surface (Raitses et al. 2005). The process of change in morphology of the erosion surface also affects the discharge operation performance of the thruster (Li et al. 2018). Therefore, wall-sputtering erosion has become one of the significant factors affecting the operational life of the Hall thruster. In recent years, several studies have been published on sputtering erosion, showing that researchers are paying attention to it.

This paper is structured as follows. Section 2 explains the wall-erosion mechanism and summarizes the key factors affecting the lifetime of Hall thrusters. Section 3 summarizes the magnetic shielding (MS), aft-magnetic, wall-less, and other long-lifetime technologies. Section 4 describes the limitations of each long-life technology and Sect. 5 concludes the paper.

2 Analysis of factors affecting hall-thruster life

As mentioned, the sputtering erosion of the wall surface is the main factor affecting the lifetime of a Hall thruster. Some ions in the channel collide with the channel wall, transferring kinetic energy to the wall, resulting in sputtering erosion of the wall material. Other factors restricting the lifetime of a Hall thruster, listed in Table 1, include (Claus et al. 1997) erosion of the cathode and magnetic circuit

Table 1 Factors affecting lifetime of Hall thruster

<i>a</i>	Sputtering erosion of wall surface
<i>b</i>	Erosion of cathode and magnetic circuit system components
<i>c</i>	Bombardment erosion of hollow cathode
<i>d</i>	Evaporation of cathode–heater materials
<i>e</i>	Aging of various thruster materials during space operation
<i>f</i>	Mechanical deformation or rupture of channel wall, cathode, and heater

system components by plasma; bombardment erosion of the hollow cathode caused by high-energy ions in a plume; evaporation of cathode–heater materials at high temperatures; aging of various thruster materials during space operation caused by temperature and radiation; and mechanical deformation or rupture of the channel wall, the cathode, and the heater caused by thermal shock during the initial process. These factors are less severe than wall-sputtering erosion (Kim 1998). Therefore, international scholars generally focus on wall erosion. However, with the development of magnetic shielding technology, hollow cathode erosion has gradually become the most dominant lifetime-limiting factor.

2.1 Interaction between plasma and wall surface

The typically large surface-to-volume ratio of a Hall thruster can cause a strong interaction between the plasma and the wall of the channel. This can be classified into three processes as follows: recombination of the plasma particles at the wall, sputter erosion of the wall, and near-wall conduction (Ahedo et al. 2003; Roy and Pandey 2002).

The recombination of plasma particles at the wall occurs because of the randomness of the ion vectors. If produced far from the outlet, the ions would probably move to the wall with a radial velocity component before reaching the channel outlet. The ions and electrons would then be compounded into atoms, losing kinetic energy and resulting in low propellant utilization and reduced thruster efficiency (Roy and Pandey 2002).

Sputter erosion occurs when the ions have a higher energy than the threshold energy when they collide with the wall. Further, ion bombardment promotes the absorption of energy at the wall, leading to overheating. A poor thermal environment will adversely affect the service life of a thruster. The near-wall conductivity is caused by fast electrons hitting the wall with energies above the potential barrier owing to the plasma sheath. As a complex physical process, the interaction comprises the properties of wall materials, sheath and magnetic-field configurations, and other factors. The interaction between the plasma and the wall is a function of the potential near the wall, which is decided by the secondary electron emission coefficient and sputtering yield (Roy and Pandey 2003).

When the secondary electron emission coefficient increases, the loss of electrons from the walls decreases and more electrons can participate in the ionization. Thus, the secondary electron emission can cause ion acoustic instability and enhance

electron cyclotron drift instability, leading to an increase in the electron temperature. Both these phenomena can increase plasma density and thus enhance the interaction between the plasma and the wall. When the secondary electron emission coefficient decreases, the primary electrons of intermediate energy are absorbed by the wall and deposit heat to the wall. Thus, the plasma temperature decreases (Hargus and Cappelli 2002). Meanwhile, the sheath potential is reduced by the decrease in the quantity of secondary electrons, and the energy of high-energy ions is reduced, thus reducing the sputtering yield. Therefore, the secondary electron emission, sputtering yield, ionization, and recombination can be used to regulate processes before the system reaches a steady state (Keidar and Boyd 2001; Roy and Pandey 2003).

Ahedo and Pablo (2007) suggested that electrons colliding with one side of the wall were mainly secondary electrons emitted from the other side, because, when the secondary electrons emitted from the wall move towards the channel center, the sheath accelerates them. Thus, these electrons have higher energy, overcoming the sheath on the wall and colliding with the other side. Ahedo and Pablo (2007) simulated the radial presheath and sheath using a one-dimensional particle-in-cell (PIC) model. The results show that nearly all secondary electrons emitted from the wall collide with the wall on the other side (Kaganovich et al. 2007). It is also found through simulation that the secondary electrons emitted from both the walls couple with each other, causing two-stream instability in some cases (Kaganovich et al. 2007). Therefore, it is necessary to study the interaction between the plasma and the wall to understand the factors affecting the discharge performance and lifetime of the Hall thruster.

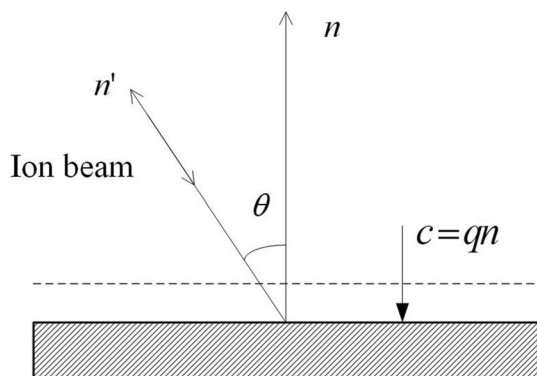
2.2 Main factors restricting the lifetime of Hall thruster

Bringa (2000) showed that the erosion caused by ion sputtering causes the surface materials to peel off and that the surface morphology evolves during the erosion process, as shown in Fig. 4. $\theta = \arccos(n \cdot n')$ is the angle between the ion incident direction and the surface normal direction. n and n' are the unit vectors representing the ion beam incident to the normal and pointing directions on the surface.

The normal erosion rate of the surface can be expressed as

$$c = qn, \quad (1)$$

Fig. 4 Schematic of substrate under incidental ion bombardment



where q is the sputter erosion rate, which can be expressed as

$$q = \frac{J_i \cdot Y(E, \theta) \cdot \cos \theta}{N}, \quad (2)$$

where J_i and E are, respectively, the ion flux to the wall and the incident ion energy, N is the atomic number density, and $Y(E, \theta)$ is the sputtering yield and its specific form is as follows (Yamamura and Tawara 1996; Seah 2005):

$$Y(E, \theta) = \frac{0.042 \cdot \alpha(M_2/M_1)}{U_0} \frac{S_n(E)}{1 + As_e(\epsilon)} \left[1 - \left(\frac{E_{th}}{E} \right)^{\frac{1}{2}} \right]^S \cdot x^f \exp \left[- \sum_f (x - 1) \right] \quad (3)$$

where $\alpha(M_2/M_1)$ is a function of the mass ratio of the ion and target atom, M_1 and M_2 are the masses of the incident ion and target atom, respectively, U_0 is the surface-binding energy, $S_n(E)$ is the nuclear-stopping cross section, A is equal to $0.35U_0$, $s_e(\epsilon)$ is the reduced electronic stopping power, ϵ is the reduced energy, E_{th} is the threshold energy for sputtering, and θ is the ion incidence angle, $x = 1/\cos \theta$, $\sum_f = \cos \theta_{opt}$. When $f=2.23$ and $\theta_{opt}=67.9^\circ$, the variance between the fitted curves obtained by Yamamura's empirical formula and the experimental data points is the smallest (Yamamura and Tawara 1996).

It can be analyzed from Eqs. (2) and (3) that the physical quantities, N , U_0 , A , and E_{th} , are related to the properties of the wall material itself. The physical quantities J_i , E , M_1 , and θ are related to the ions bombarding the wall. Therefore, the factors affecting the sputtering erosion rate q are also the factors restricting the thruster's lifetime. The factors can be placed into two categories. The wall's anti-sputtering capability is related to the substrate composition, microstructure, surface morphology, and other intrinsic properties of the channel-wall materials (Yim et al. 2006). The other is related to ion flux, energy, and incident angle (Garnier et al. 1999; Cheng 2007). Therefore, many scholars have studied the two major factors restricting the lifetime of Hall thrusters by combining numerical simulation calculations and experimental research.

As far as research on the effect of ion flux and energy on the life of the Hall thruster is concerned, Koizumi et al. (2008) used a two-dimensional (2D) mixed PIC method to simulate ionization, acceleration, and the near-field plume region of a Hall thruster working for 2000 h. They predicted the erosion effect on the channel wall with the deformed-mesh method. The results show that the sputtering erosion occurred in an area 10 mm upstream from the channel outlet, as this region corresponds to the position of the potential drop. The electric field accelerates ions and converts them into high-energy particles with energy higher than the threshold of sputtering erosion energy. Meanwhile, the erosion of the outer wall is more intense than that of the inner wall. This difference is caused by the magnetic-field configuration and ion-movement trajectory in the channel. Cho et al. (2013) simulated a 600-W class laboratory model magnetic-layer type Hall thruster under different conditions using the 2D-3 V particle-in-cell method combined with the Monte Carlo technique. The results show that, with the increase in the magnetic-field intensity,

the electric field inside the channel increases and the plasma is more confined to the internal channel, resulting in an increased average energy of the ions eroding the wall via sputtering. Thus, they increase the wall erosion rate.

Peterson and Manzella (2003) carried out a prominent anti-sputtering wall-material research on the lifetime of the Hall thruster and performed a 200-h test on the NASA-120 M Hall thruster equipped with five different boron–nitride (BN) insulation rings. Then they compared the erosion thicknesses of the five materials. The results showed that the materials differed in their sputtering properties. The increase in the content of BN and B_2O_3 was conducive to improving the erosion resistance of the materials. However, an increase in the content of SiO_2 reduced the materials' erosion resistance. The impact of Ca and other components on erosion resistance is still not clear. Reducing the cost of an extended lifetime is a very significant consideration (Peterson and Manzella 2003).

Based on the abovementioned analysis, the lifetime of a Hall thruster can be improved using mainly two methods: controlling the ion movement to reduce the bombardment on the wall and improving the anti-sputtering performance of the wall to slow down the erosion rate.

3 Long-life technologies

3.1 Magnetic shielding technology

High-energy ions sputtering on the channel wall is the key factor determining the operational life of the Hall thruster. However, MS technology provides a solution for the problem, effectively promoting long life.

The 4.5-kW BPT-4000 Hall thruster prototype, jointly developed by Aerojet and Lockheed Martin Space Systems, has been used for experimentation (Grys et al. 2010). The experimental results show that when the BPT-4000 accumulates 5600 h, the eroded-wall morphology does not change over the next 5000 h (see Fig. 5), and thruster performance remains stable (see Fig. 6). This is a significant and unusual discovery about the physical principles of the MS Hall thruster.

In 2010, the Jet Propulsion Laboratory (JPL) formally proposed the design concept of the MS Hall thruster (Mikellides et al. 2013a). The concept was to match the proper field configuration with the channel-wall topography while maintaining traditional design to form a high-potential zone close to the wall via the isothermal characteristics of the magnetic line and its isopotential condition. This confined the high-energy ions in the central region of the channel and fundamentally solved the problem of ion sputtering in the acceleration zone. The results showed that the wall-erosion rate was reduced by at least 2 or 3 orders; even zero erosion occurred under some conditions (Mikellides et al. 2013a; Mikellides et al. 2014). Thus, the most critical lifetime-restricting factor of channel-wall erosion has been completely eliminated, solving the long service life problem that has plagued the Hall thruster for decades.

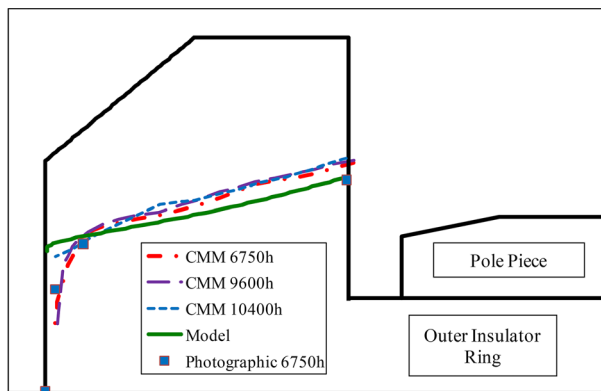


Fig. 5 Comparison of outer insulator ring erosion profile measurements and model prediction (Grys et al. 2010)

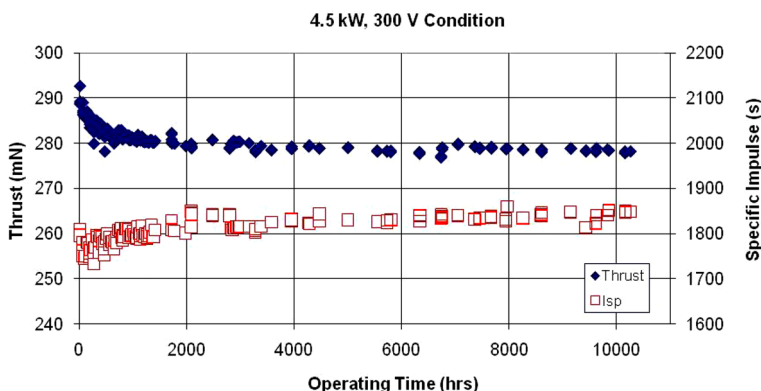


Fig. 6 Measured thrust and specific impulse as a function of time under the operating condition of 4.5 kW, 300 V (Grys et al. 2010)

The principle of the MS Hall thruster is shown in Fig. 7 (Mikellides et al. 2014). Because the electrons emitted by the cathode gain energy from the electric field and ionize the neutral gas to lose energy, there is a peak in the profiles of the electron temperature, causing it to be higher, as shown in Fig. 7a. The electrons are magnetized in the thruster; the parameters are $\Omega_e = \frac{\omega_{ce}}{v_e} \gg 1$, where ω_{ce} represents the electron cyclotron and v_e represents the total collision frequency. The temperature of the electron is approximately constant along the field lines ($\nabla_{\parallel} T_e \approx 0$). Moreover, in the absence of a resistive contribution to the electric field in this direction, the electron momentum equation becomes simplified to $E_{\parallel} \approx -T_e \ln n_e$, where n_e is the electron density. Thus, for each magnetic-field line (Mikellides et al. 2014),

$$\begin{aligned} T_e &\approx T_{e0}, \\ \emptyset &\approx \emptyset_0 + T_{e0} \ln(n_e/n_{e0}), \end{aligned} \quad (4)$$

where T_{e0} , \emptyset_0 , and n_{e0} denote integration constants that vary with the magnetic-field lines. The value at the intersection of the magnetic-field line and the centerline of the channel is generally considered. Equation (4) shows that if the temperature of the electron along the magnetic-field line is small or the density distribution is uniform, the magnetic-field line can be considered as equipotential (Mikellides et al. 2014). The magnetic field in the acceleration area of the traditional Hall thruster is nearly perpendicular to the wall along the radial direction, as shown in Fig. 7b. Owing to the temperature of the electron in the acceleration zone being higher and the channel-center density being higher than the near-wall area, the potential is unequal along the magnetic-field lines. The electric-field component, E_{\parallel} , is perpendicular to the surface of wall, causing high-energy ions to impact and erode the channel wall in the accelerating region. Furthermore, the potential drop of the wall sheath is larger at higher electron temperatures (Hobbs and Wesson 1967). Thus, the ions gain considerable energy before hitting the wall, increasing the erosion intensity. After fully understanding the disadvantages of the traditional thruster design, the main concept of the MS Hall thruster is to make full use of the isothermal characteristics of magnetic-field lines and the condition of equipotential field lines to form a high-potential area near the wall surface to restrict high-energy ions to the central area of the channel (Mikellides et al. 2014). The specific implementation principle is shown in Fig. 7c, where the magnetic-field lines near the wall of the accelerating zone are extended to the depth of the channel near the anode. The wall morphology of the accelerating zone should be adjusted accordingly. Because the potential near the anode is very high and the electron temperature is very small (Fig. 7a), the magnetic-field line has good equipotential. A high potential corresponding to the anode potential is formed near the wall surface of the accelerating region. Thus, the radial electric-field component points to the center of the channel, preventing high-energy ions from moving towards the wall surface (Mikellides et al. 2014). Meanwhile, the

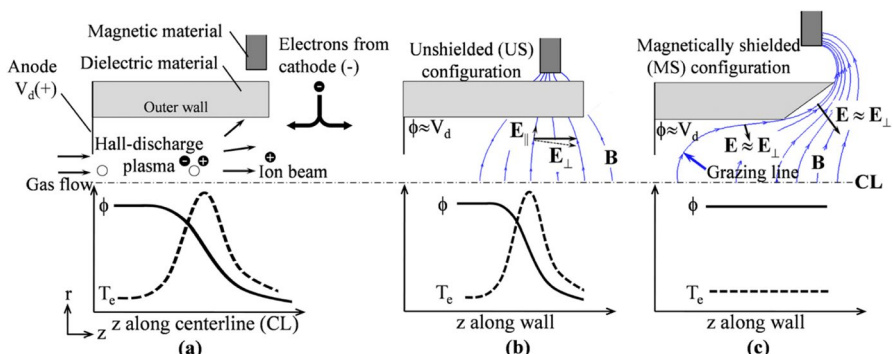


Fig. 7 Schematics of the upper half of the annular acceleration channel in a typical magnetic-layer Hall thruster (top) and typical profiles of ϕ and T_e (bottom) established during ion acceleration. Left: basic features of the accelerator and typical profiles along the centerline (CL). Middle: representative magnetic-field lines and profiles along the wall in an unshielded (US) configuration. Right: Representative magnetic-field lines and profiles along the wall in a magnetically shielded (MS) configuration (Mikellides et al. 2014)

low electron temperature characteristics of the wall's magnetic-field line ensure that the sheath potential drop is small. Thus, even if the ions hit the wall, the energy gain from the sheath is negligible.

The magnetic-field distribution of the Hall thruster, designed under the guidance of the theory of MS technology, has a prominent feature—the maximum magnetic-field intensity point is located outside the discharge channel (Shastry et al. 2011; Hofer et al. 2013; Grimaud et al. 2016), as shown in Fig. 8. Because the magnetic field controls the distribution of the plasma parameters, the variation of the magnetic-field distribution will inevitably affect the discharge characteristics. From the discharge-condition photos of the thruster with an MS configuration, it is determined that the plasma structure in the discharge chamber is evidently different from that of the conventional thruster. The unshielded (US) configuration discharge fills the chamber in close proximity to the walls. However, the MS discharge contains a zone of intense emissions with noticeable gaps on either side of the channel between the wall and the primary emission zone. These types of discharge zones have been seen on different types of MS thrusters (Conversano et al. 2014; Mazouffre et al. 2014a; Conversano et al. 2015). Figure 9 displays the plasma structure of the amplified H6 thruster discharge chamber. In this view, we can clearly see the anode past the discharge chamber via the gaps. This phenomenon qualitatively embodies our expectation that MS can significantly reduce the interaction between the plasma and the wall. It is also the first sign that the H6 thruster may achieve MS.

The effectiveness of MS technology has been validated by the JPL on Hall thrusters of different power levels. Research in this field is mainly conducted via numerical simulations and experiments. The emphasis on numerical simulation demonstrates the real existence of the physical effects of MS, enabling researchers to apply the theory of MS technology to thruster design. By simulating the MS effect in the discharge acceleration zone and testing the ion sputtering erosion rate, it has been proven that MS technology can effectively prolong thruster life. The principle of MS

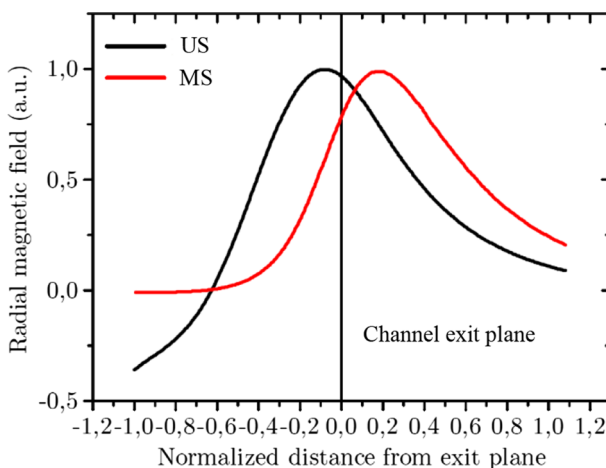


Fig. 8 Magnetic-field intensity distribution on the centerline of the channel (Grimaud et al. 2016)



Fig. 9 Operation of the H6 in the MS configuration (Hofer et al. 2014)

technology is refined based on the simulation of the physical discharge processes of the BPT-4000 at different stages of its life, comparing the results with experimental results (Mikellides et al. 2011). To reveal the physical mechanism of the MS technology and its impact on the discharge characteristics of the Hall thruster, the JPL established the simulation platform Hall2De based on the fluid model (Mikellides and Katz 2012; Katz and Mikellides 2011).

Using the Hall2De simulation platform, Katz et al. (2011) obtained the distribution condition of potential and electronic energy in the US and MS configurations, as shown in Fig. 10. It is evident that the main plasma potential drop region and the electron temperature peak position move toward the outside of the channel in the MS.

From the thermochemical potential distribution graph, we determined that the plasma potential drop at the expanding wall inside and outside the MS was only 6–13 V. By contrast, potential drops of greater than 270 V appeared closer to the US channel outlet. Therefore, the acceleration of ions in the US near-wall region was much higher than that in the MS near-wall region. Higher acceleration can increase the kinetic energy of ions entering the sheath. Because the electron temperature on the same magnetic line is approximately equal, the electron temperature in the shielding area is much lower than that in the US area, owing to the magnetic line penetrating into the channel of the MS (Mikellides et al. 2014). The sheath energy along the wall decreases with the decrease in electron temperature. Calculation results show that with 25% of the channel outside, the sheath energy declined by nearly an order. Further, the acceleration of ions was mostly perpendicular to the wall, owing to the significant decrease in the electric-field component parallel to the expanding walls of the nearby MS configuration. The accelerating ions caused a significant decrease in ions in the channel shielding area. Therefore, there was not enough ion flux to cause detectable erosion. In other words, the MS effect mainly formed a high-potential area near the wall, significantly reducing the transfer of high-energy ions to the channel wall. Thus, it weakens or even eliminates the erosion impact (Mikellides et al. 2014).

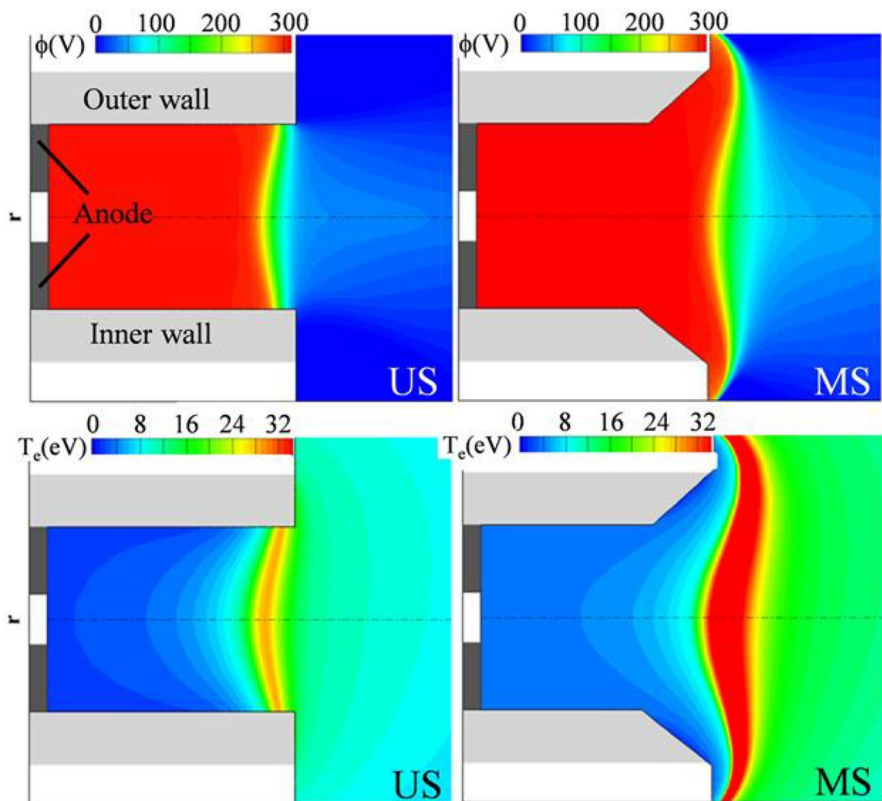


Fig. 10 Comparison of numerical simulation results in US (left) and MS (right) thruster configurations. Top: plasma potential. Bottom: electron temperature (Mikellides and Ortega 2014)

To further verify the correctness of this theory and to understand the operational mechanism of the MS Hall thruster in further detail, the plasma parameter distribution and performance were studied experimentally by the JPL. The H6 prototype with 6 kW power was the main testing object. The experimental prototype operated between 4.5 and 12 kW (Haas et al. 2007). The theory of MS effect was applied to improving the structural design of the H6 thruster (Hofer et al. 2014), including the discharge channel configuration and magnetic circuit structure of the acceleration zone.

The diagnostic method using a wall probe is adopted in the experiment. This method measures the distribution of plasma parameters on the wall, as direct evidence for the action principle of the MS technology. Figure 11 shows the plasma potential and electron temperature at the channel centerline measured under the US and MS configurations (Hofer et al. 2014). The experimental results show that the near-wall MS theory is consistent with the experiment. On one hand, the potential near the outlet wall maintains the same level as the anode potential under the MS condition. On the other hand, compared to the

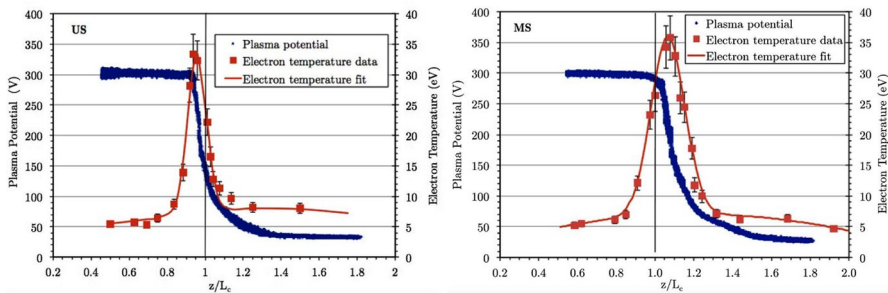


Fig. 11 Plasma potential (relative to cathode) and electron temperature measured at the channel centerline in the US (left) and MS (right) configurations (Hofer et al. 2014)

traditional Hall thruster, the axial electron temperature of the MS Hall thruster is distributed across a wider range, and the electron temperature in the near-wall region decreases by approximately 70%. Simultaneously, the ion-current density decreases by 1–2 orders. The simulation results are in good agreement with the experimental results on the flux and energy characteristics of the ions hitting the internal and external outlet walls (Hofer et al. 2014). Under MS, whereas there are many ions bombarding the outer wall, the ion energy does not reach the material sputtering threshold. The erosion rate is 0; few ions hit the inner wall; and the ion energy is less than 50 eV, which is far less than the ion energy of 200 eV obtained with the US configuration. Thus, the erosion rate decreases significantly. These findings are consistent with the predictions of the MS theory.

The measured thruster performance was compared with that of the H6 thruster prior to improvement. When H6 was set at the rated operating conditions (6 kW power and 300 V discharge voltage), experimental measures showed that there was little change in the thruster performance after adopting MS technology. The thrust decreased by 4.2%, specific impulse increased by 2.6%, total power decreased by 1.1%, and wall temperature decreased by 12–16%. The peak-to-peak value for oscillation of discharge current increased by 25% (Hofer et al. 2014). However, from Fig. 12, we find that the erosion rate of the H6 thruster with an MS configuration was significantly controlled. The erosion rate of the outer wall was zero, and the erosion rate of inner wall was reduced by 2–3 orders. The MS Hall thruster weakened the interaction between the plasma and the wall remarkably, bringing it down to a negligible extent.

The ceramics-erosion pattern after the discharge experiment shows the particularity of the MS configuration thruster (Hofer et al. 2014). With traditional Hall thrusters, the sputtering rate is generally much higher than the carbon deposition rate. Therefore, erosion is dominant on the wall of the acceleration zone, revealing the white color of the BN ceramic body, as shown on the left side of Fig. 13. However, the JPL found that when MS technology was applied, the wall of the acceleration zone was greyish black, as shown on the right side of Fig. 9. Furthermore, using the precise method of quartz crystal microbalance, they demonstrated

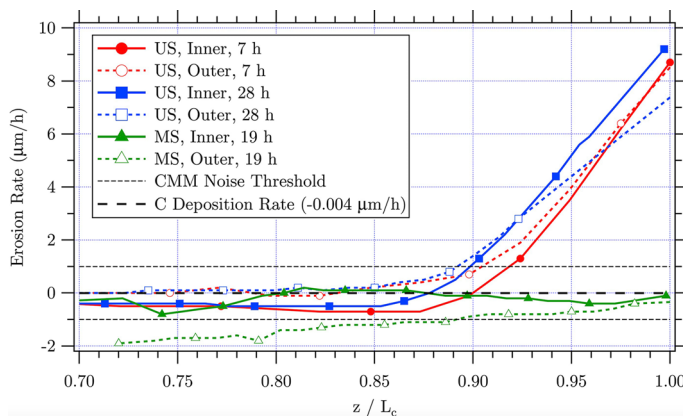


Fig. 12 Average erosion rate of US and MS rings for various run times as measured by the coordinate measuring machine (Hofer et al. 2014)



Fig. 13 Comparison of ceramics-erosion pattern between the US (left) and MS (right) configurations (Hofer et al. 2014)

that a layer of carbon film attached to the wall because the sputtering rate was lower than the carbon deposition rate.

It was observed through The possible reason, measured with the $E \times B$ probe, that the number of multicharge ions in the MS configuration had increased significantly compared to the US configuration, as shown in Fig. 14. The calculation shows that the Xe^+ current in the US configuration accounts for 75.5% of the total ion current, whereas the Xe^+ current in the MS configuration only accounts for 57.5%. Unexpectedly, the peak value of electron temperature in the discharge chamber, measured in the MS configuration, increased only by 3 eV. In addition, the ion beams in both cases mainly comprised ions with four or fewer valence states. The right semi-logarithmic coordinate graph also showed evidence that there may be Xe^{5+} (or xenon ions with higher valences), Xe^{6+} , or others with even higher valence states.

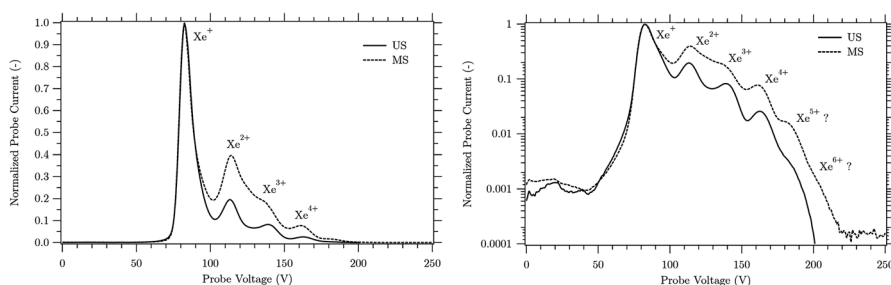


Fig. 14 Spectra of ion current for US and MS configurations on linear (left) and semi-log (right) scales normalized to maximum Xe^+ current (Hofer et al. 2012)

After comprehensive analysis, it was determined that the peak does not originate from the diatomic substances nitrogen (N_2) or BN. Therefore, Xe^{5+} may appear in the Hall thruster discharge for the first time (Hofer et al. 2012). The appearance of multivalent ions is mainly related to the peak of electron temperature in the plume region. Because there is no cooling of the wall to electrons, the electrons have a high temperature in the plume region. Thus, multivalent ionization may occur easily (Hofer et al. 2012).

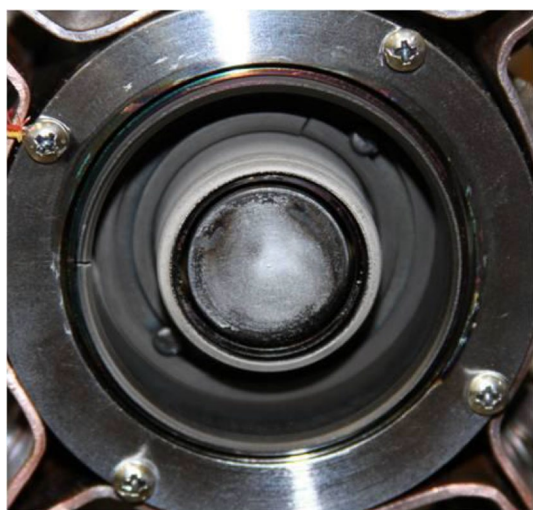
When the discharge voltage and power of the H6 are, respectively, increased to 800 V and 9 kW (Mikellides et al. 2013b; Hofer 2013), the thruster operates at a high specific impulse (3000 s) mode. Whereas no erosion could be detected at the outer wall after adopting MS technology, the erosion rate of the inner wall increased by an order, and the MS effect declined, compared to the H6 operating at 6 kW, after adopting MS technology. Further analysis shows that this was caused by the magnetic circuit system of the H6 being saturated under high-discharge-voltage conditions, leading to the deviation of the magnetic-field configuration by the MS. This problem can be eliminated by designing a more powerful magnetic circuit for a high discharge voltage. Therefore, the H9 MS Hall thruster with 9 kW power has been proposed. The H9, inheriting the geometry of the LaB6 cathode anode/gas distributor and the discharge chamber of the H6 thruster with a modified magnetic circuit, has a high degree of MS in the case of discharge voltages greater than 300 V (Hofer et al. 2017). Experimental results show that the specific impulse can reach 2950 s at 800 V and 9 kW and that the ceramic wall is free from corrosion. In addition, the H9 thruster has been proven to test well on multiple devices, exhibiting good stability and consistency (Cusson et al. 2017).

The JPL has applied MS technology to small Hall thrusters. With cooperation from the University of California and the Los Angeles Electric Propulsion Test Facility, the JPL developed a 325-W MS miniature thruster with a rated voltage 275 V and channel diameter of 4 cm (Conversano et al. 2015). Owing to the inherent higher surface-to-volume ratio of the small Hall thruster, the ceramic wall eroded quickly and there was significant loss of ion energy. The application of MS technology was expected to solve the problem fundamentally and effectively prolong the service life of the small Hall thruster. The discharge performance result, measured from the experiment, showed that within a discharge voltage range of 150–300 V,

the thrust level of the MaSMi thruster was 11–13 mN and the anode efficiency was 21–24% (Conversano et al. 2014). After the experiment, by testing the sputtering condition of the channel wall it was found that the external ceramic wall provided strong shielding without any ion sputtering. While the internal ceramic wall was shown to provide weak shielding, there were still some signs of ion sputtering (see Fig. 15). The possible reason for this phenomenon is that the localized magnetic circuit saturation makes the shielding of the inner wall weaker, which makes the ion sputtering rate of the inner wall higher. Compared with the Hall thruster with US configuration, the channel-erosion rate was reduced by approximately 3 orders, indicating a significant decrease in channel erosion by ions and a corresponding significant increase in operating life. The experimental results show that while demonstrating discharge performance, the MaSMi thruster also exhibited the expected MS effect. Therefore, the MS technology was successfully verified on the small Hall thruster.

From these research results, we recognized that the low-power MS Hall thruster had low operational efficiency. To explore the underlying physical mechanism, Conversano et al. carried out simulations and experimental research based on the discharge behavior of the new low-power MaSMi-60 MS Hall thruster (Conversano et al. 2017a). They found that the low-power MS Hall thruster had several disadvantages: low current utilization; inadequate magnetic-field intensity, which could not adequately restrain electrons from moving towards the anode, leading to an increase in the electrical current and a decrease in the current utilization; low propellant utilization; small channels of low-power thrust with shorter ionization regions; and a longer mean ionization-free path. Many non-ionized neutral particles escape from the channel. Low plume divergence efficiency is also a disadvantage. The convex curvature in the magnetic-field topology local to the discharge channel walls directed the electric-field vector off-axis relative to the channel centerline, yielding beam divergence. However, the concave curvature near-channel centerline directed

Fig. 15 MaSMi internal and external ceramics-erosion pattern (Conversano et al. 2015)



the electric-field vector toward the channel centerline, yielding beam focus. Therefore, it presented a larger plume divergence angle, leading to performance degradation (Conversano et al. 2017b). These characteristics have become a major obstacle for designing low-power MS Hall thrusters. In addition, notwithstanding the power level of the thruster, the increase in the curvature of the magnetic field close to the discharge channel outlet caused by the shielding magnetic field inevitably leads to an increase in the plume divergence angle (Conversano et al. 2017b).

The MaSMi-DM version of the MaSMi has also been improved further (Conversano et al. 2017c) using the new internally mounted low-current ultra-compact hollow cathode (MaSMi's LUC), as shown in Fig. 16. It also adopted an improved gas distributor and magnet coil design, yielding a uniform propellant flow through the discharge channel and a low requirement of magnetic power. A barium-depletion life model for MaSMi's LUC design has an operating lifetime longer than 36 kh, supplying a sufficient life margin. The objective is to achieve thruster lifetime of more than 10 kh. According to a prediction of the impressive discharge performance via simulation, the MaSMi-DM can reach nearly 50% anode efficiency and 1600 s specific impulse.

Inspired by the American MS technology, the Centre National de la Recherche Scientifique conducted research on the MS Hall thruster, including a PPS-Flex with 1.5 kW power and an ISCT200-MS with 200 W power. Experiments show that both produced discharge effects with MS characteristics. However, owing to the change in electron transfer characteristics and the weakened ability of the wall to control plasma, both the discharge performance parameters and stability were degraded (Mazouffre et al. 2014b, 2015; Grimaud et al. 2016).

The sputtering erosion of high-energy ions to the channel wall has become the most critical factor restricting the life of the Hall thruster. In the field of ion-sputtering protection, many research institutes have promulgated solutions from a variety of angles. Among them, optimizing the magnetic field's impact on the plasma

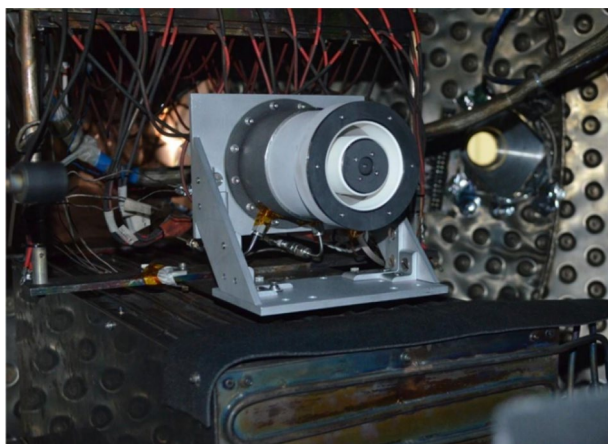


Fig. 16 MaSMi-DM mounted on thrust stand of the JPL High Bay vacuum facility (Conversano et al. 2017c)

parameter distribution is one of most significant regulation matters. Based on these research results, we found that the MS technology, based on the optimized magnetic field, was presently the most effective means for ion-sputtering protection. Research on the long service life characteristics of the MS Hall thruster has gradually become the consensus among prominent aerospace countries worldwide, inevitably propelling the development of electric propulsion technology.

3.2 Wall-less technology

The wall-less Hall thruster locates its anode at a channel outlet, with ionization and acceleration occurring in a plume region. The ionization zone and acceleration zone are completely moved outside the discharge channel to restrict the interaction between the plasma and the channel walls. This was first proposed by Kapulkin et al. (1995) in the 1990 s. Thereafter, the external electric field concept was proposed for the Hall thruster. However, owing to a presumed ion-current limitation linked to plasma instabilities, researchers moved from the standard one-stage architecture to a two-stage architecture. Semenkin (1997) researched the concept of moving the electric field out of the channel for a thruster-with-anode layer (TAL). Researchers demonstrated the possibility of efficient and stable operations under a high voltage. In 2014, Mazouffre et al. (2014c) presented the wall-less Hall thruster to reduce the interaction between the plasma and the channel walls based on this concept.

Figure 17 depicts the standard configuration of a traditional Hall thruster and a wall-less Hall thruster. Thus, in a traditional Hall thruster (shown in Fig. 17a), the anode is generally located at the bottom of the channel. The cathode (i.e., electron source and neutralizer) is located outside the channel. A radial directed magnetic field with a bell-shaped intensity distribution along the centerline is generated by coils or permanent magnets. The maximal magnetic-field intensity is close to the channel outlet. The ceramic channel constrains the propellant and

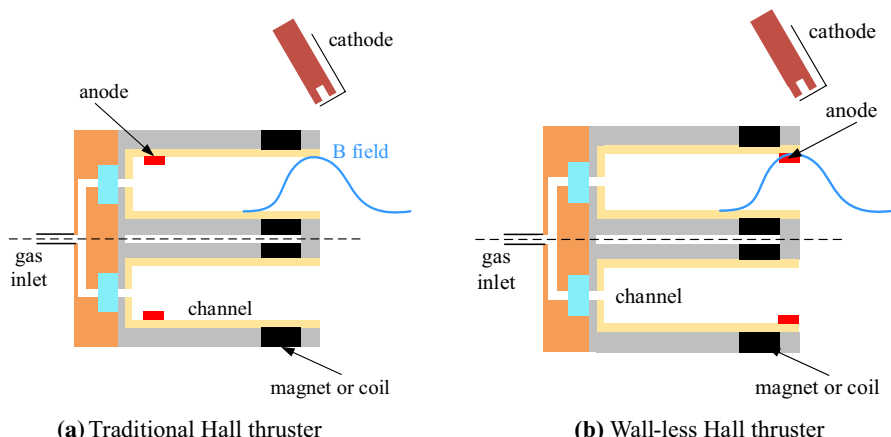


Fig. 17 Configurations of **a** traditional and **b** wall-less Hall thrusters (Mazouffre et al. 2014c)

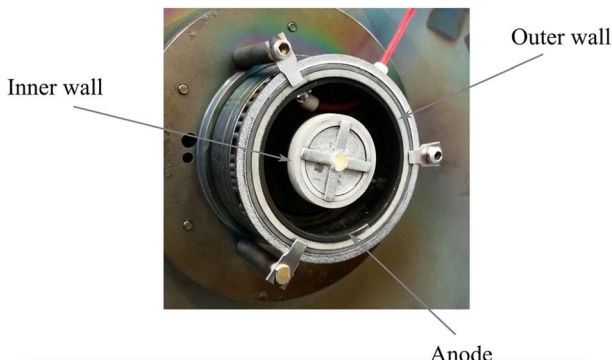


Fig. 18 Photograph of 200-W class wall-less Hall thruster prototype (Mazouffre et al. 2014c)

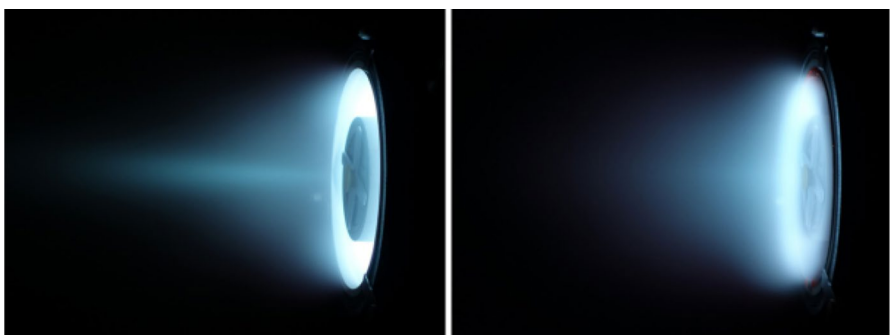


Fig. 19 Photos of low-power traditional Hall thruster (left) and wall-less Hall thruster (right) (Mazouffre et al. 2014c)

maintains a high atomic density for subsequent ionization processes. Therefore, for the wall-less Hall thruster, the anode is located at the channel outlet, as shown in Fig. 17b, to achieve ionization and acceleration in the plume region (Mazouffre et al. 2014c).

Figure 18 shows the 200-W wall-less Hall thruster prototype. The anode comprises a conducting ring located at the channel exit plane around the external wall. The channel is made of BN–SiO₂. The magnetic field of the thruster is generated by a permanent magnet. Figure 19 depicts the images of a low-power ion source working with Xe propellant in the traditional 200-W class Hall thruster and the wall-less Hall thruster with a ring anode (Mazouffre et al. 2014c). The discharge voltage is 200 V and the anode mass-flow rate is 1 mg/s. The photo (right) of the channel outlet under hard light shows that the discharge zone was pushed out of the ceramic channel, as expected, in the wall-less Hall thruster. The evident distinction between them is that the boundary of the ion beam in the wall-less Hall thruster is less distinct. This indicates that the plume divergence angle in a wall-less configuration is greater. Greater plume divergence angle may degrade thruster performance,

bringing about magnetic-pole erosion and creating other problems. Moreover, a large beam divergence means that the plasma from the thrusters has a negative effect on spacecraft elements (Mazouffre et al. 2014c).

Compared to the traditional Hall thruster, the wall-less Hall thruster has a larger current under the same conditions. However, the standard deviation of the discharge current is lower in the wall-less mode. Similar to the traditional Hall thruster, the low-frequency oscillations of a wall-less Hall thruster fall within 10–30 kHz, corresponding to the well-known breathing mode (Choueiri 2001b), as shown in Fig. 20. The wall-less Hall thruster has a small power spectrum at 100 Hz, encompassing phenomena such as rotating instabilities and ion transit time instabilities. The potential distribution measurement results also demonstrate that the acceleration zone of the wall-less Hall thruster was completely pushed out of the channel, as shown in Fig. 21 (Mazouffre et al. 2014c).

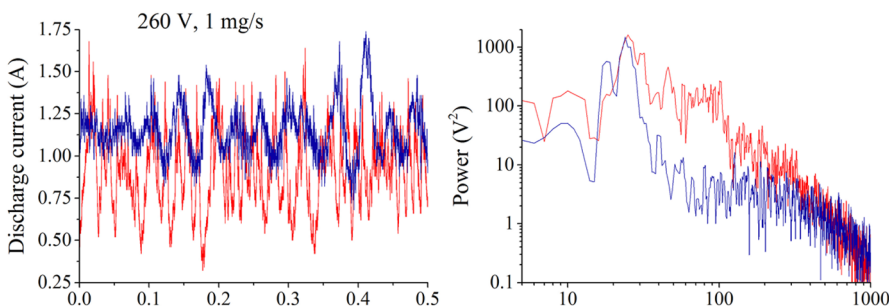


Fig. 20 Discharge current waveforms of thruster in traditional configuration (red line) and in wall-less configuration (blue line) (Mazouffre et al. 2014c)

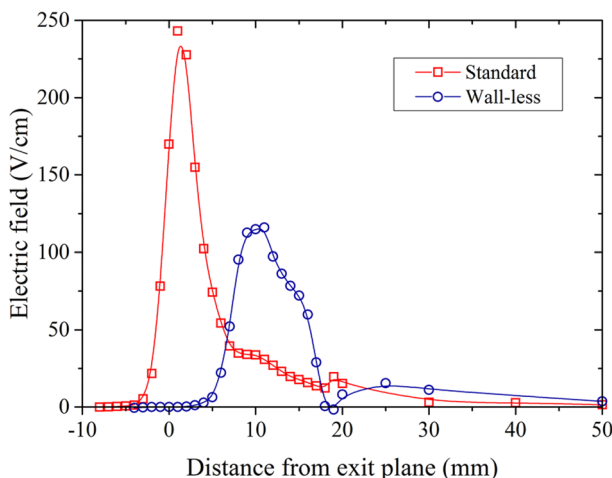


Fig. 21 Accelerating electric-field distribution along channel axis of ion source in the standard (square) and the wall-less Hall thruster (circle) configurations (Mazouffre et al. 2014c)

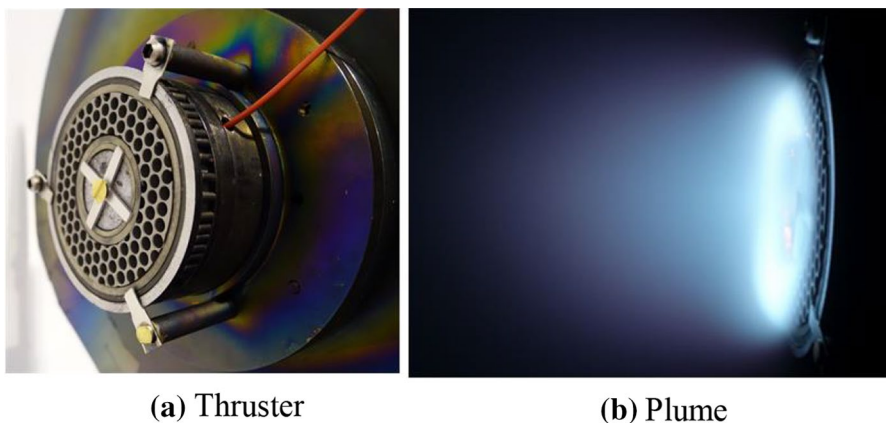


Fig. 22 Second prototype of wall-less Hall thruster with gridded anode (Mazouffre et al. 2014c)

Furthermore, Mazouffre et al. (2014c) presented an improved wall-less Hall thruster. The anode ring at the channel outlet was changed to a gridded anode. The gridded anode had a transparency of 68% with a 3-mm diameter hole, as shown in Fig. 22a. To sufficiently homogenize the central gas, a 3-mm thick gridded anode covering the channel outlet was designed. To limit the plasma diffusion in the discharge channel, the anode width was decreased. Other components and assemblies were almost the same as in the prototype.

Figure 22b shows a photo of the second prototype of the wall-less Hall thruster with a gridded anode firing Xe with a discharge voltage of 200 V. The anode mass-flow rate was 1 mg/s. It can be observed from the light at the channel outlet that ionization occurred outside the channel. Moreover, the plume is divergent and the ion beam boundary is hazy. This implies that there was a degradation in the performance. The gridded anode occupies the channel outlet and some magnetic lines directly intersect the anode, particularly in the area nearest to the channel wall. Thus, it creates a short circuit for the electrons. Under several conditions, the anode changes to red, indicating a temperature above 1000 K (Mazouffre et al. 2014b).

Figure 23 reflects the interaction between the annular anode and the B-field lines. The magnetic circuit of the original wall-less Hall thruster prototype is shown in Fig. 23 (left). It is based on the classical Hall thruster design. The anode was placed at the channel outlet and the ionization was pushed out of the channel. Thus, no change was registered on the magnetic field. The magnetic line near the outlet was almost perpendicular to the channel wall, intersecting the anode. Thus, the electronic restraining capability decreased. Moreover, many high-energy electrons emitted from the cathode were trapped along the magnetic-field lines, eventually arriving at the anode. Therefore, the electronic current was relatively large and the propellant utilization was low. To solve the significant loss problem of the anode electron energy, an optimal magnetic circuit was used (Vaudolon et al. 2015), as shown in Fig. 23 (right). The magnetic-field lines were injected axially and the peak magnetic-field intensity was pushed downstream towards the channel exit. The curved

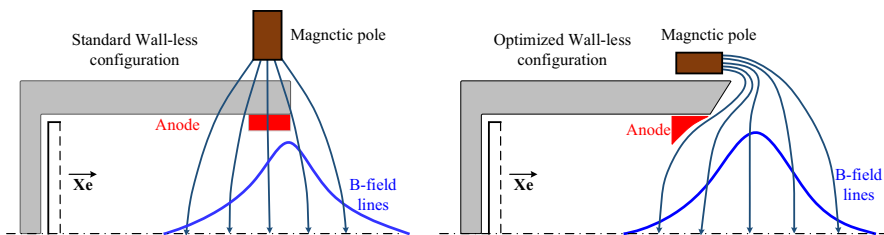


Fig. 23 Schematics of original (left) and optimized (right) wall-less Hall thruster prototype (Vaudolon et al. 2015)

anode, located at the exit, was so shaped that it did not intersect the field lines. This ensured that the magnetic field could trap electrons and effectively produce thrust. This type of optimization may seem similar to the MS Hall thruster, but the striking difference is that in the wall-less magnetic configuration, it is not necessary to extend deeply into the cavity to capture electrons. Therefore, it is quite easy to generate the required magnetic circuit (Vaudolon et al. 2015).

Some experiments have been performed based on the 1.5-kW PPS-Flex Hall thruster (Vaudolon et al. 2015). As expected, the discharge current was significantly reduced by the adjustment of the magnetic topology and the positioning of the anode in parallel. To improve the propellant utilization and achieve higher thrust, specific impulse, and anode efficiency, the thruster was operated at a voltage of 500 V. However, the exciting current did not allow the generation of a wall-less topology with a peak magnetic-field value above 90 Gs, which significantly impacted the operation at high voltage. Further optimization was necessary to increase the thruster efficiency and reduce discharge current oscillations. An improved Hall thruster, based on PPS-Flex and capable of forming a stronger magnetic-field intensity, is currently under development. The impact of the ceramic channel length of the thruster is a critical factor that requires further study. It is possible that the channel length could be reduced while ionization takes place near the channel outlet plane. However, it should also be maintained sufficiently long to ensure the homogenization of the neutral gas (Vaudolon et al. 2015).

Karadag et al. (2018a) presented the external discharge plasma thruster (XPT), very similar to the wall-less thruster. A magnetic mirror configuration is used to restrain the discharge of plasma in the plume region. The thruster has no discharge channel or magnetic conductive element. Its magnetic circuit comprises a pair of hollow cylindrical permanent magnets. A circular anode is placed downstream of the magnetic-field maximum. Figure 24 shows the XPT thruster head cross section (left) and thruster firing (right) (Karadag et al. 2018b).

Propellant gas is injected upstream of the anode cavity from the holes azimuthally arranged on the dielectric front wall. A magnetic field is generated from the permanent magnet, which is stronger at the magnetic cusps on the front wall than that at the anode centerline, owing to the curvature of the magnetic-field lines. Electrons captured by the magnetic mirror reciprocated between two mirror points to form an electronic cloud along the $E \times B$ direction. Neutral atoms

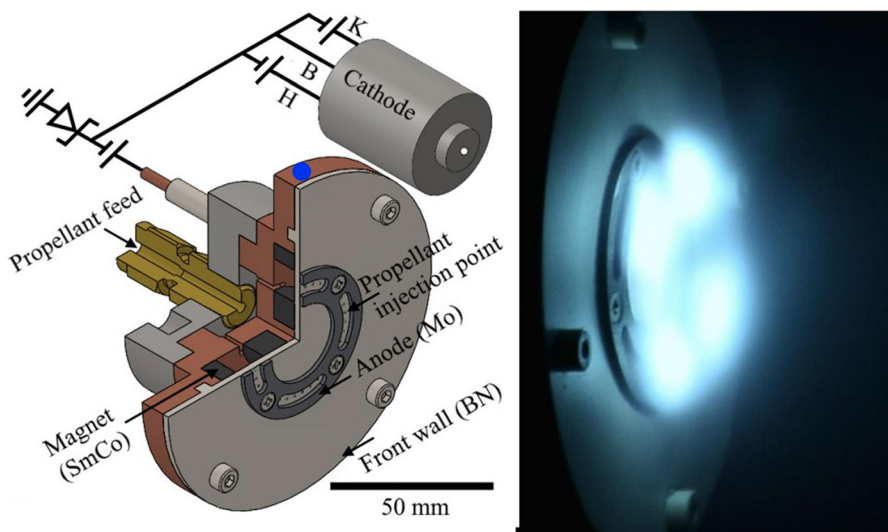


Fig. 24 XPT thruster head cross section and thruster firing (Karadag et al. 2018b)

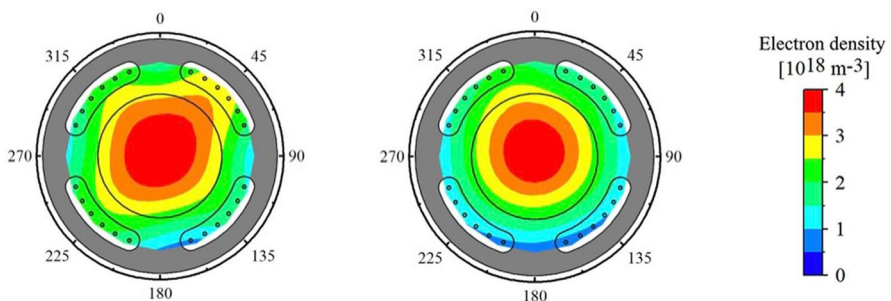


Fig. 25 2D electron density maps for the operating conditions 150 V, 1.43 mg/s (left) and 250 V, 1.43 mg/s (right) (Karadag et al. 2018b)

injected at the upstream end of the anode cavity entered the rotating electron cloud and generated ionization. The radial magnetic field reduced the axial electron mobility, so that the neutral plasma maintained a strong axial electric field. Ions accelerated under the action of the electrical field and generated thrust according to the Lorentz force law: $F = q(E + v \times B)$. The XPT was the first Hall thruster to operate without any annular or cylindrical discharge channel walls (Karadag et al. 2018b).

Figure 25 presents the 2D electron density maps for different operating conditions. It can be observed from Fig. 24 that the plume was unevenly close to the anode because of the non-uniformity of the gas distributor. Figure 25 displays the results 10-mm away from the external wall, where the electron density was relatively even along the circumference. This suggests that the plasma flow adjusted

itself to be uniform in the azimuthal direction as the axial distance increases when the propellant injection scheme was highly non-uniform (Karadag et al. 2018b).

Wall-less Hall thrusters place the anode at the channel outlet and push the ionization zone and acceleration zone out of the channel. The interaction between the plasma and the wall decreases significantly. Therefore, the impact of the channel material on thruster performance is alleviated. More significantly, it is then possible for the thruster to operate at a higher voltage and with an extended lifetime. However, owing to the lack of channel limitation, the plume divergence angle is high and the thruster performance is low. In addition, the reduction of the plasma–wall interaction can lead to higher electron temperatures and positive points, resulting in efficient ionization of propellants (e.g., krypton and argon).

3.3 Aft-magnetic field with large gradient technology

Ding et al. (2016) studied the aft-magnetic field with large gradient technology to improve the life of the Hall thruster. The distribution of the magnetic field in the channel is shown in Fig. 26. Compared to the traditional Hall thruster, the difference mainly lies in the maximal magnetic-field intensity in the plume region and the great magnetic-field gradient. Compared to the MS Hall thruster, the difference mainly lies in the intersection of the magnetic-field lines and the wall and a high magnetic-field gradient, which is good for shortening the length of the ionization zone. The maximal magnetic-field intensity in the plume region can effectively control ionization in the channel outlet, effectively decreasing the bombardment of high-energy ions onto the wall and improving the lifetime of the Hall thruster (Ding et al. 2016).

The ratio between Brexit (the magnetic-field intensity at the channel outlet at the channel centerline) and Brmax (the maximal magnetic-field intensity at the channel centerline) is used to indicate the aft-magnetic degree. A smaller ratio represents a larger aft-magnetic degree. Ding et al. (2016) adopted a permanent magnet excitation, realizing a different aft-magnetic degree by adjusting the channel length for different values of the Brexit/Brmax ratio and calculated the change in the ratio based on thruster performance between 0.75 and 1, as shown in Table 2. With the decrease in the ratio, while the plume divergence angle increases and the propellant utilization decreases (i.e., decrease in thruster efficiency), the power deposition of plasma on the wall decreases significantly, which is good for improving thruster efficiency. Therefore, a suitable Brexit/Brmax ratio corresponds to high efficiency. Simulation

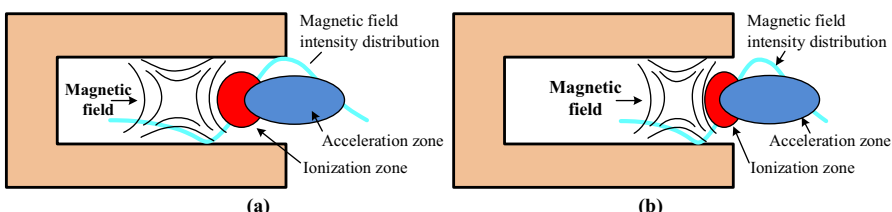


Fig. 26 Schematic of ionization and acceleration in thruster channel: **a** Traditional Hall thruster, **b** aft-magnetic field with a large-gradient Hall thruster. Reprinted with permission from Ding et al. (2016) Copyright 2016 IOP

Table 2 Performance parameters with different Brexit/Brmax ratios (Ding et al. 2016)

Brexit/Brmax	Power (W)	Thrust (mN)	Anode-specific impulse (s)	Anode efficiency (%)
0.75	1413	81.1	1655	46.6
0.80	1389	83.5	1704	50.0
0.85	1368	85.8	1751	53.5
0.90	1353	88.9	1814	58.4
0.95	1338	87.6	1788	57.4
1	1326	86.6	1767	56.5

results indicate that the efficiency is high when the ratio is 0.9 or 0.95, because primary ionization can be maintained inside the channel, and primary acceleration can be pushed down to the plume region. This can maintain a high level of propellant utilization and decrease the energy and flux of ions and electrons bombarding the walls. Furthermore, when the Brexit/Brmax ratio decreases from 1 to 0.75, the power deposition of plasma on the wall reduces by nearly 30 times (Ding et al. 2016). Furthermore, the length of high-energy ions bombarding the wall reduces remarkably (as shown as Fig. 27), which is good for improving thruster life. Therefore, a suitable Brexit/Brmax ratio should be selected for the Hall thruster to guarantee higher propellant utilization and lower wall-energy loss. Thus, both the thruster performance and lifetime can be improved (Ding et al. 2016).

The impact of the magnetic-field gradient in the discharge channel of a Hall thruster on the ionization and power deposition on the wall was studied by adopting 2D-3 V PIC and Monte Carlo collision models (Ding et al. 2017a). Figure 28 depicts the magnetic-field distribution, in which Br is the magnetic-field intensity along the radial direction. The study showed that when maximal magnetic-field

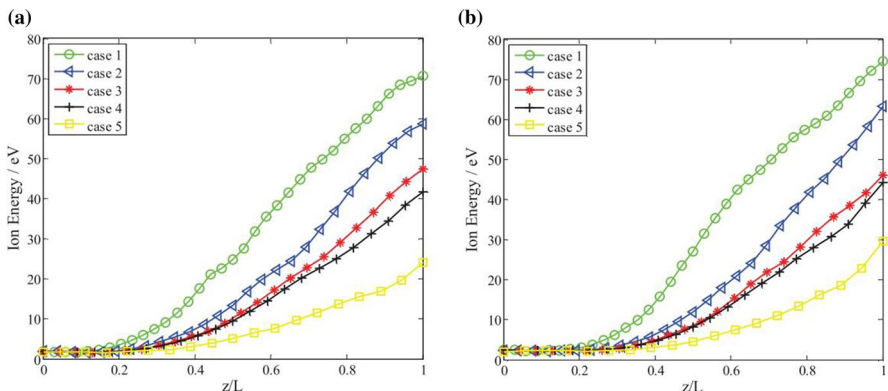


Fig. 27 Axial ion energy distribution at the walls: **a** Inner wall and **b** outer wall. The Brexit/Brmax ratios for cases 1–5 are, respectively, 1, 0.95, 0.9, 0.85, 0.8, and 0.75. Reprinted with permission from Ding et al. (2016) Copyright 2016 IOP

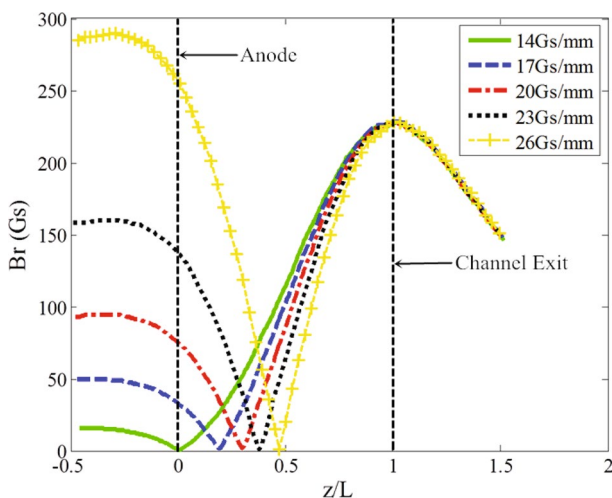


Fig. 28 Magnetic-field gradient distribution at the channel centerline. Reprinted with permission from Ding et al. (2017a) Copyright 2017 JPP

intensity and an unchanging anode position are maintained with an increase in the magnetic-field gradient, the ionization zone moves into the channel outlet. Thereafter, the second ionization zone appears close to the anode. Simultaneously, the power deposition on the channel wall decreases and then increases. To reduce the power deposition of electrons and ions generated in the second ionization zone on the wall, during the change in the magnetic-field gradient, the anode is constantly maintained at the zero magnetic-field position and the power deposition on the wall decreases with an increase in the magnetic-field gradient. Thus, the temperature and thermal load on the discharge channel can be effectively decreased (Ding et al. 2017a).

Ding et al. (2017b) designed a 200-W permanent magnet aft-magnetic Hall thruster with high gradient. The magnetic field possessed symmetrical double-peak characteristics, as shown in Fig. 29. A photograph of the thruster is shown in Fig. 30.

The thruster possesses several characteristics. Its magnetic field is generated with a permanent magnet. The gas distributor and the anode are made of non-magnetic stainless materials. The thruster and other metal structures are made of titanium, and there is no other magnetic conductor. No magnetic screen is used. The thruster adopts the hollow anode structure and its front-end face is at the internal magnetic separatrix position. The distance from the zero magnetic field zone to the channel outlet is shorter than that of other Hall thrusters. Thus, the magnetic-field gradient is larger than that of traditional Hall thrusters. Channel length can be adjusted by combining different ceramic rings. Thus, 50% of the hollow treatment is performed for the thruster shell surface, which is conducive to thermal radiation of the ceramic channel during thruster operation. This effectively reduces the temperature (Ding et al. 2017b).

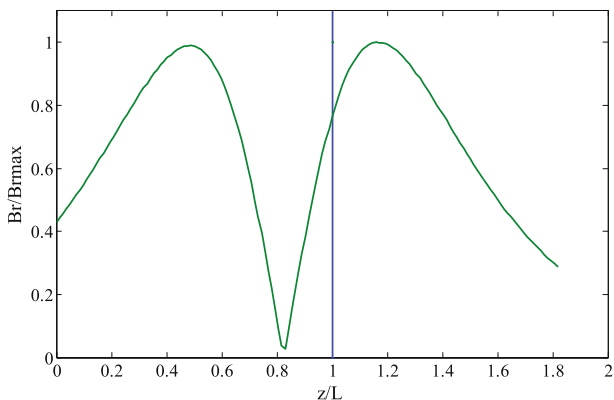


Fig. 29 Distribution of magnetic-field intensity at the channel centerline. Reprinted with permission from Ding et al. (2017d) Copyright 2017 IOP



Fig. 30 Thruster and inner and outer walls after discharge. Reprinted with permission from Ding et al. (2017d) Copyright 2017 ELSEVIER

Experiments showed visual evidence of ion suppression and electron energy loss on the wall (Ding et al. 2017c). When discharging with a straight channel and an indented channel, the thruster can realize zero wall loss ($B_{exit}/B_{rmax} = 0.75$). When the discharge power is 200 W, the maximal anode efficiency can reach 29.1 and 34.2% (i.e., oblique channel). When $B_{exit}/B_{rmax} = 0.9$, the anode efficiency can be as high as 42% (Ding et al. 2017c). Figure 30 shows the photographs of the inner and outer walls after a discharge with $B_{exit}/B_{rmax} = 0.75$. Near the outlet of the inner ceramic wall, there is a dark yellow area approximately 1 mm long. The outer ceramic wall is almost completely black because it is covered by a black deposition. Therefore, it can be inferred that low-energy ions have bombarded the channel wall. There are almost no high-energy ions bombarding the wall and causing erosion (Ding et al. 2017d). This further demonstrates that technology can greatly reduce the bombardment of high-energy ions on the wall, thus

realizing a long service life. In addition, thrust, specific impulse, and efficiency test lead to different Brexit/Brmax ratios, further validating the numerical simulation results (Ding et al. 2017e).

As far as the Hall thruster with an aft-magnetic field and a large gradient is concerned, there is a short distance from the zero magnetic field to the channel outlet, and the ratio between the mean ionization-free path and the characteristic length of the channel is less, which is poor for sufficient ionization of neutral gas. Therefore, it is necessary to achieve gas homogenization and sufficient ionization at such a short distance. Ding et al. (2017f) studied different anode positions and shapes to improve the density and evenness of neutral gases and improved the propellant utilization and efficiency of the thruster. They successively performed a four-anode study, as shown in Fig. 31, focusing on the impact of the different anodes on the discharge characteristics of a thruster to obtain theoretical support for the performance improvements of Hall thrusters with long lifetimes.

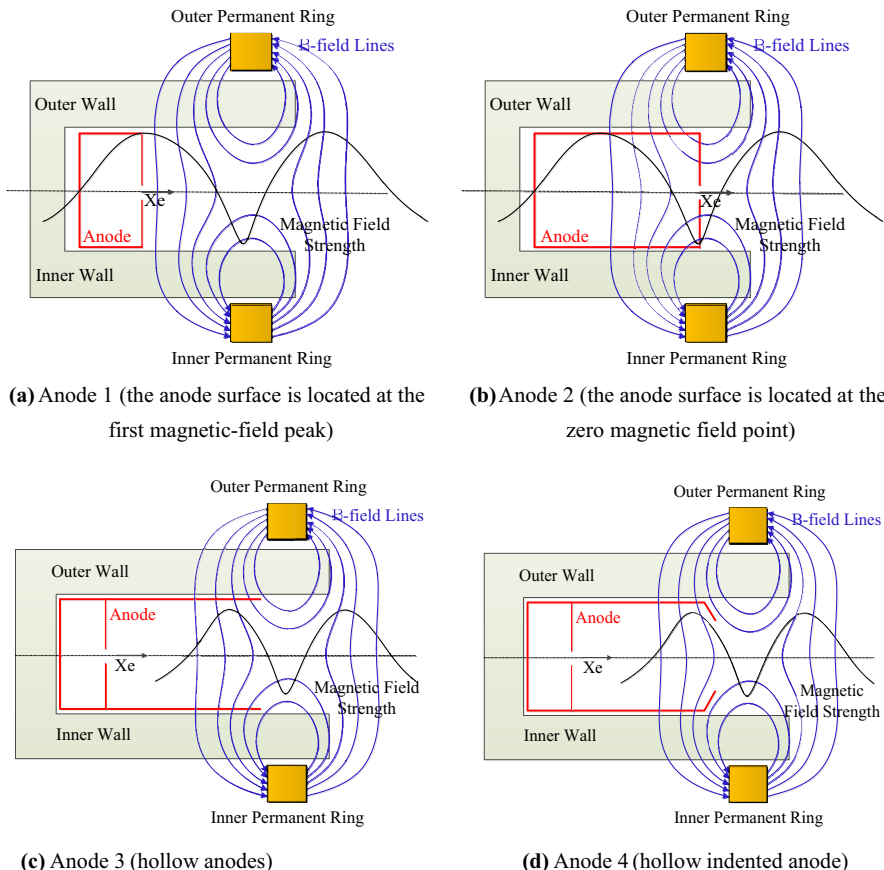


Fig. 31 Schematic of magnetic-field configuration. Reprinted with permission from Ding et al. (2017f, g). Copyright 2017 ELSEVIER and IOP Publishing

It is shown in Ding et al.'s study (2017f) that under the same magnetic fields, the discharge voltage, anode mass-flow rate, and hollow indented anode (Anode 4) are most efficient. Thus, with respect to the anode in the first magnetic-field peak (Anode 1), the ionization rate is the highest (as shown in Fig. 31a), the interaction area between the plasma and the wall is long, and the deposition energy on the wall is high. Therefore, under the same conditions, the efficiency at Anode 1 is lower than those of Anode 2, 3, and 4 (Ding et al. 2017f). For the anode at the zero magnetic field point (Anode 2), while its maximum ionization rate is higher than those of the hollow anodes (Anodes 3 and 4) and the power deposition on the walls is slightly smaller, the propellant utilization and voltage utilization are lower than those of the hollow anodes. Furthermore, its overall performance is poorer than those of the hollow anodes (Anodes 3 and 4) because of the shorter ionization length and larger divergence plume.

The hollow anode study was performed to improve the neutral gas pre-ionization and efficiency. The hollow anodes are shown in Fig. 31c (i.e., hollow straight anode) and Fig. 31d (i.e., hollow indented anode) (Ding et al. 2017g). Neutral gas-flow simulation results show that compared to the hollow straight anode, the hollow indented anode can effectively improve the neutral gas density in the discharge channel, as shown in Fig. 32 (Ding et al. 2017g). The simulation results indicate that the hollow indented anode can increase propellant utilization in the channel and the pre-ionization of the anode. Therefore, the hollow indented anode can be considered an essential design concept for improving thruster performance (Fig. 33).

Further experiments indicate that under the same operation conditions, compared to the hollow-straight anode, the hollow-indented anode effectively improved thruster efficiency. The maximum absolute difference of anode efficiency was 7.23%, with a discharge voltage of 300 V and an anode mass-flow rate of 1.2 mg/s. The maximum difference of the propellant utilization was 8.35%, with an anode voltage of 400 V and mass-flow rate of 1.1 mg/s (Ding et al. 2017g).

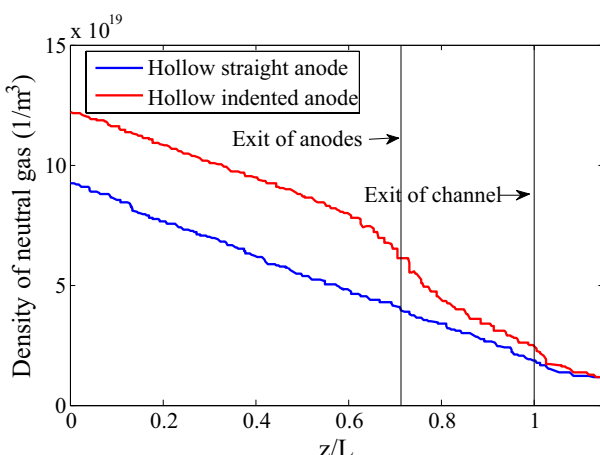


Fig. 32 Density distribution of neutral gas along medium diameter of discharge channel. Reprinted with permission from Ding et al. (2017g) Copyright 2017 ELSEVIER

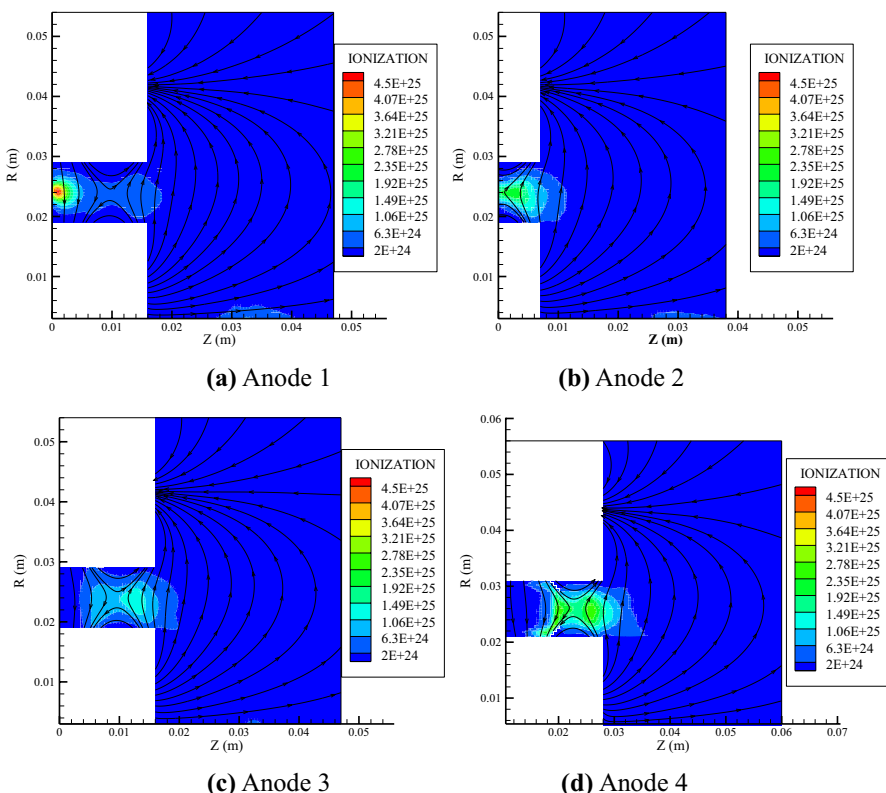
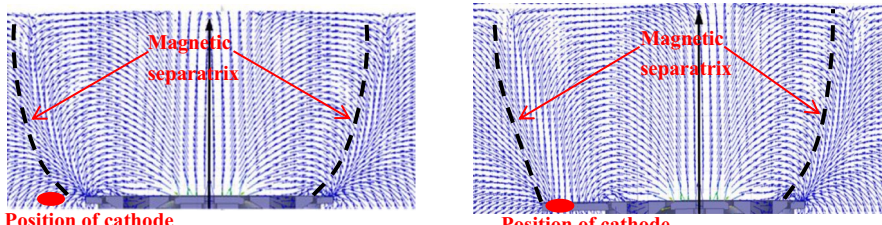


Fig. 33 Ionization distribution. Reprinted with permission from Ding et al. (2017g) Copyright 2017 ELSEVIER and IOP Publishing

The implementation of aft-magnetic technology for the Hall thruster was mainly performed on the permanent-magnet Hall thruster. The magnetic field of such thrusters usually has the significant feature of the magnetic separatrix, and the relative position of the cathode and magnetic separatrix has a significant impact on the ignition process. In this work, a new convex external magnetic pole structure is proposed. The structure can change the location of the magnetic separatrix. When the cathode position is not changed, the cathode can be located inside and outside the magnetic separatrix, as shown in Figs. 34 and 35.

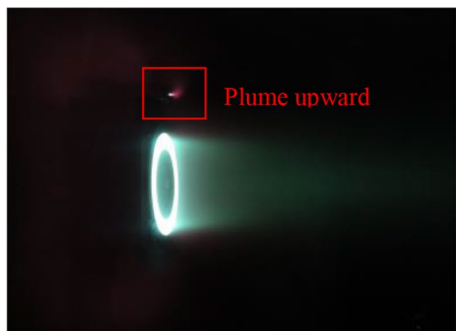
Figure 35 shows two magnetic pole structures and photographs of the discharge plume. It can be clearly seen from the photos that when the outer magnetic poles have not extended (Fig. 35a), the anode will be located outside the magnetic separatrix. A large number of electrons emitted from the cathode are captured by the magnetic-field line outside the magnetic separatrix. In this case, a pink electron drift belt forms beyond the magnetic separatrix, and the corresponding electron does not participate in the ionization process. When the outer magnetic pole extends (Fig. 35b), the magnetic separatrix is pulled outwards. Therefore, the cathode is located inside



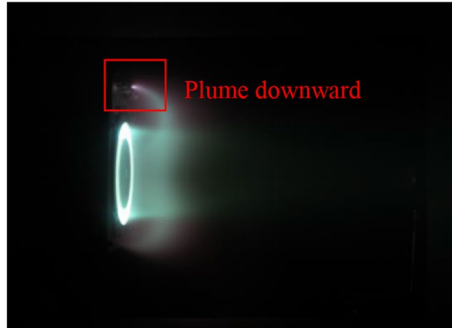
(a) Magnetic-field distribution with traditional external magnetic pole structure

(b) Magnetic-field distribution with extended structure of external magnetic pole

Fig. 34 Magnetic-field distribution with traditional outer magnetic pole structure and extended structure of outer magnetic pole. Reprinted with permission from Ding et al. (2018b) Copyright 2018 ELSEVIER



(a) Non-extended outer magnetic pole and its plume



(b) Extended outer magnetic pole and its plume

Fig. 35 Comparison between discharge plumes of extended and non-extended structures of outer magnetic pole. Reprinted with permission from Ding et al. (2018b) Copyright 2018 ELSEVIER

the magnetic separatrix. Most electrons emitted from the cathode are captured by the magnetic-field line in the magnetic separatrix. Subsequently, they participate in the ionization and contribute to conduction. The pink electric belt disappears, and a

plasma bridge is formed between the cathode and the discharge channel (Ding et al. 2018b).

The ignition process of the thruster, when the cathode is inside and outside the magnetic separatrix, is studied with a high-speed charge-coupled device camera (Li et al. 2019). The thruster plume images during ignition, when the cathode is inside and outside the magnetic separatrix at different times, are shown in Figs. 36 and 37, respectively, having three apparent differences. First, at the initial time (t_2), a weak light intensity can be observed at the exit of the cathode and discharge channel when the cathode is inside the magnetic separatrix. However, when the cathode is outside the magnetic separatrix, no significant brightness is observed, owing to the cathode being inside the magnetic separatrix. The electrons enter the discharge channel along the magnetic-field lines within the magnetic separatrix, and the electron energy loss is less. However, the electrons must pass through the magnetic-field lines outside the magnetic separatrix to enter the discharge channel. The energy loss of the electrons is large but not enough to reach the ionization threshold of the Xe atom. Therefore, no apparent brightness is observed. Second, at the end of the avalanche ionization phase (t_5), a plasma bridge can be observed between the cathode exit and the inner pole of the thruster when the cathode is inside the magnetic separatrix. Third, during the thruster transitions from the ignition process to the normal state (t_6-t_{11}), when the cathode is outside the magnetic separatrix, the thruster occurs at a typically low-frequency oscillation, because during the establishment of the discharge process the electrons must traverse more magnetic-field lines, causing the discharge of the plasma to be unstable.

The ignition impulse current of the thruster, under two different configurations, was also measured. The results indicate that the ignition duration was longer when the cathode was outside the magnetic separatrix than when it was located inside the magnetic separatrix. However, the peak value of the pulse current was small, and during the transition from the end of the ignition process to the normal discharge, the thruster discharge occurred at a typically low-frequency oscillation. However, after ignition, the current entered the normal discharge process in the same fashion.

In summary, the relative position of the cathode and magnetic separatrix had a significant impact on the ignition process of the Hall thruster owing to the different conduction paths followed by the electrons emitted into the acceleration channel.

Experiment results indicate that when the cathode is located inside the magnetic separatrix, the effective acceleration voltage is higher and the coupling voltage between the cathode and thruster is lower. Thus, the thruster performances are improved. When the cathode is located outside the magnetic separatrix, the effective acceleration voltage is lower and the coupling voltage between the cathode and thruster is higher. Thus, the thruster performance declines. When the cathode is located inside the magnetic separatrix, the thrust and specific impulse of the thruster is improved by 2.3%, compared to the cathode outside the magnetic separatrix. The anode efficiency is improved by a maximum of 4.6%. This study provides a new method for the design of the magnetic separatrix and is of significance for the coupling-matching design of the cathode and thruster.

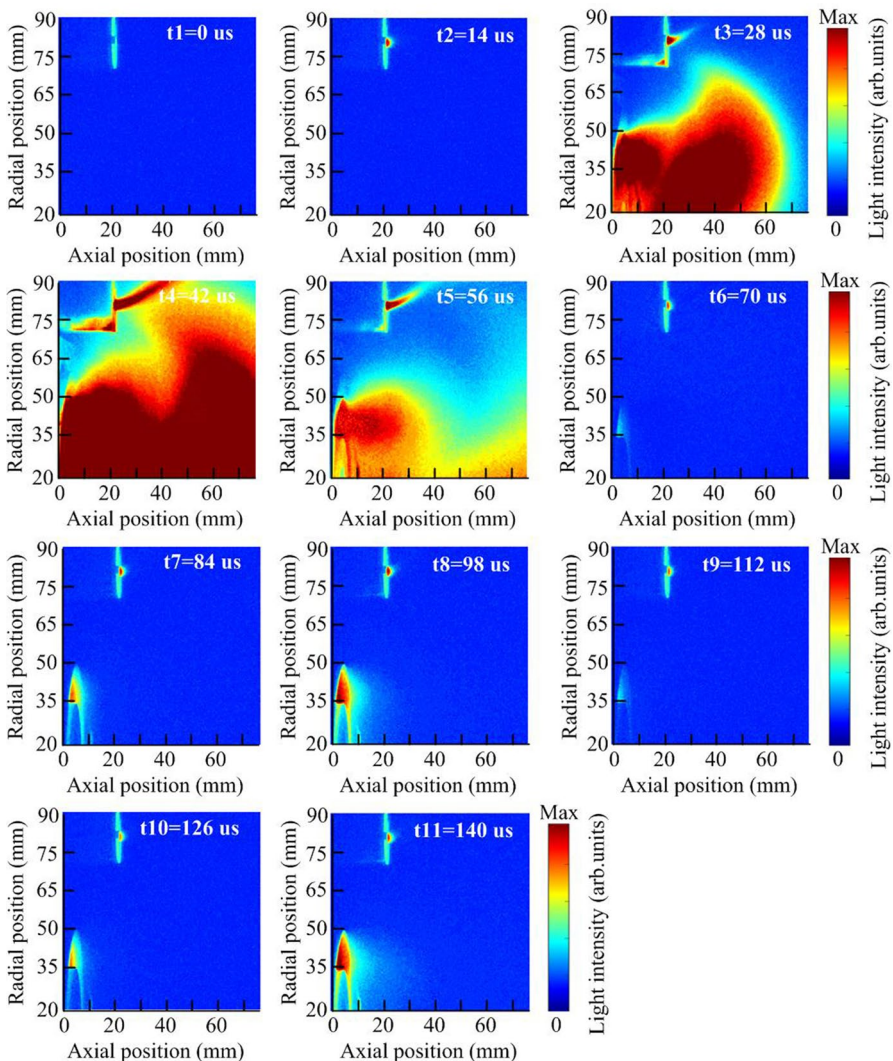


Fig. 36 Images of plasma plume from Hall thruster during ignition when the cathode is located inside the magnetic separatrix. The light intensity mostly originates in Xe emission lines and portrays the Xe^+ ion density. Reprinted with permission from Li et al. (2019) Copyright 2019 ELSEVIER

3.4 Cylindrical Hall thruster

The idea of the cylindrical Hall thruster (CHT) comes from low-power applications for reducing erosion. Differing from the traditional Hall thruster, the CHT comprises a cylindrical ceramic channel, ring-shaped anode, magnetized cores, and magnetized sources. Its cross section is shown in Fig. 38 (Ellison et al. 2012).

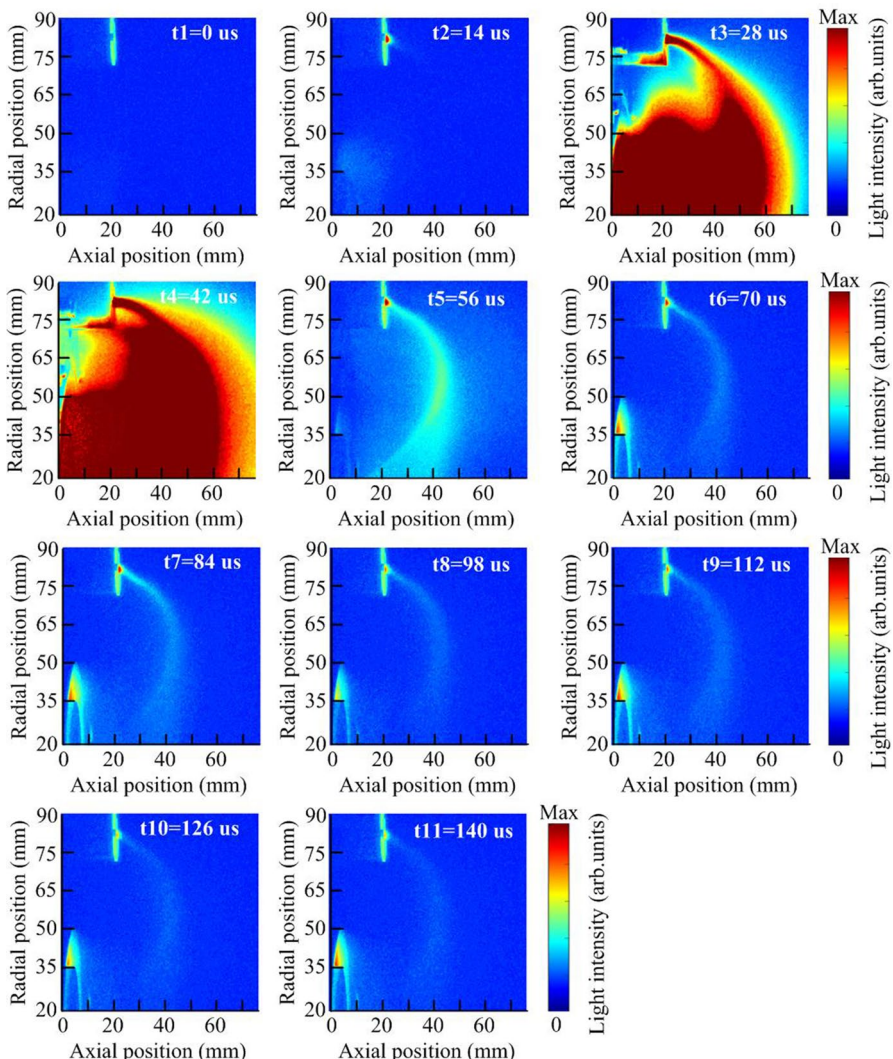
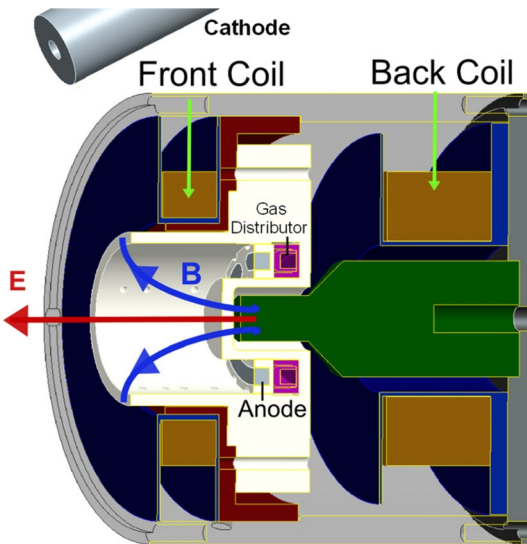


Fig. 37 Images of the plasma plume from the Hall thruster during ignition when the cathode is located outside the magnetic separatrix. The light intensity mostly originates in Xe emission lines and portrays the Xe^+ ion density. Reprinted with permission from Li et al. (2019) Copyright 2019 ELSEVIER

The most significant features of the CHT are its short inner magnetic pole and its cylindrical channel, which dramatically reduce its channel surface. While its discharge characteristics are similar to those of traditional Hall thrusters, the CHT performs better than traditional Hall thrusters because of its higher propellant ionization efficiency caused by the doubly charged ions produced by the ionization of Xe^+ , less large-amplitude low-frequency oscillations, and the possibility of operating at a smaller power (Raitses and Fisch 2001; Smirnov et al. 2002; Garrigues et al.

Fig. 38 Cross section of CHT
(Ellison et al. 2012)



2008). By analyzing the characteristics of the plasma parameters measured by the Langmuir probe, it can be concluded that the potential drop in a CHT mainly takes place in the cylindrical part and the plume. This conclusion strongly supports the fact that the structure of CHT can reduce surface erosion. Plume-narrowing in the CHT is significant, leading to an increase in the anode efficiency (Smirnov et al. 2004; Raitses et al. 2007). Meanwhile, the interaction between the characteristics of CHT's plasma parameters and the cathode is gradually revealed. It was experimentally found that the cathode electron emission above the CHT's self-sustained level led to a reduction of plume divergence, a suppression of low-frequency oscillations, and a higher ion energy (Granstedt et al. 2008; Raitses et al. 2009). Furthermore, a series of subjects were developed on the CHT structure, such as using a permanent magnet instead of an electromagnet coil and changing the length or width of the discharge channel. An unusual halo shape appears in the angular ion-current density distribution when a permanent magnet is used. The propellant utilization and ion energy distribution function have substantial connections with the channel length. Thrust and efficiency also increase with increasing channel length. For constant channel width, smaller thrusters have higher current and propellant utilization but lower anode efficiency (Raitses et al. 2010; Lee et al. 2011; Seo et al. 2013a).

The differences between CHTs and traditional Hall thrusters caused by the lack of an internal surface are mainly multiply charged ions, a rotating spoke, and variation in the interactions between the plasma and the surface caused by different magnetic fields near the anode. The uneven density of the azimuthal plasma, caused by rotating spokes, leads to varying interactions between the plasma and the surface, influencing the CHT's life. Compared to a traditional Hall thruster, the CHT has more multiply charged ions, which hit the surface and easily produce erosion. The difference in the magnetic field near the anode leads to a difference in the electron residence time and causes the ionization to vary. With the electromagnetic field action,

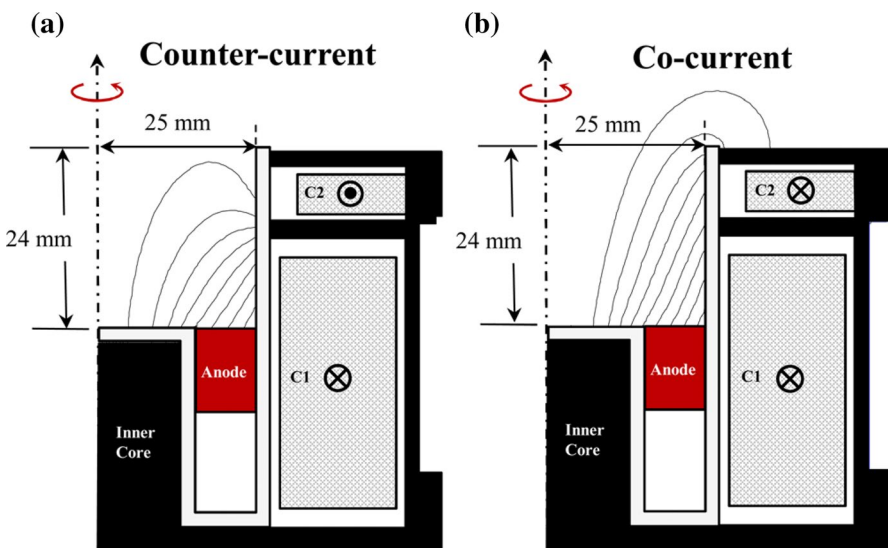


Fig. 39 Schematic of CHT with magnetic-field lines for **a** counter current and **b** co-current configurations (Kim et al. 2015)

the ions hit the surface and affect the CHT's lifetime. Thus, this review summarizes early work on rotating spokes, multiply charged ions, and magnetic fields near the anode to provide suggestions for the design of a CHT with long lifetime (Kim et al. 2015).

As CHT research has advanced, multiple-charged ions have become the focus of research. The differences in the fractions of ions are related to the magnetic-field configuration. Figure 39 shows the difference in the magnetic-field lines between the counter-current and co-current configurations. When the current in Coil 2 flows opposite to that in Coil 1, the CHT produces a counter-current configuration. However, when the coil currents flow in the same direction, the CHT produces co-current configurations (Kim et al. 2015). The magnetic field is shown in Fig. 40a and d, which is similar to that shown in Fig. 39. The contours of the magnetic flux density in the discharge channel are shown in Fig. 40b and e. It shows that the co-current configuration has an evidently higher magnetic flux density near the anode than the counter-current configuration. For the co-current configuration, the axial magnetic-field intensity B_z along the thrust axis is much higher, implying that the magnetic mirror ratios from the inner magnetic core to the outer channel wall are higher than the counter-current configuration. Thus, more electrons are confined inside the channel at a larger magnetic mirror ratio. However, the counter-current configuration has a higher maximum radial magnetic-field intensity B_r along the outer channel wall. The color map images depicted in Fig. 40c and f are based on the photograph of the plasma plume (Kim et al. 2017; Jiang et al. 2018).

As can be seen in Fig. 41, the peaks for the $E \times B$ probe voltage of both the counter-current and the co-current are similar. However, the ion-current fractions are evidently different. At an anode voltage of 300 V, it can be concluded that the

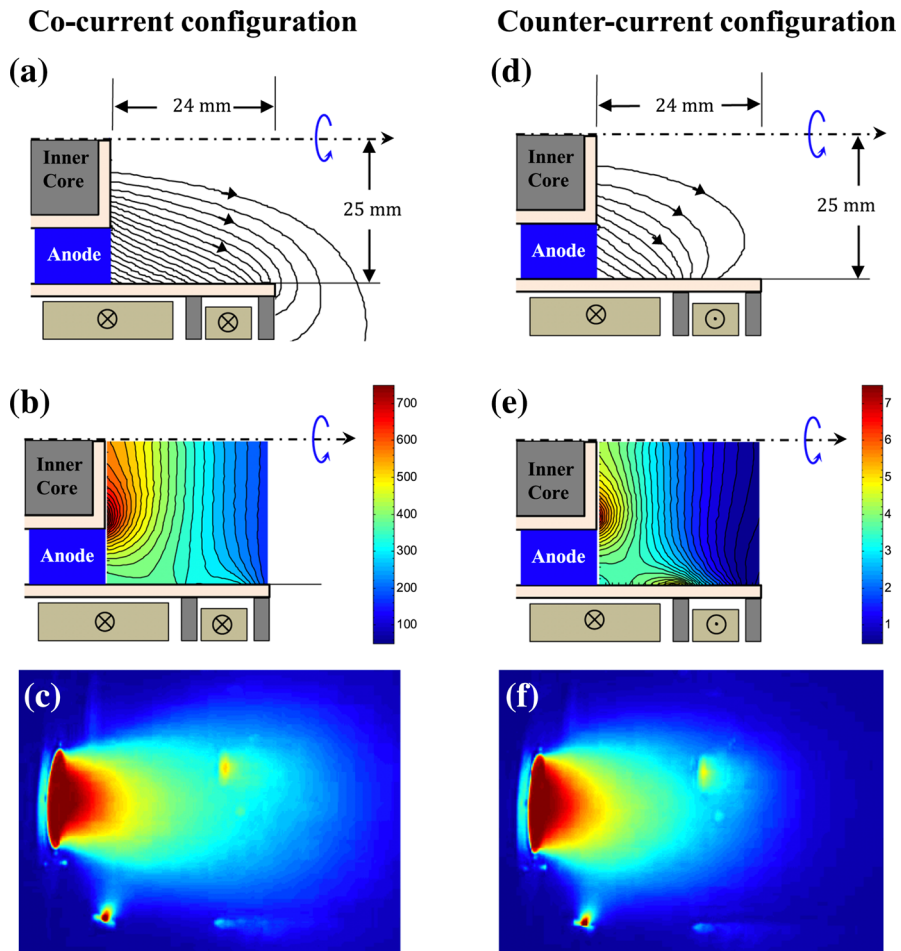


Fig. 40 **a** Magnetic-field lines, **b** magnetic flux density contours, and **c** color map image for the co-current field configuration. Those for the counter-current configuration are depicted in **d–f** (Kim et al. 2017)

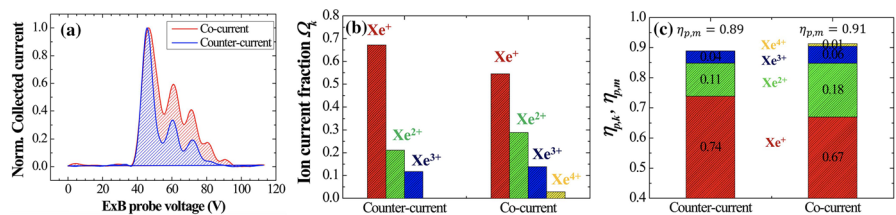


Fig. 41 **a** Normalized $E \times B$ spectra, **b** histogram of ion-current fractions, and **c** modified propellant efficiency of the counter-current and co-current configurations at an anode voltage of 300 V (Kim et al. 2015)

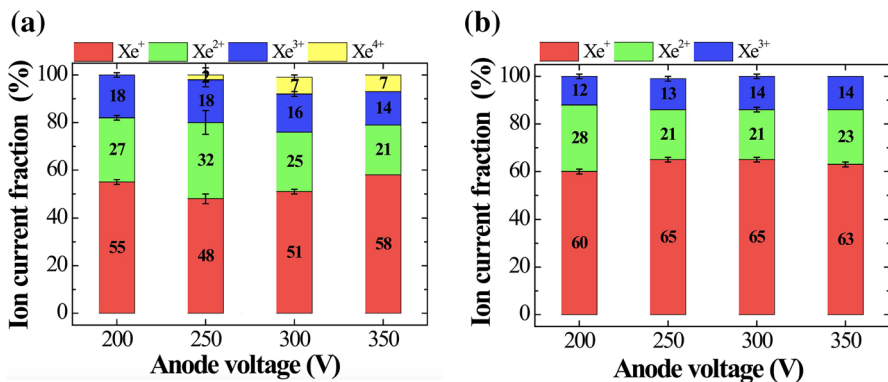


Fig. 42 Ion current fractions of **a** the co-current and **b** counter-current configurations (Kim et al. 2017)

population of Xe^{2+} and Xe^{3+} for a co-current configuration is higher than that for the counter-current configuration. Moreover, there exists additional Xe^{4+} in the co-current configuration. With the change in anode voltage, a dynamic change in the ion-current fractions is shown in Fig. 42. At anode voltages of 200–350 V, it can still be inferred that the sum of multiply charged ion fractions is higher in the co-current configuration. Furthermore, 7% of Xe^{4+} was observed at 300–350 V in the co-current configuration (Kim et al. 2015; 2017). For co-current configurations, the strong magnetic mirror effect retains electrons such that slow ions have a long residence time inside the discharge channel. The ion density becomes high in the channel because of the increased ionization rate. It could also extend residence time through an enhanced ambipolar potential. These effects lead to the generation of multiply charged ions (Kim et al. 2015).

The magnetic field near the anode plays a significant role in improving CHT performance. Thus, a series of techniques have been designed to control the magnetic field. For example, the MS rings can effectively control the magnetic field. As can be seen in Fig. 43, the intensive magnetic-field lines are distributed near the anode in case C1 without the magnetic shield ring. However, in cases C2 and C3, the magnetic-field intensities near the anode are weakened by the magnetic shield rings (Gao et al. 2016a). The decreasing magnetic field near the anode promotes the electron cross-field transport leading to the increase in ionization collision frequency and the ionization region's shift towards the anode. This work significantly enhances the performance of CHT, including thrust, specific impulse, and efficiency. In experiments, the emission intensity in the discharge channel is higher when the magnetic-field intensity near the anode decreases. In addition, changing the radial position of gas holes in the distributor's and anode's inner radii are effective methods of controlling the magnetic field to enhance CHT performance (Gao et al. 2016b, 2017).

The magnetic field near the anode can also be controlled via the depth of the annular region, L_a (Fig. 44). The thruster can vary the magnetic field near the anode at will, according to the change in L_a . With the increase in L_a , the magnetic field near the anode also becomes strong because of the principles of electron cross-field transport and magnetic mirror. The thrust and anode efficiency decrease, but

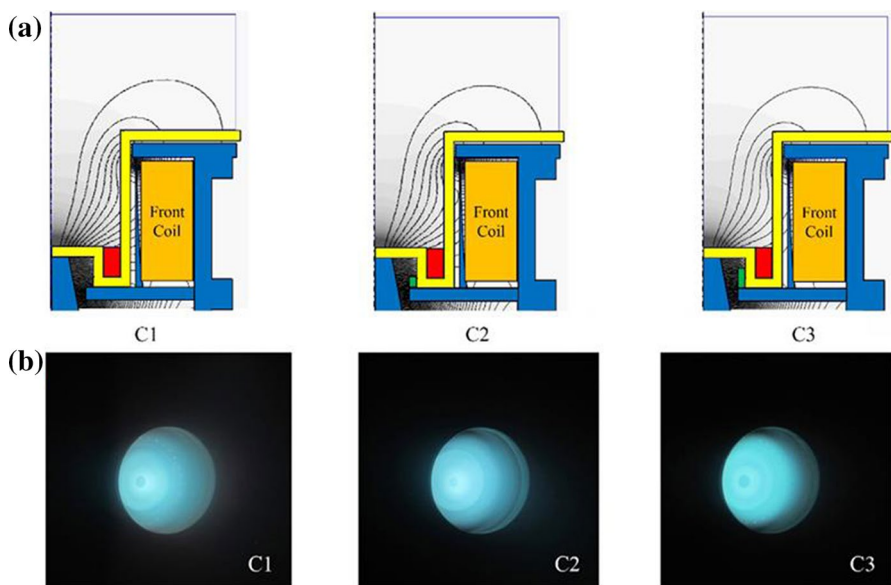


Fig. 43 **a** Simulated results of the thrusters with different MS rings and **b** photographs of plasma discharge in the channel for different configurations: C1, C2, and C3 (Gao et al. 2016a)

the plume angle does not change remarkably. Therefore, thruster performance will improve when L_a is shorter (Seo et al. 2013b).

Ding et al. (2017h, 2018c) studied the changes in magnetic field near the anode zone using a magnetically insulated anode, as shown in Fig. 45. Unlike the magnetic-field line generated by the non-magnetically insulated anode parallel to the anode surface, magnetically insulated anodes can guide the magnetic-field distribution in the channel to change the intersection position between the characteristic magnetic-field lines passing through the anode and the wall, as shown in Fig. 45b. Based on the structure of the magnetically insulated anode, the characteristic magnetic-field line stops being parallel to the anode surface and the intersection point between the characteristic magnetic-field lines passing through the anode and the wall moves to the outlet. Based on the thermalization potential theory (Mikellides and Ortega 2014), the magnetic-field line is isopotential. Thus, the characteristic magnetic line passing through the anode is isopotential with the anode. The intersection point between the characteristic magnetic-field line and the channel can move towards the channel outlet to guarantee that the wall near the anode is in its high-potential state. It can repel the ions and further decrease the length of the sputtering belt along the channel, thereby enhancing performance and improving lifetime (Ding et al. 2017h, 2018c). It is shown experimentally that when a magnetically insulated anode structure is adopted, the length of the sputtering belt decreases significantly. The magnetically insulated anode is conducive to decreasing the erosion and bombardment of ions into walls (Ding et al. 2017h). Furthermore, upon adoption of the magnetically insulated anode structure, the initial position of the sputtering belt is in front of the

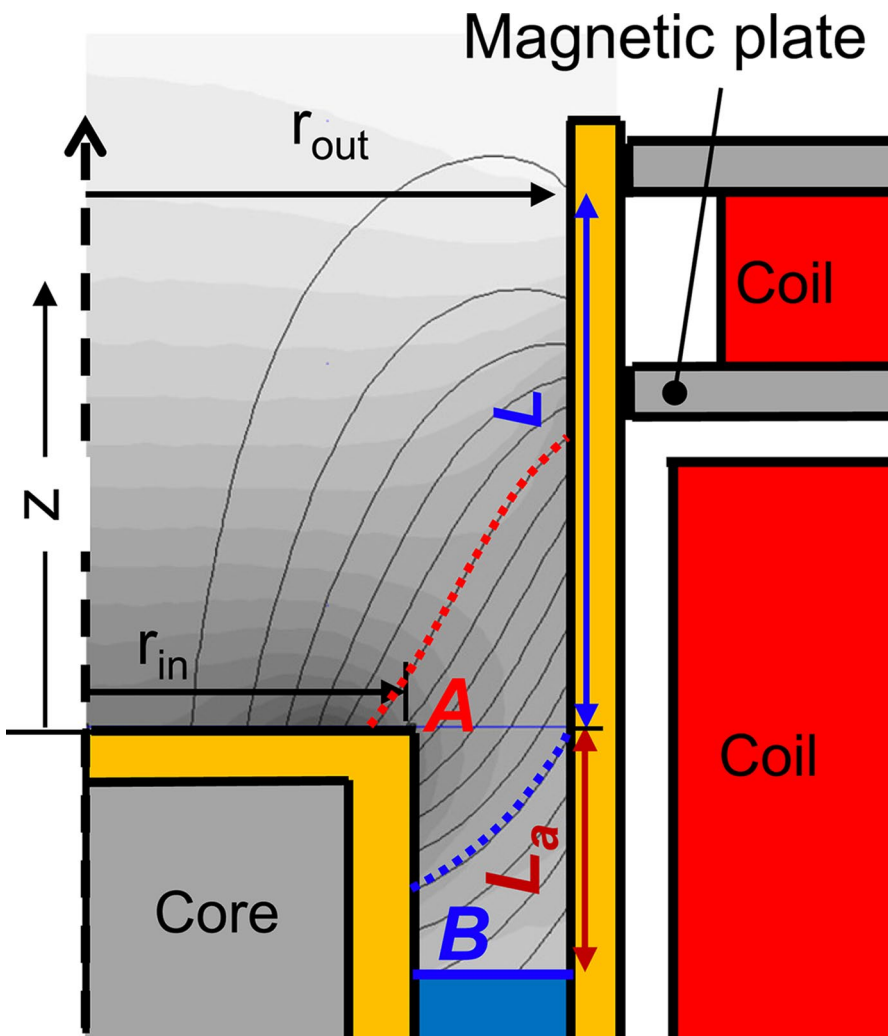


Fig. 44 Schematic of experimental CHT plotted with magnetic-field lines (Seo et al. 2013b)

magnetic pole, meaning that even if the channel wall is eroded and damaged, the magnetic pole will not be subject to ion sputtering. Therefore, even under long-term discharge, the magnetic field in the channel caused by magnetic pole erosion will not change as it does in the traditional Hall thruster. Therefore, the thruster lifetime is improved significantly (Ding et al. 2017h).

The magnetically insulated anode also forms a “zero magnetic field” zone, as shown in Fig. 45. The zone effectively increases the dwell time of electrons in the channel, improving the ionization. Through PIC simulation, it is found that after adopting the magnetically insulated anode, the potential near the wall increases (as shown in Fig. 46). The wall then repels more ions and the interaction between

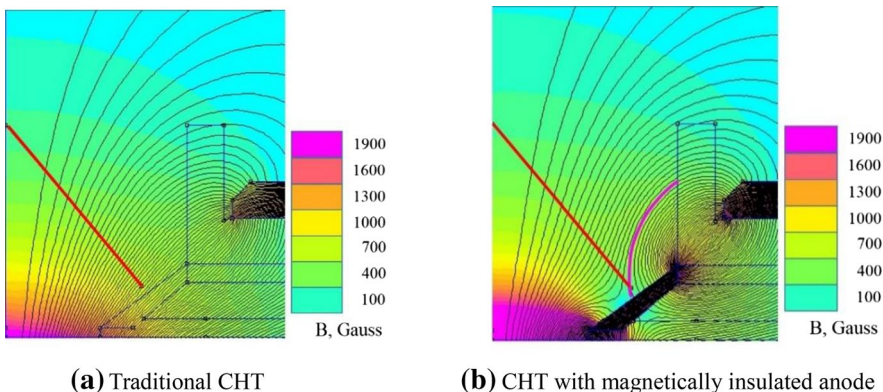


Fig. 45 Magnetic-field topology. Reprinted with permission from Ding et al. (2017b) Copyright 2017 IOP

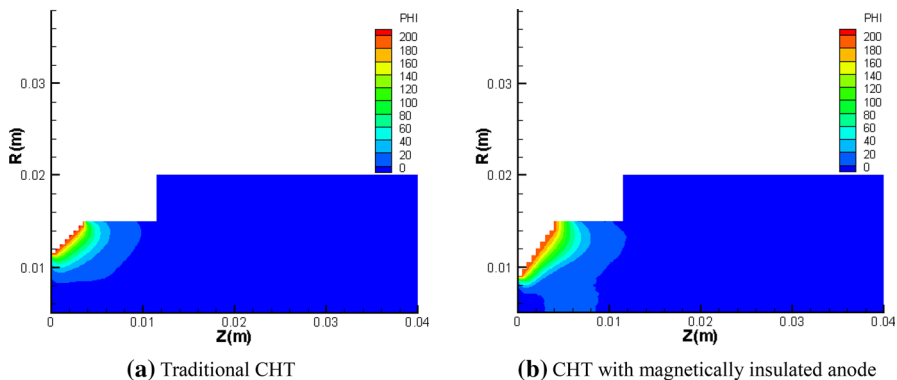


Fig. 46 Potential distribution. Reprinted with permission from Ding et al. (2018c) Copyright 2018 PST

the ions and the wall and the sputtering belt length decreases, which is conducive to improving the lifetime of the thruster (Ding et al. 2018c).

As research on the CHT has developed, a rotating spoke of increased plasma density and light emission has been discovered. Figure 47 shows the characteristic azimuthal rotation of the spoke of increased light emission in a 2.6-cm CHT. The spoke rotates in the $E \times B$ direction at 1.2–2.8 km/s. Hollow and filament cathodes are used in this research. The change in cathodes proves that the rotating spoke behavior is not related to the type of cathode. As can be seen in Fig. 46, for the hollow cathode, the spoke is visible at $I_k \leq 2.0$ A and invisible at $I_k = 2.5$ A. For the filament cathode, the spoke is visible at $I_f = 5.7$ A and invisible at $I_f \geq 6$ A. High-frequency oscillations of the order ~1 MHz are excited in the discharge current. The spoke is visible at $I_f = 7.5$ A and invisible at $I_f = 9.6$ A. To control this type of spoke, the boundary condition at the anode is adjusted. It has been proven experimentally that the properties of the azimuthal mode can be changed by varying the voltage and relative phases at

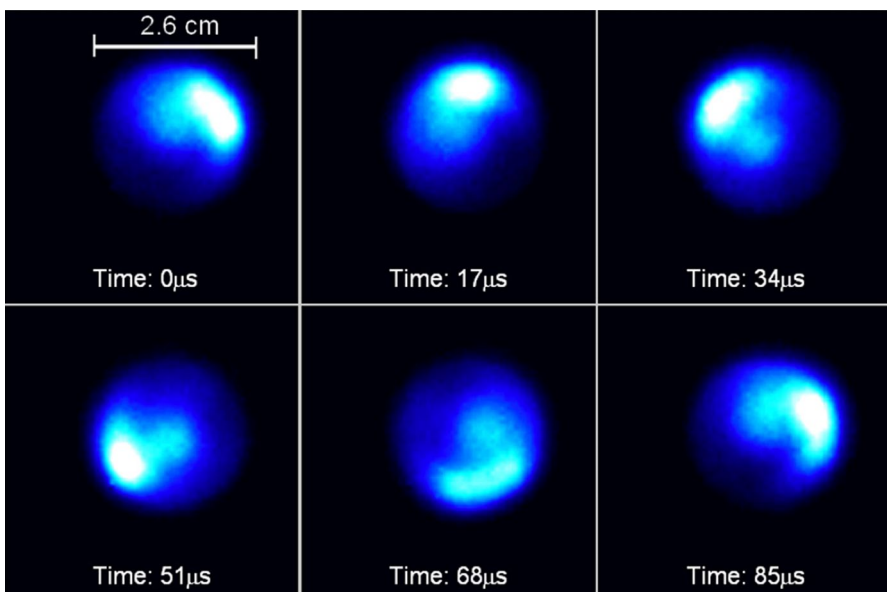


Fig. 47 Sequence of camera images showing a spoke of increased light emission propagating in $E \times B$ direction (Ellison et al. 2012)

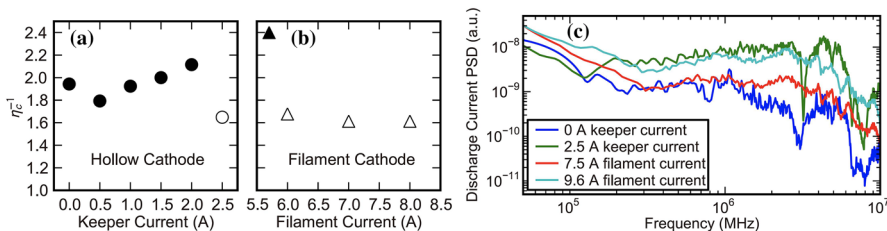


Fig. 48 **a** Keeper current of the hollow cathode, **b** filament current, and **c** power spectral density of the discharge current (Parker et al. 2010)

the anode. The rotating spoke produced this way is distinct from the natural spoke. The effect is strongest near the anode and gradually weakens in the plume (Parker et al. 2010; Ellison et al. 2012; Shi et al. 2018). To explore the mechanism of the rotating spoke, the 3D PIC code, STOIC, was applied to simulate this type of phenomenon in a 100-W CHT. Figure 47 shows the spoke and non-spoke regimes of the CHT. The spoke-like structure can be observed when the cathode current is 0.25 A, but it disappears when the cathode current increases from 0.25 to 0.5 A (Fig. 48).

The rotating spoke significantly impacts the performance of the thruster, including electron density (Fig. 49), ion flow and potential drop inside the thruster channel. The ion-flow velocity is presented in Fig. 50. The contours clearly show that the ion acceleration takes place mainly in the plume instead of in the discharge channel

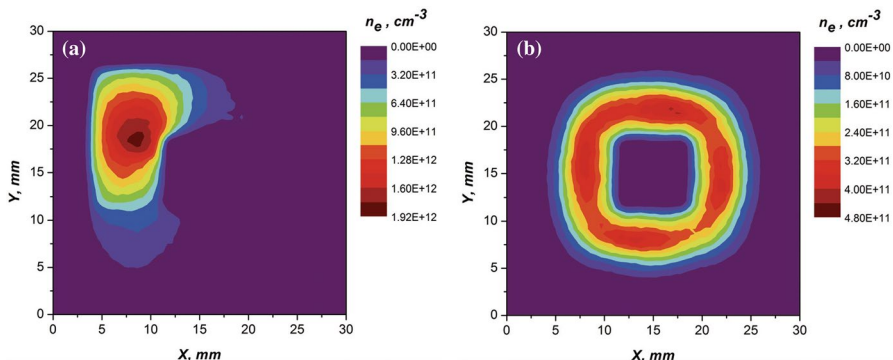


Fig. 49 Electron density in annular channel of CHT thruster: **a** spoke regime and **b** non-spoke regime (Matyash and Schneider 2013)

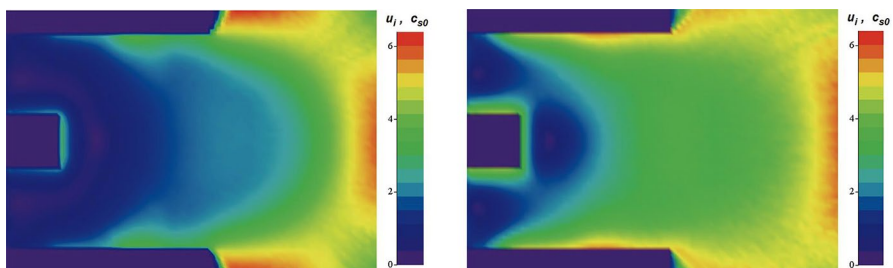


Fig. 50 Map of total ion velocity: spoke (left) and non-spoke regime (right) (Matyash and Schneider 2013)

of the spoke regime. By contrast, for the non-spoke regime, the ion acceleration takes place mainly inside the thruster channel. This type of phenomenon illustrates that the potential drop is larger inside the channel for the non-spoke regime. However, in the spoke regime, the potential drop at the same position is much smaller. The difference can be explained by the increased plasma conductivity caused by the rotating spoke. These simulation results prove that the rotating asymmetry in the ion flow is caused by the rotating spoke (Matyash and Schneider 2013).

As the rotating spoke has been identified, its precise mechanism has not been fully understood. It may relate to the process of ionization but there is no accurate conclusion thus far.

3.5 Adopting low sputtering yield materials

Material is one of the most essential factors for space equipment (Levchenko et al. 2017, 2018c, g). Consequently, for the Hall thruster, the wall material is a critical element that determines performance, especially for specific impulse and efficiency. Table 3 provides several most popular materials tested under thruster conditions.

Table 3 Currently used wall materials for thrusters

<i>a</i>	Boron nitride (BN)
<i>b</i>	Borosil (BN + SiO ₂ /Al ₂ O ₃ /ZrO ₂ /AlN/SiC)
<i>c</i>	Alumina (Al ₂ O ₃)
<i>d</i>	Silicon carbide (SiC)
<i>e</i>	Graphite
<i>f</i>	Titanium

The walls of the traditional Hall thrusters are mainly made of BN material (Boeuf 2017) owing to the following reasons (Barral et al. 2003; Gascon et al. 2003; Goebel et al. 2015):

1. insulating surfaces do not short out the electric field in the thruster acceleration region;
2. low secondary electron emission coefficient minimizes the electron power loss to the wall.

Via powder sintering, BN has poor anti-sputtering capability (Meng et al. 2014; Jiang et al. 2009), restricting the lifetime of the Hall thruster (Mikellides et al. 2011). To improve the anti-sputtering capability of BN, many scholars have tested BN composite materials (Eichler and Lesniak 2008; Zhang et al. 2002; Chen et al. 2004) by adding SiO₂, Al₂O₃, ZrO₂, AlN, SiC, or other materials to BN. Duan et al. (2014, 2016) and Li et al. (2018) have carried out research on the BN erosion mechanism and analyzed the damage situation when Xe ions impact perpendicular to and parallel to the direction of the *h*-BN layers, obtaining sputtering yields dependent on complex surface morphologies and relative density. B–N bond breaking and BN layer delamination are the main sputtering damage mechanisms of *h*-BN grains sputtered by Xe ions. Researchers have pointed out an increase in mullite as an additive, and that an increase in the sintering pressure can reduce the sputtering yield of *h*-BN (Duan et al. 2014). Figure 51 shows the damage model of *h*-BN crystal via Xe ion sputtering from different directions.

To further reduce the sputtering yield of BN, ZrO₂ (Duan et al. 2013a, b), Al₂O₃ (Duan et al. 2013b), and SiO₂ are considered as additives to improve BN density and reduce sputtering yield. Research shows that ZrO₂_{*p*}(3Y)/BN–SiO₂ composite ceramics can be obtained via hot-pressed sintering (Zhou et al. 2011). Zirconia particles with two types of phases (*t*-ZrO₂, *m*-ZrO₂) are embedded uniformly in the BN and SiO₂ matrix (see Fig. 52). The *h*-BN, SiO₂, *t*-ZrO₂, and *m*-ZrO₂ phases are present in the composites before and after plasma sputtering. The anti-sputtering capability acquired by the addition of ZrO₂ is significantly higher than that of BN. Moreover, when increasing the ZrO₂ content, the erosion rate of composite ceramics decreases significantly.

Research has shown that by adding Al₂O₃ into BN–SiO₂, the sputtering yield is mainly affected by atomic number density and crystal structure. With increase in the *h*-BN_{*p*} volume fraction, the hardness and density decrease when the *h*-BN_{*p*}

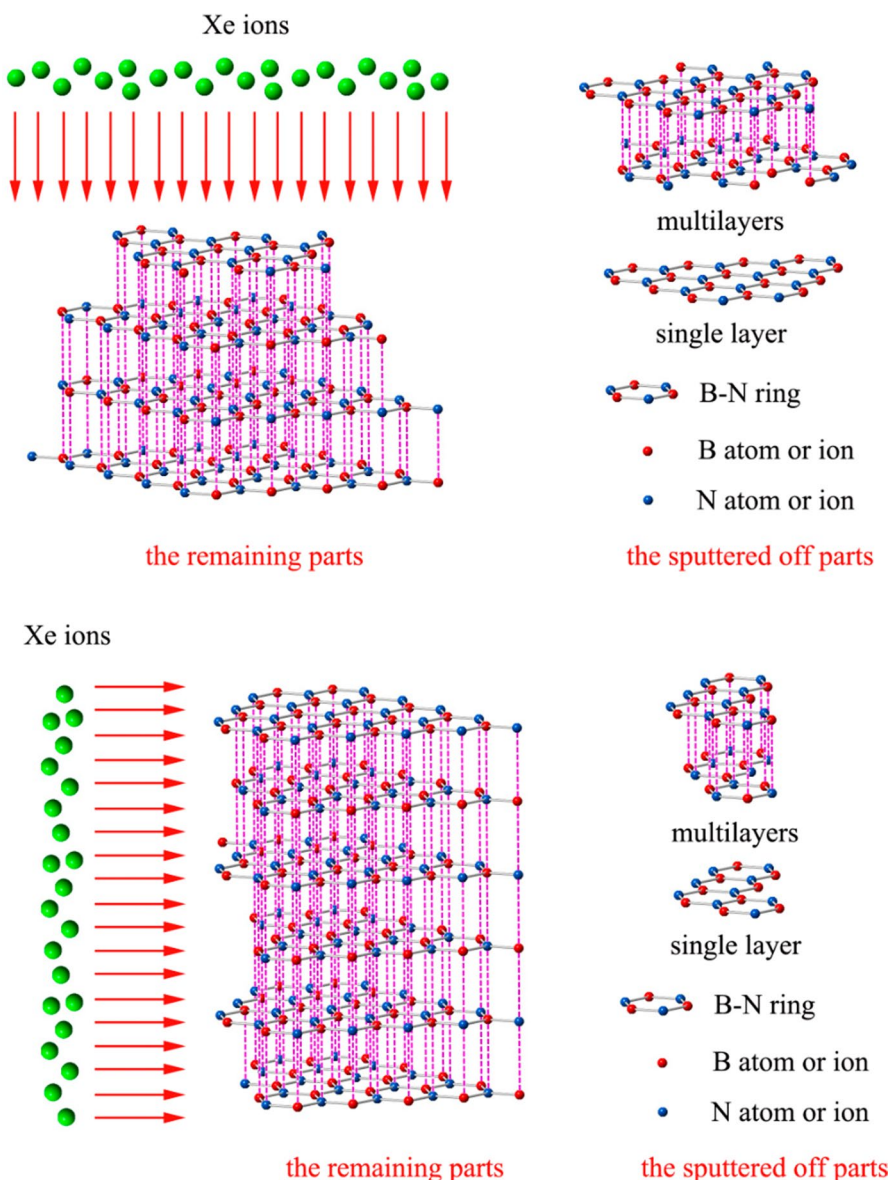
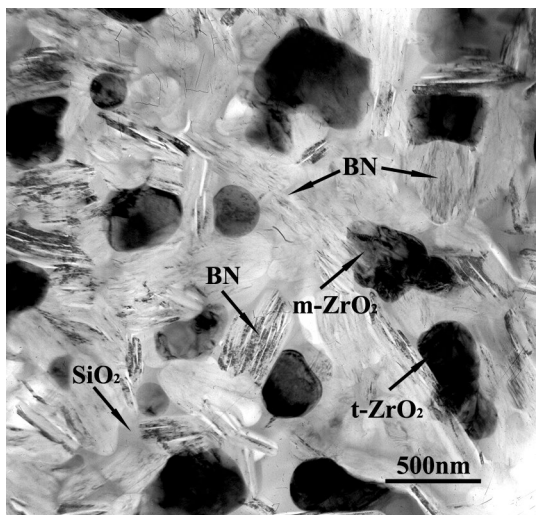


Fig. 51 Damage model of *h*-BN crystal by Xe ion sputtering: damage situation when Xe ions impact **a** perpendicular to and **b** parallel to the direction of *h*-BN layers (Duan et al. 2016)

volume fraction increases. The composite ceramics with 40% (volume fraction) BN_p show that the elastic modulus, fracture toughness, and flexural strength are 257 GPa, 3.99 MPa·m^{1/2}, and 284.3 MPa, respectively (Duan et al. 2013b). Figure 53 shows the SEM images of BN_p/Al₂O₃–SiO₂ ceramics with 10–60% *h*-BN_p volume fractions (Tian et al. 2016).

Fig. 52 XRD patterns of surface of $\text{ZrO}_{2p}(3\text{Y})/\text{BN}-\text{SiO}_2$ composite ceramics (Duan et al. 2013b)



Although the anti-sputtering performance of materials can be improved by adding different materials to BN, the impact of improvement is limited. Graphite and titanium provide less sputtering yield than BN (Eckstein 2007). Therefore, many researchers have performed discharge research with graphite and titanium as the wall material.

It is well known that changes in the discharge channel material lead not only to changes in the sputtering yield but also to changes in the secondary electron emission coefficient (Seiler 1983; Doerner et al. 2003; Chang et al. 2018). These changes also impact the discharge characteristics of Hall thrusters. Compared to BN, graphite has advantages such as strong anti-sputtering capability, high heat conductivity, radiation coefficients, and light weight. Further, graphite, which possesses a low secondary electron emission coefficient (Thomas et al. 2017), has a significant impact on thruster performance. The performance of the graphite channel in the Hall thruster with a traditional magnetic-field configuration is much lower than that of a BN ceramic channel. The main drawback of the traditional Hall thruster is that the wall material largely determines the discharge properties. Consequently, the performance level and operational lifetime (Vaudolon et al. 2015). Gascon et al. (2003) experimented with BN, graphite, Al_2O_3 , and SiC as discharge channels. The results show that the maximum difference in the efficiency was as high as 20% (absolute value) owing to the conductivity and low secondary electron emission coefficient provided by graphite compared with the BN wall, as shown in Fig. 54.

Thanks to the presentation and development of MS technology (Hofer et al. 2010) and aft-magnetic technology (Ding et al. 2016), many scholars have again begun to study graphite as a discharge channel (Goebel et al. 2015; Ding et al. 2018d; Grimaud et al. 2018) to improve the lifetime of the Hall thruster to meet the increasing demands of tens of thousands of hours of lifetime and total impulse, realize on-orbit mission diversity, and meet the orbital transfer and station-keeping demands.

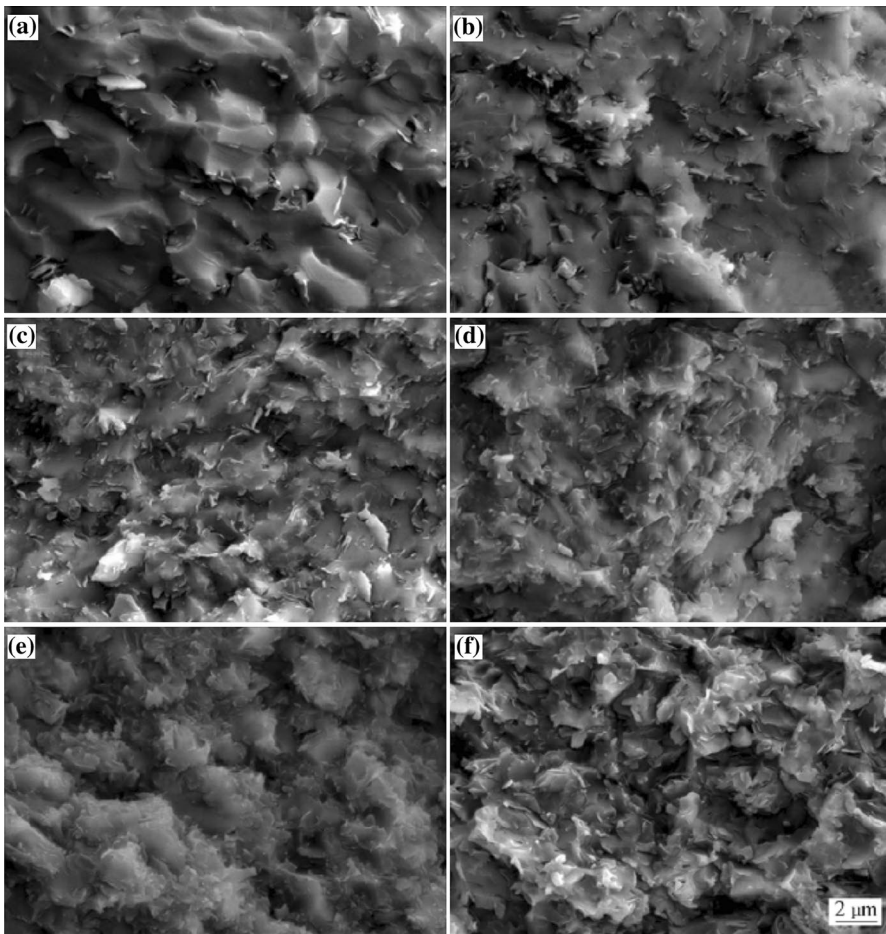


Fig. 53 Fracture surface SEM images of BNp/Al₂O₃–SiO₂ ceramics with different *h*-BNp volume fractions: **a** 10%, **b** 20%, **c** 30%, **d** 40%, **e** 50%, **f** 60% (Duan et al. 2013b)

The remarkable characteristic of MS technology and aft-magnetic technology is that the maximum electron temperature is located in the plume region, not in the channel. This is a significant difference from the traditional Hall thruster, as shown in Fig. 10. The electron temperature interacting with the channel wall is reduced from 20–30 eV to several eV (Mikellides and Ortega 2014). As decrease in the temperature at which the electrons bombard the wall implies that the difference in the secondary electron emission coefficient of the wall materials has no evident effect on the discharge (only when the electron energy exceeds a certain threshold, secondary electrons can be emitted). Therefore, many scholars have carried out research by adopting graphite as the discharge channel in MS and aft-magnetic Hall thrusters (Goebel et al. 2014, 2015).

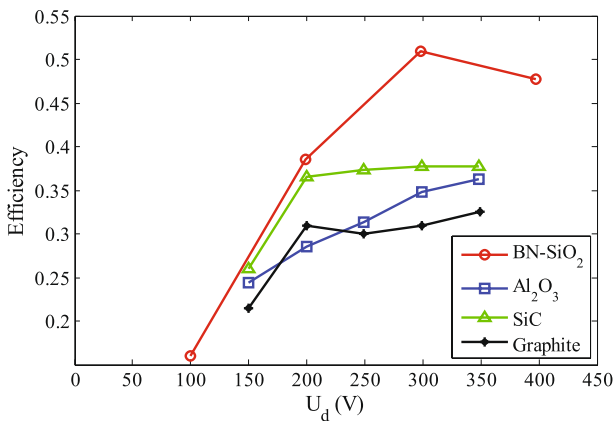


Fig. 54 Efficiency of SPT-100 thruster with different wall materials (Gascon et al. 2003)

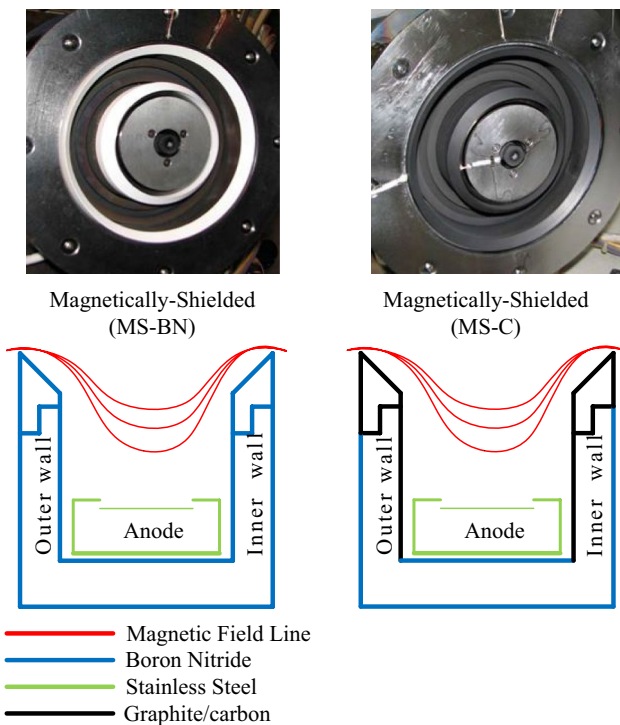


Fig. 55 MS BN channel (left) and graphite channel (right) (Goebel et al. 2015)

Goebel et al. (2015) have carried out relevant studies on the 5-kW MS H6 thruster with BN and graphite walls, as shown in Fig. 55. Because the magnetic-field line of the H6 MS Hall thruster is almost parallel to the channel, which significantly

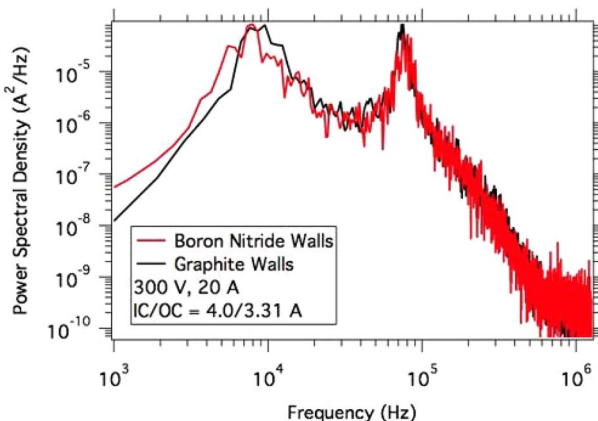


Fig. 56 Power spectral density in the MS H6 thruster with BN and graphite walls (Goebel et al. 2015)

reduces the interaction between the plasma and the wall, the impact of the difference in the secondary electron emission coefficient on the discharge characteristics of materials can be dramatically reduced. The difference in thrust and specific impulse between thrusters adopting the BN channel and graphite channel is less than 3% and the difference in efficiency is less than 2% (absolute value) (Goebel et al. 2015). Compared with the results obtained by Gascon et al. (2003) on SPT-100, the discharge efficiency of graphite is significantly reduced owing to low secondary electron emission coefficient and conductivity.

Goebel et al. (2015) have also identified in their research that under the same discharge voltage, the anode mass-flow rate, optimal magnetic field, and discharge current remain unchanged, and the oscillation is almost the same on graphite and BN walls. The discharge current oscillation power spectral density diagrams of the graphite and BN walls of the MS Hall thruster are very similar (Goebel et al. 2015) (Fig. 56).

Grimaud et al. (2017, 2018) and Ding et al. (2018d) carried out a study on the applications of graphite wall material in low-power (200 W) Hall thrusters. Grimaud and Mazouffre (2017) took up MS magnetic fields and traditional magnetic fields for comparing the discharge characteristics, respectively, with graphite and BN as the wall material. A contrast experiment can be performed by replacing the graphite with a BN ring.

Figures 57 and 58 depict, respectively, the differences observed in the discharge performances of BN and graphite channels adopted by Grimaud et al. (2018) for the US and MS Hall thruster. The discharge current, thrust, specific impulse, and efficiency of Hall thrusters with US magnetic-field configuration are quite different for different discharge channels. The maximum difference in the efficiency reaches more than 20% (absolute value), which is similar to the experiment results of Gascon et al. (2003) on the US magnetic thruster SPT-100. It can be seen from Fig. 56 that for the Hall thruster with MS magnetic-field configuration, the differences in the discharge currents and efficiencies are less when different discharge channels are

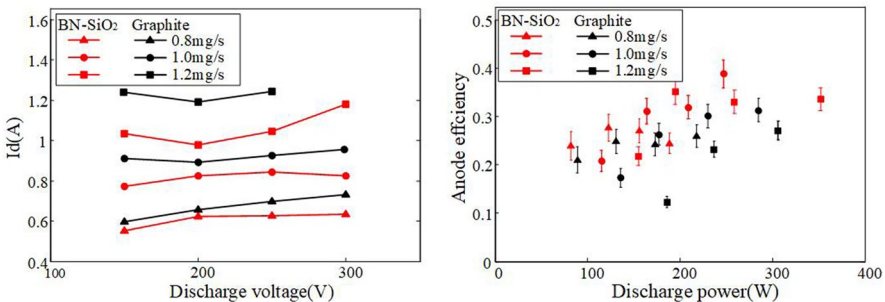


Fig. 57 Discharge current and anode efficiency of ISCT200-US (Grimaud et al. 2018)

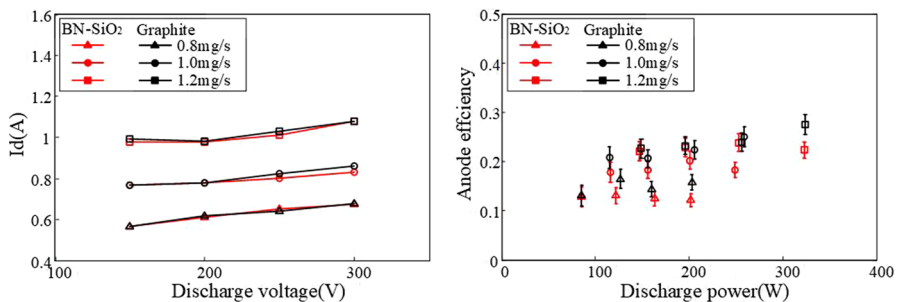


Fig. 58 Discharge current and anode efficiency of ISCT200-MS (Grimaud et al. 2018)

adopted. The maximal efficiency difference can be as much as 5% (absolute value), similar to the results of experiments performed by Goebel et al. (2015), and so on, on the MS thruster. Therefore, it is further demonstrated that the MS Hall thruster is insensitive to discharge materials. Graphite can be employed as the wall material to achieve long service life.

The 200-W permanent magnet Hall thruster NWLHT-200 W was designed by Ding et al. (2018b, c, d) based on aft-magnetic technology. Magnetic-field topology can effectively extrapolate the ionization and acceleration regions to the outlet of the discharge channel. There is little interaction between high-energy ions and the wall. The wall is bombarded only by low-energy ions and electrons. A contract experiment was performed on NWLHT-200 W with BN, graphite, and titanium as the wall materials (Ding et al. 2017i, 2018d).

Figure 59 shows the plume pictures under the same magnetic field and an anode mass-flow rate with BN, graphite, and titanium as the discharge walls. It can be seen from the plume pictures that there are no significant differences among the three wall materials. All the ionization regions (i.e., whitening and shining) are close to the channel outlet. It is further verified that the aft-magnetic field can effectively extrapolate the ionization region to the discharge channel outlet, or even to the plume region, which is conducive to long service life.

The experimental results show that the thrust, specific impulse, and efficiency are almost the same for the graphite and BN walls. However, the discharge oscillation



Fig. 59 Plume pictures with different wall materials. Reprinted with permission from Ding et al. (2017i, 2018d) Copyright 2017 IOP and 2018 ELSEVIER

is slightly different (Ding et al. 2018d). The discharge performance of titanium as a discharge channel is slightly lower than that of the BN channel. The efficiency thereof is lower by approximately 2–3% (Ding et al. 2017i). This may be related to the fact that graphite and BN belong to porous materials, whereas titanium is a dense metal.

Metal materials used for channel walls can be traced back to the 1960s. The assumption of TAL was proposed and verified by scientists from the former Soviet Union. The typical characteristics of TAL are its short discharge channel (Raitses et al. 2000; Fujita et al. 2014) and the channel wall made of metal (Choueiri 2001a; Boy 2000; Keidar et al. 2004), which can further improve the anti-sputtering capability of the wall and prolong the thruster lifetime.

In summary, to improve the anti-sputtering capability of wall materials, additives are used with BN to reduce the sputtering yield. Graphite, titanium, and other materials with low sputtering yields are used as wall materials. With the emergence of MS and aft-magnetic technology, further research is inclined towards using mainly graphite as the wall material.

4 Limitations of the long-life technologies

Whereas using wall materials with low sputtering yield can reduce the wall erosion rate and improve the lifetime of the Hall thruster, using MS technology, aft-magnetic technology, and wall-less technology can significantly reduce ion energy and flux bombardment on the discharge channel wall, improving the thruster lifetime. However, each technology has certain limitations.

The discharge performances of MS and aft-magnetic Hall thrusters are the same with BN and graphite channel walls (Goebel et al. 2015; Ding et al. 2018d; Grimaud et al. 2018). While the sputtering yield of graphite is relatively low, it also has characteristics such as low compactness and high porosity (Arbab et al. 2018).

Low compactness means that graphite will absorb more air than BN if exposed to the atmosphere for a long time. For the first ignition, owing to the heating effect of the plasma on the wall, more air will be released from the graphite wall. The released air will participate in ionization and the electrons generated will participate in ionization and conduction, thereby generating excessive discharge current (Hargus and Pote 2002) for a long duration, exceeding the normal power of the thruster. With a gradual release of air, the discharge current gradually decreases to

the normal level, as shown in Fig. 60. If the Hall thruster with a graphite wall realizes its first ignition in orbit, enough exhaust time shall be reserved for the graphite wall. Insufficient exhaust time will generate excessive ignition current for a long duration at the first instance. Thus, the power supply will be protected and ignition will not be completed.

Regarding MS technology, the magnetic-field line parallel to the wall can effectively reduce the ion erosion of the ceramic wall. Optimizing the magnetic-field lines and configurations can facilitate wall discharge without erosion (Hofer et al. 2014). In recent years, with the implementation of the lifetime test of the MS Hall thruster, new problems have been exposed. Whereas the magnetic pole end surfaces protected by ceramics have not eroded, those against the plume direction have eroded (Mikel-lides and Ortega 2014; Goebel et al. 2014; Polk et al. 2017). Figure 59 shows the inner magnetic pole of the HERMeS thruster after working for 1000 h (Frieman et al. 2018). It can be observed that erosion has occurred on the inner magnetic pole end surface (Fig. 61).

To further evaluate the erosion rate of the magnetic pole, Frieman et al. (2018) tested the erosion rate of the inner magnetic pole, as shown in Fig. 62. Its

Fig. 60 Change in discharge current after ignition (Hargus and Pote 2002)

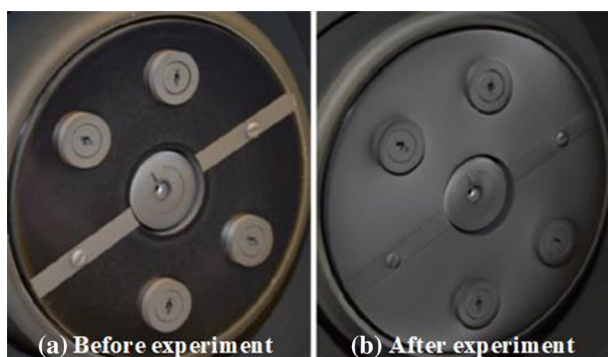
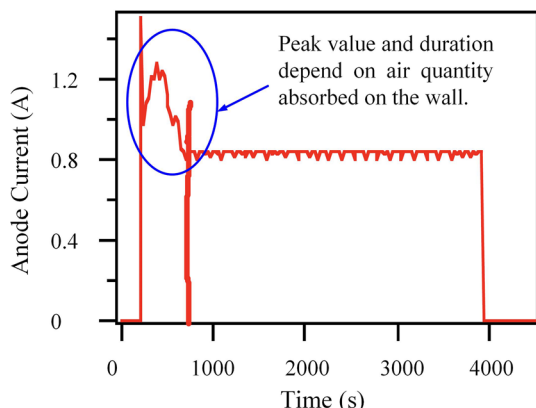


Fig. 61 Inner magnetic pole end surface of HERMeS thruster (Frieman et al. 2018)

erosion rate reached 20–100 $\mu\text{m/kh}$. Calculated based on the erosion rate, the erosion amount of the inner magnetic pole would reach 0.6–3 mm within 30,000 h. It is well known that the magnetic field in the channel completely depends on the magnetic circuit structure. 0.6–3-mm erosion will inevitably change the magnetic-field topology and intensity of the circuit, causing the magnetic-field intensity to vary from the design value. Thus, the discharge conditions should be deteriorated and the efficiency should be reduced. There are also uncertainties about the HERMeS completing a 50,000-h lifetime examination.

To further analyze the magnetic pole erosion mechanism, Jorns et al. (2016) and Ortega and Mikellides (2018) carried out numerical simulations. The results indicate that for MS Hall thrusters, the potential at the channel outlet is higher than that of the traditional Hall thruster, as shown in Fig. 63 (Ortega and Mikellides 2018). This means that the potential difference between the channel outlet and the pole surface is higher

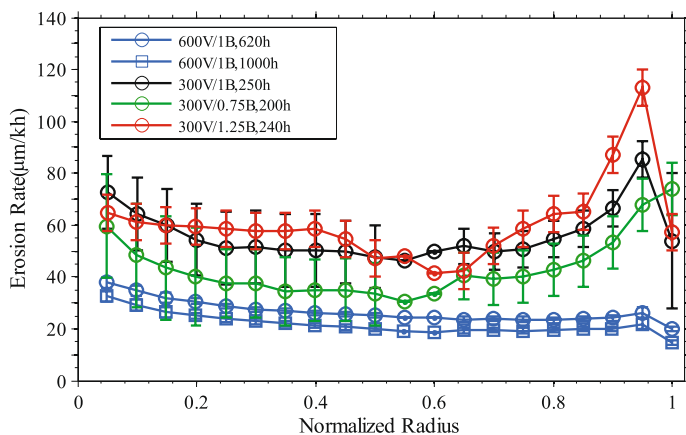


Fig. 62 Erosion rate of the inner magnetic pole (Frieman et al. 2018)

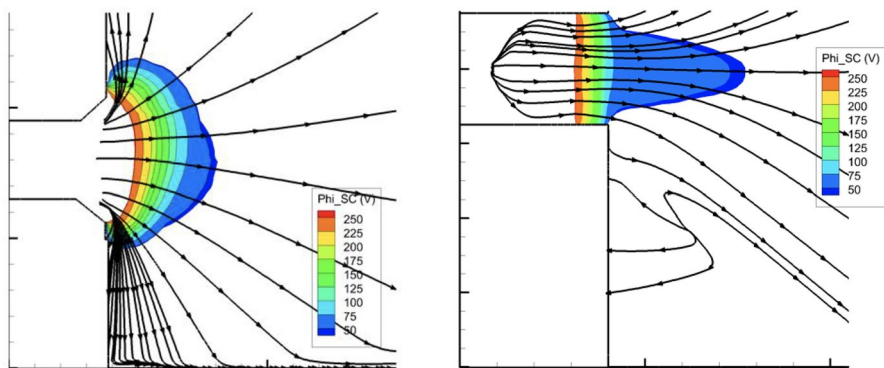


Fig. 63 Stream traces of 250-eV ions and plasma potential contours in the MS thruster (left) and US thruster (right) (Ortega and Mikellides 2018)

than that for the traditional Hall thruster. The ions ejected from the channel will bombard the magnetic pole surface via the potential difference between the magnetic pole and the channel outlet, further leading to magnetic-pole erosion. It can be observed from Fig. 64 that many ions bombard the end surface of the inner magnetic pole (Ortega and Mikellides 2018).

It can be seen from Fig. 62 that under the same magnetic-field conditions, the erosion rate is higher when the discharge voltage is low. Thus, the erosion rate is higher at 300 V than at 600 V. This is mainly because the mismatch between the magnetic field and the discharge voltage lead to an increasingly diverging plume under a discharge voltage of 300 V (Frieman et al. 2018). Erosion of the cathode also indirectly proves that plume divergence can aggravate the erosion of magnetic poles. Figure 65 shows the 3D micro-morphology of the cathode keeper at different times (after erosion).

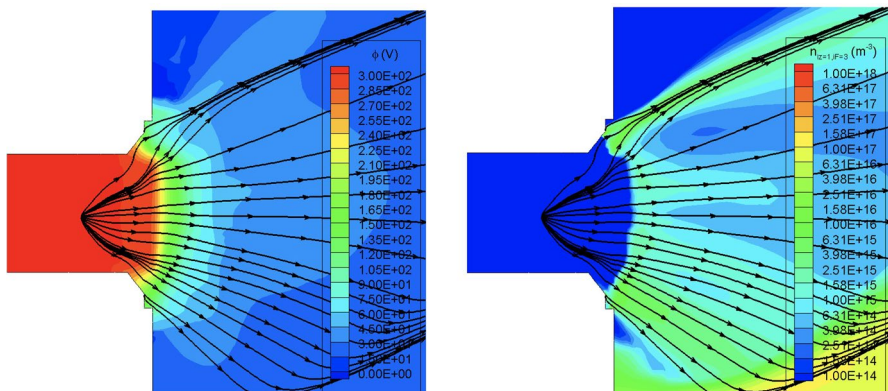


Fig. 64 Plasma potential contours, ion densities, and trajectories for ions with energy between 120 and 170 V for simulation with superimposed plasma potential with nearest extrapolation and free ion velocity in acceleration region (Ortega and Mikellides 2018)

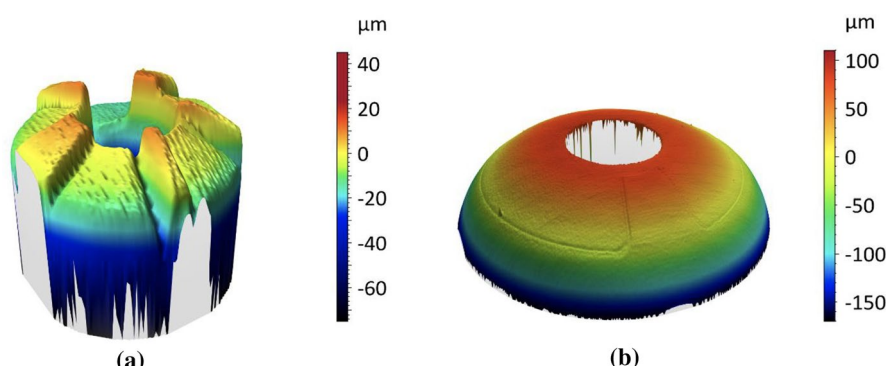


Fig. 65 3D view of the cathode keeper after **a** short duration and **b** long duration wear test (Frieman et al. 2018)

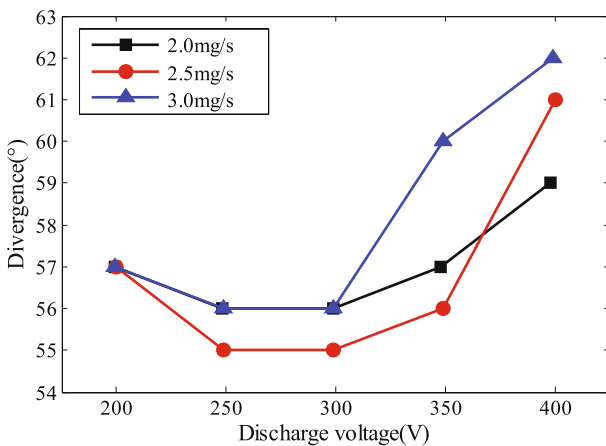


Fig. 66 Divergence of wall-less Hall thruster (Vaudolon et al. 2015)

For a Hall thruster adopting wall-less technology, because the anode is located at the channel outlet, all ionization occurs in the plume region. The density of the neutral gas is lower than that in the channel owing to the lack of channel restraint, leading to a more divergent ionization distribution in the plume region. The divergence of the ionization distribution leads to a higher plume divergence angle of thrust. The results from both Vaudolon et al. (2015) and Karadag et al.'s (2018b) experiments show that the plume divergence angle of the wall-less Hall thruster is greater than that of the traditional Hall thruster (45°). Figure 66 shows the plume divergence angle of the wall-less Hall thruster (Vaudolon et al. 2015).

Large plume divergence angles can reduce the efficiency of Hall thrusters (Hofer and Gallimore 2006; Linnell and Gallimore 2006). The efficiency η_v of Hall thrusters comprises the acceleration efficiency η_{acc} and plume divergence efficiency η_{div} (Linnell and Gallimore 2006), as shown in the following formula:

$$\eta_v = \eta_{acc} \eta_{div} = \frac{\dot{m}_i(\theta) V_z(\theta)}{\dot{m}_b V_D}, \quad (5)$$

$$\eta_{acc} = V_a / V_D, \quad (6)$$

$$\eta_{div} = \frac{\dot{m}_i(\theta) V_z(\theta)}{\dot{m}_b V_a}. \quad (7)$$

When the plume diverges, a decrease in η_{div} can reduce the thruster efficiency. Figure 67 shows the anode efficiency of the external discharge and wall-less Hall thrusters. It can be seen that the anode efficiency is lower than that of the traditional Hall thruster. The maximal anode efficiency of the external discharge plasma thruster is approximately 25% when the discharge power is 100–400 W. Compared with the anode efficiency of 30–45% of traditional Hall thrusters (Grimaud et al. 2018), that of wall-less Hall thrusters is reduced by approximately 5–15%. However,

when the discharge power is 1.5 kW, the anode efficiency of the wall-less Hall thruster is only 30%, which is reduced by 15–20% compared to the anode efficiency of 45–55% (Li et al. 2018) of the traditional Hall thruster. Therefore, with respect to the wall-less Hall thruster, it is still necessary to further restrict the ionization range and reduce the plume divergence angle to improve the anode efficiency.

The discharge characteristics of the aft-magnetic Hall thruster depend largely on the Brexit/Brmax ratio. Lower the ratio, higher is the aft-magnetic. When the Brexit/Brmax ratio is relatively low, discharge catastrophes may occur (Ding et al. 2017). Figures 68 and 69 are the contrast diagrams between the discharge plume and discharge current, respectively, before and after catastrophe. It can be seen from the figures that when the Brexit/Brmax ratio is low enough, the plume changes from a focusing mode to a divergent mode and the mean value and amplitude of the discharge current increases significantly.

Further measurements show that the thrust increases after the mode catastrophe. However, the increasing range is smaller than that of the discharge current, as shown in Fig. 70a. It can be seen from Fig. 70b that I_i/I_d decreases from 85 to 60%, indicating that after the mode catastrophe, the increase in the discharge

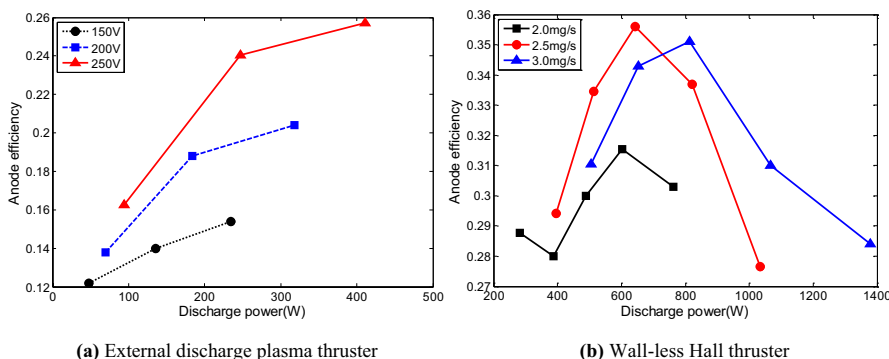


Fig. 67 Anode efficiency (Vaudolon et al. 2015; Karadag et al. 2018b)



Fig. 68 Plume pictures. Reprinted with permission from Ding et al. (2017j) Copyright 2017 ELSEVIER

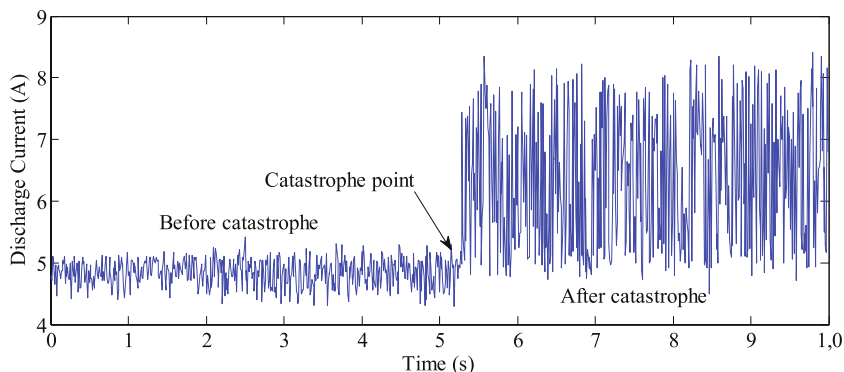


Fig. 69 Discharge current before and after catastrophe. Reprinted with permission from Ding et al. (2017j) Copyright 2017 ELSEVIER

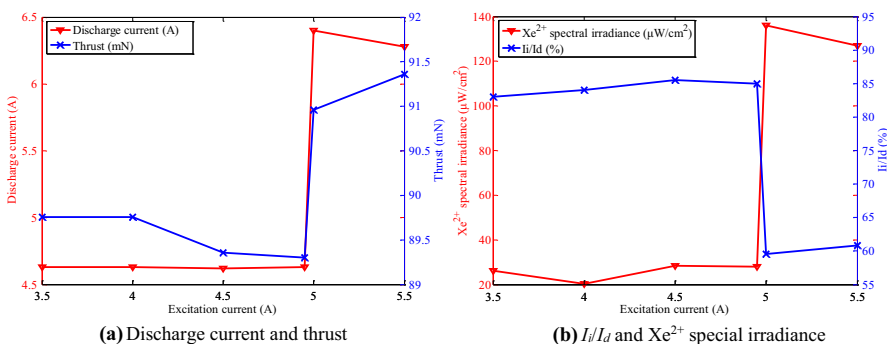
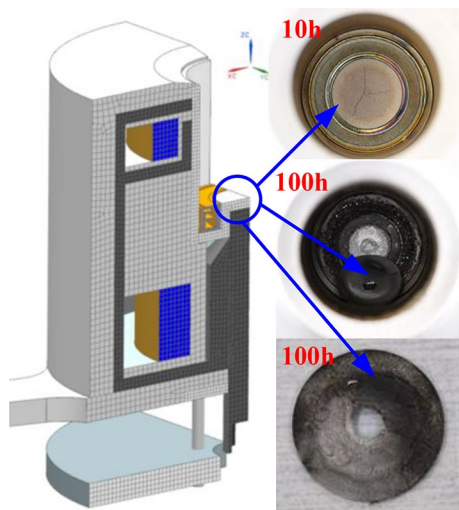


Fig. 70 Discharge parameters with excitation current (different values of Brexit/Brmax ratio). Reprinted with permission from Ding et al. (2017j) Copyright 2017 ELSEVIER

current is mainly caused by the electronic current. Therefore, the increasing range of the thrust is smaller than that of the discharge current. In addition, the ion energy increases after the mode catastrophe. Combined with the Xe^{2+} spectral irradiance enhancement, subject to spectral measurement and an increase in ion energy after the mode catastrophe, it can be concluded that, with a gradual decrease in the Brexit/Brmax ratio, the ionization position gradually moves to the plume region (Ding et al. 2017j). When the Brexit/Brmax ratio is less than the threshold value, ionization occurs in the plume region. Similar to wall-less thrusters, the divergence of neutral gas in the plume region leads to an increase in the plume divergence angle. In addition, because the maximum magnetic intensity is in the plume region, the electron temperature in the plume region is higher than that in the channel. When the electron energy is high enough to cause secondary ionization of neutral gas, the additional electrons generated participate in conductivity, leading to increased discharge current and decreased efficiency. Therefore, the Brexit/Brmax ratio must be selected properly to achieve a low discharge

Fig. 71 Erosion of permanent magnet ceramic cover plate (Pigeon 2017)



current and a high-performance discharge when adopting aft-magnetic technology (Ding et al. 2017j) (Fig. 71).

For CHT, whereas there is no inner wall surface, the erosion phenomenon also appears on the ceramic cover plate for protecting the permanent magnet. After performing a 100-h experiment for the 200-W CHT, Pigeon (2017) found there were crack and erosion phenomena on the permanent magnet ceramic cover plate and that the 2-mm thick ceramic cover plate was completely eroded by ion bombardment, as shown in Fig. 71. Currently, there is no literature on the erosion mechanism of a ceramic cover plate. To achieve a long service life for the CHT, the erosion of the ceramic cover plate must be paid attention to and solved.

5 Conclusions and outlook

Aimed at future deep space explorations such as Moon, Mars, and planetoid explorations, Hall thrusters, as the main thrust power platform, must have higher total and specific impulse. Therefore, they are subject to increasing demands of long service life. Plasma bombardment on the ceramic wall is the main factor restricting the lifetime of Hall thrusters. Improving the anti-sputtering ability of the wall and significantly reducing its ion energy and flux bombarding are the main measures adopted for improving the lifetime of a Hall thruster. MS technology, wall-less technology, and aft-magnetic technology can significantly reduce the ion energy and flux bombarding the wall. These are now mainstream technologies that help achieve long service life. At present, the main technical characteristic is that the maximum magnetic field is located in the plume region. With respect to the magnetic-field distribution, while discharge can be achieved at the wall without erosion, the plume-oriented magnetic poles are eroded by ion bombardment, which is not conducive to achieving long service life. When the magnetic pole of a Hall thruster is eroded to a certain

extent, the magnetic-field intensity and distribution in the channel drastically deviate from their design values, and such deviations worsen the discharge conditions and make the Hall thruster unusable. Therefore, it is still necessary to find a way to further resolve the problem of erosion of the magnetic pole end surface and to ultimately achieve the erosion-free long life of the discharge wall and magnetic poles. In further research, the service life of Hall thrusters should be prolonged mainly by efforts in the following respects:

1. Magnetic-field design technology will still be crucial for prolonging the service life of Hall thrusters. The emphasis of future studies will be to further integrate the magnetic shielding (MS), magnetic focusing, and aft-magnetic-field technology; weaken the interaction between the plasma and discharge channel; and sharply decrease the ion energy and flux bombarding the walls. However, the integration of the abovementioned multiple magnetic-field design technologies should not impair the performance of Hall thrusters.
2. To improve the lifetime of the Hall thruster, the sputtering resistance of the wall material of the discharge channel will be another area for research focus. Further increase in the sputtering threshold of the discharge channel material and decrease in the erosion rate, while considering the secondary electron emission characteristic of the material, will be required. The magnetic pole can be protected by employing anti-sputtering material against the bombarding of high-energy ions, which will be effective for prolonging the service life of Hall thrusters.
3. The Hall thrusters accelerated life assessment research method is another key technology to reduce the life test cost and promote the development of design technology that facilitates long service life. The key point is verifying the design method through short-time tests and simulation. A lot of work is required to improve the material properties modeling, parallel calculation method, and erosion model of the thruster.
4. The effect of cathode life on Hall thrusters' service lives is not discussed in this paper. However, the shape and intensity of the magnetic field around the cathode in the plume region and the local ion beam characteristic of the cathode on cathode erosion is also a main influencing factor on thruster lifetime. Therefore, the magnetic field in the plume region during magnetic-field design, and particularly the magnetic field around the cathode, requires attention.
5. Considering the large number of applications of Hall thrusters in space explorations in the future, studies on the lifetime of Hall thruster have been transformed from being based on a single machine to being based on mass production. Therefore, research on the screening of components and independent testing technology are also noteworthy issues in the further development of the applications.
6. Plasma oscillation has a significant impact on thruster discharge characteristics, and there are various forms of oscillations. At present, there has been little research on the impact of plasma oscillation on thruster life; related research results have not been reported in the literature. Thus, this will also be one of the focus areas of further studies on the service lives of thrusters.

Acknowledgements The authors wish to acknowledge financial support from the National Natural Science Foundation of China (Grant Nos. 51777045 and 51736003).

References

- A. Semenkin, External anode layer thruster parameters at a high specific impulse regimes. IEPC 1997-055 (1997)
- Agrawal R, Nieto A, Chen H, Mora M, Agarwal A (2013) Nanoscale damping characteristics of boron nitride nanotubes and carbon nanotubes reinforced polymer composites. *ACS Appl. Mater. Interfaces.* 5(22):12052–12057. <https://doi.org/10.1021/am4038678>
- Ahedo E, Pablo VD (2007) Combined effects of electron partial thermalization and secondary emission in Hall thruster discharges. *Phys. Plasma* 14:083501. <https://doi.org/10.1063/1.2749237>
- Ahedo E, Gallardo JM, Martinez-Sanchez M (2003) Effects of the radial plasma-wall interaction on the Hall thruster discharge. *Phys. Plasma* 10(8):3397–3409. <https://doi.org/10.1063/1.1584432>
- A.L. Ortega, I.G. Mikellides, Investigations of pole erosion mechanisms in the 12.5 kW HERMeS Hall thruster using numerical simulations and ion velocity measurements. AIAA 2018-4647 (2018). <https://doi.org/10.2514/6.2018-4647>
- A.M. Kapulkin, A.D. Grishkevich, V.F. Prisnyakov, Outside electric field thruster. In: Proceedings 45th IAF Congress; Space Technol. (Pergamon, UK), 15, 391–394 (1995)
- Arbab AA, Mengal N, Sahito IA, Memon AA, Jeong SH (2018) An organic route for the synthesis of cationic porous graphite nanomaterial used as photocatalyst and electrocatalyst for dye-sensitized solar cell. *Electrochim. Acta* 266:43–53. <https://doi.org/10.1016/j.electacta.2018.02.012>
- B. Welander, C. Carpenter, K. Grys, Life and operating range extension of the BPT-4000 qualification model Hall Thruster. AIAA 2006-5263 (2006). <https://doi.org/10.2514/6.2006-5263>
- B.A. Jorns, C. Dodson, J. Anderson, D.M. Goebel, R.R. Hofer, M. Sekerak, A.L. Ortega, I. Mikellides. Mechanisms for pole piece erosion in a 6-kW magnetically-shielded Hall thruster. AIAA 2016-4839 (2016). <https://doi.org/10.2514/6.2016-4839>
- Baranov O, Bazaka K, Kersten H, Keidar M, Cvelbar U, Xu S, Levchenko I (2017) Plasma under control: advanced solutions and perspectives for plasma flux management in material treatment and nano-synthesis. *Appl. Phys. Rev.* 4(4):041302. <https://doi.org/10.1063/1.5007869>
- Becatti G, Goebel DM, Polk JE, Guerrero P (2018) Life evaluation of a lanthanum hexaboride hollow cathode for high-power Hall thruster. *J. Propul. Power* 34(4):893–900. <https://doi.org/10.2514/1.B36659>
- Behroozfar A, Daryadel S, Morsali SR, Moreno S, Baniasadi M, Bernal RA, Minary-Joland M (2017) Microscale 3D printing of nanotwinned copper. *Adv. Mater.* 30(4):1705107. <https://doi.org/10.1002/adma.201705107>
- Boeuf JP (2017) Tutorial: physics and modeling of Hall thrusters. *J. Appl. Phys.* 121(1):011101. <https://doi.org/10.1063/1.4972269>
- Boy ID (2000) Computation of the plume of an anode-layer Hall thruster. *J. Propul. Power* 16(5):902–909. <https://doi.org/10.2514/2.5658>
- R.R. Hofer, I.G. Mikellides, I. Katz, D.M. Goebel, BPT-4000 Hall Thruster discharge chamber erosion model comparison with qualification life test data. IEPC 2007-267 (2007)
- Brandhorst HW, Neill MJ, Jones PA, Cassady RJ (2002) POWOW-An alternative power source for Mars exploration. *Acta Astron.* 51(1):57–62. [https://doi.org/10.1016/S0094-5765\(02\)00073-5](https://doi.org/10.1016/S0094-5765(02)00073-5)
- C. Claus, M. Day, V. Kim, Y. Kondakov, T. Randolph, Preliminary study of possibility to ensure large enough lifetime of SPT operating under increased powers. AIAA 97-2789 (1997). <https://doi.org/10.2514/6.1997-2789>
- C. Pigeon, Development of a miniature low power cylindrical Hall thruster for microsatellites. Master Thesis. University of Toronto, pp. 60–61 (2017)
- Chang HY, Alvarado A, Marian J (2018) Calculation of secondary electron emission yields from low-energy electron deposition in tungsten surfaces. *Appl. Surf. Sci.* 450(30):190–199. <https://doi.org/10.1016/j.apsusc.2018.04.155>
- Chen L, Wang YJ, Shen HF, Rao JC, Zhou Y (2004) Effect of SiC content on mechanical properties and thermal shock resistance of BN-ZrO₂-SiC composites. *Mater. Sci. Eng. A-Struct. Mater. Prop. Microstruct. Process.* 590:346–351. <https://doi.org/10.1016/j.msea.2013.10.054>

- Chiu YH, Austin BL, Williams K, Dressler RA, Karabadzhak GF (2006) Passive optical diagnostic of Xe-propelled Hall thrusters. I. Emission cross sections. *J. Appl. Phys.* 99:1–10. <https://doi.org/10.1063/1.2195018>
- Cho S, Komurasaki K, Arakawa Y (2013) Kinetic particle simulation of discharge and wall erosion of a Hall thruster. *Phys. Plasma* 20:063501. <https://doi.org/10.1063/1.4810798>
- Choueiri EY (2001a) Fundamental difference between the two Hall thruster variants. *Phys. Plasma* 8:5025. <https://doi.org/10.1063/1.1409344>
- Choueiri EY (2001b) Plasma oscillations in Hall thrusters. *Phys. Plasma* 8:1411. <https://doi.org/10.1063/1.1354644>
- Choueiri EY (2004) A critical history of electric propulsion: the first fifty years (1906–1956). *J. Propul. Power* 20(2):193–203. <https://doi.org/10.2514/1.9245>
- R.W. Conversano, D.M. Goebel, I.G. Mikellides, R.R. Hofer, T.S. Matlock, R.E. Wirz, Magnetically shielded miniature Hall thruster: performance assessment and status update. AIAA2014-3896 (2014). <https://doi.org/10.2514/6.2014-3896>
- Conversano RW, Goebel DM, Hofer RR, Matlock TS, Wirz RE (2015) Development and initial testing of a magnetically shielded miniature Hall thruster. *IEEE Trans. Plasma Sci.* 43(1):103–117. <https://doi.org/10.1109/TPS.2014.2321107>
- Conversano RW, Goebel DM, Mikellides IG, Hofer RR, Wirz RE (2017a) Performance analysis of a low-power magnetically shielded Hall thruster: computational modeling. *J. Propul. Power* 34(4):992–1001. <https://doi.org/10.2514/1.B36231>
- Conversano RW, Goebel DM, Hofer RR, Mikellides IG, Wirz RE (2017b) Performance analysis of a low-power magnetically shielded Hall thruster: experiments. *J. Propul. Power* 34(4):975–983. <https://doi.org/10.2514/1.B36230>
- D. King, D. Tilley, R. Aadland, K. Nottingham, R. Smith, C. Roberts, Development of the BPT family of U.S.-designed hall current thrusters for commercial LEO and GEO applications. AIAA 1998-3338 (1998). <https://doi.org/10.2514/6.1998-3338>
- Ding YJ, Peng WJ, Wei LQ, Sun GS, Li H, Yu DR (2016) Computer simulations of Hall thrusters without wall losses designed using two permanent magnetic rings. *J. Phys. D Appl. Phys.* 49(46):465001. <https://doi.org/10.1088/0022-3727/49/46/465001>
- Ding YJ, Li P, Zhang X, Wei LQ, Sun HZ, Peng WJ, Yu DR (2017a) Effects of the magnetic field gradient on the wall power deposition of Hall thrusters. *J. Plasma Phys.* 83(2):905830205. <https://doi.org/10.1017/S0022377817000241>
- Ding YJ, Xu Y, Peng WJ, Wei LQ, Su HB, Sun HZ, Li P, Li H, Yu DR (2017b) A type of cylindrical Hall thruster with a magnetically insulated anode. *J. Phys. D Appl. Phys.* 50:145203. <https://doi.org/10.1088/1361-6463/aa6019>
- Ding YJ, Peng WJ, Sun HZ, Wei LQ, Zeng M, Wang FF, Yu DR (2017c) Visual evidence of suppressing the ion and electron energy loss on the wall in Hall thrusters. *Jpn. J. Appl. Phys.* 56(3):038001. <https://doi.org/10.7567/JJAP.56.038001>
- Ding YJ, Peng WJ, Sun HZ, Xu Y, Wei LQ, Li H, Zeng M, Wang FF, Yu DR (2017d) Effect of oblique channel on discharge characteristics of 200-W Hall thruster. *Phys. Plasma* 24(2):023507. <https://doi.org/10.1063/1.4976104>
- Ding YJ, Sun HZ, Wei LQ, Li P, Su HB, Peng WJ, Yu DR (2017e) A 200 W Hall thruster with hollow indented anode. *Acta Astron.* 139:521–527. <https://doi.org/10.1016/j.actaastro.2017.08.001>
- Ding YJ, Sun HZ, Li P, Wei LQ, Su HB, Peng WJ, Li H, Yu DR (2017f) Application of hollow anode in Hall thruster with double-peak magnetic fields. *J. Phys. D Appl. Phys.* 50(33):335201. <https://doi.org/10.1088/1361-6463/aa7bbf>
- Ding YJ, Li P, Sun HZ, Wei LQ, Xu Y, Peng WJ, Su HB, Li H, Yu DR (2017g) Simulation of double stage Hall thruster with double-peaked magnetic field. *Eur. Phys. J. D* 71:192. <https://doi.org/10.1140/epjd/e2017-80124-8>
- Ding YJ, Sun HZ, Li P, Wei LQ, Xu Y, Peng WJ, Su HB, Yu DR (2017h) Influence of hollow anode position on the performance of a Hall-effect thruster with double-peak magnetic field. *Vacuum* 143:251–261. <https://doi.org/10.1016/j.vacuum.2017.06.030>
- Ding YJ, Sun HJ, Peng WJ, Xu Y, Wei LQ, Li H, Li P, Su HB, Yu DR (2017i) Experimental test of 200 W Hall thruster with titanium wall. *Jpn. J. Appl. Phys.* 56(5):050312. <https://doi.org/10.7567/JJAP.56.050312>
- Ding YJ, Su HB, Li P, Wei LQ, Li H, Peng WJ, Xu Y, Sun HZ, Yu DR (2017j) Study of the catastrophic discharge phenomenon in a Hall thruster. *Phys. Lett. A* 381:3482–3486. <https://doi.org/10.1016/j.physleta.2017.09.002>

- Ding YJ, Peng WJ, Sun HZ, Wei LQ, Zeng M, Wang FF, Yu DR (2017k) Performance characteristics of No-Wall-Losses Hall thruster. *Eur. Phys. J. Spec. Top.* 226:2945–2953. <https://doi.org/10.1140/epjst/e2016-60247-y>
- Ding YJ, Li H, Wei LQ, Hu YL, Shen Y, Liu H, Ning ZX, Mao W, Yu DR (2018a) Overview of Hall electric propulsion in China. *IEEE Trans. Plasma Sci.* 46(2):2263–2282. <https://doi.org/10.1109/TPS.2017.2776257>
- Ding YJ, Li H, Li P, Jia BY, Wei LQ, Su HB, Sun HZ, Wang L, Yu DR (2018b) Effect of relative position between cathode and magnetic separatrix on the discharge characteristic of Hall thrusters. *Vacuum* 154:167–173. <https://doi.org/10.1016/j.vacuum.2018.05.005>
- Ding YJ, Li H, Jia BY, Li P, Wei LQ, Xu Y, Peng WJ, Sun HZ, Cao Y, Yu DR (2018c) Simulation of the effect of a magnetically insulated anode on a low power cylindrical Hall thruster. *Plasma Sci. Technol.* 20:035509. <https://doi.org/10.1088/2058-6272/aa9fe7>
- Ding YJ, Li H, Sun HZ, Wei LQ, Jia BY, Su HB, Peng WJ, Li P, Yu DR (2018d) A 200-W permanent magnet Hall thruster discharge with graphite channel wall. *Phys. Lett. A* 382:3079–3082. <https://doi.org/10.1016/j.physleta.2018.08.017>
- D.M. Goebel, B.A. Jorns, R.R. Hofer, I.G. Mikellides, I. Katz. Pole-piece interactions with the plasma in a magnetically shielded Hall thruster. *AIAA 2014-3899* (2014). <https://doi.org/10.2514/6.2014-3899>
- Doerner RP, Whyte DG, Goebel DM (2003) Sputtering yield measurements during low energy xenon plasma bombardment. *J. Appl. Phys.* 93(9):5816–5823. <https://doi.org/10.1063/1.1566474>
- Duan XM, Jia DC, Zhou Y, Yang ZH, Wang YJ, Ren FQ, Yu DR, Ding YJ (2013a) Mechanical properties and plasma erosion resistance of BN_p/Al₂O₃-SiO₂ composite ceramics. *J. Cent. South Univ.* 20:1462–1468. <https://doi.org/10.1007/s11771-013-1635-3>
- Duan XM, Jia DC, Meng QC, Yang ZH, Yu Y, Zhou Y, Yu DR, Ding YJ (2013b) Study on the plasma erosion resistance of ZrO₂(3Y)/BN-SiO₂ composite ceramics. *Compos. B Eng.* 46:130–134. <https://doi.org/10.1016/j.compositesb.2012.10.027>
- Duan XM, Ding YJ, Jia DC, Jing N, Yang ZH, He PG, Tian Z, Wang SJ, Wang YJ, Zhou Y, Yu DR (2014) Ion sputtering erosion mechanisms of h-BN composite ceramics with textured microstructures. *J. Alloy. Compd.* 613:1–7. <https://doi.org/10.1016/j.jallcom.2014.05.221>
- Duan XM, Yang ZH, Chen L, Tian Z, Cai DL, Wang YJ, Jia DC, Zhou Y (2016) Review on the properties of hexagonal boron nitride matrix composite ceramics. *J. Eur. Ceram. Soc.* 36:3725–3737. <https://doi.org/10.1016/j.jeurceramsoc.2016.05.007>
- Dudeck M, Doveil F, Arcis N, Zurbach S (2012) Plasma propulsion for geostationary satellites for telecommunication and interplanetary missions. *IOP Conf. Ser. Mater. Sci. Eng.* 29:012010. <https://doi.org/10.1088/1757-899x/29/1/012010>
- Eckstein W (2007) Sputtering yields. *Sputtering by particle Bombardment*. Springer, Berlin, pp 33–187
- Eichler J, Lesniak C (2008) Boron nitride (BN) and BN composites for high-temperature applications. *J. Eur. Ceram. Soc.* 28:1105–1109. <https://doi.org/10.1016/j.jeurceramsoc.2007.09.005>
- Ellison CL, Raitses Y, Fisch NJ (2012) Cross-field electron transport induced by a rotating spoke in a cylindrical Hall thruster. *Phys. Plasma* 19:013503. <https://doi.org/10.1063/1.3671920>
- E.M. Bringa, Ion tracks insolids: sputtering and surface modification. Ph.D. thesis, University of Virginia, pp. 82–83 (2000)
- Frieman JD, Kamhawi H, Williams G, Herman D, Peterson PY, Gilland J, Hofer R (2018) Long duration wear test of the NASA HERMeS Hall thruster. *AIAA*. <https://doi.org/10.2514/6.2018-4645>
- Fujita D, Kawashima R, Ito Y, Akagi S, Suzuki J, Schonherr T, Koizumi H, Komurasaki K (2014) Operating parameters and oscillation characteristics of an anode-layer Hall thruster with argon propellant. *Vacuum* 110:159–164. <https://doi.org/10.1016/j.vacuum.2014.07.022>
- Gao YY, Liu H, Hu P, Huang HY, Yu DR (2016a) The effect of magnetic field near the anode on CHT. *Plasma Sources Sci. Technol.* 25:035011. <https://doi.org/10.1088/0963-0252/25/3/035011>
- Gao YY, Liu H, Hu P, Huang HY, Yu DR (2016b) Performance characteristics according to the radial position of gas distributor holes in a low power cylindrical Hall thruster. *Phys. Plasma* 23:083514. <https://doi.org/10.1063/1.4960663>
- Gao YY, Liu H, Hu P, Huang HY, Yu DR (2017) Effect of anode position on the performance characteristics of a low-power cylindrical Hall thruster. *Phys. Plasma* 24:063518. <https://doi.org/10.1063/1.4986091>
- Garnier Y, Viel V, Roussel J-F, Bernard J (1999) Low-energy xenon ion sputtering of ceramics investigated for stationary plasma thrusters. *J. Vac. Sci. Technol., A* 17:3246–3254. <https://doi.org/10.1116/1.582050>

- Garrigues L, Hagelaar JM, Boeuf JP, Raitses Y, Smirnov A, Fisch NJ (2008) Simulations of a miniaturized cylindrical Hall thruster. *IEEE Trans. Plasma Sci.* 36(5):2034–2042. <https://doi.org/10.1109/TPS.2008.2003976>
- Gascon N, Dukeck M, Barral S (2003) Wall material effects in stationary plasma thrusters. I. Parametric studies of an SPT-100. *Phys. Plasma* 10(10):4123–4136. <https://doi.org/10.1063/1.1611880>
- Goebel DM, Hofer RR, Mikellides IG, Katz I, Polk JE, Dotson BN (2015) Conducting wall Hall thrusters. *IEEE Trans. Plasma Sci.* 43(1):118–126. <https://doi.org/10.1109/TPS.2014.2321110>
- Granstedt EM, Raitses Y, Fisch NJ (2008) Cathode effects in CHTs. *J. Appl. Phys.* 104:103302. <https://doi.org/10.1063/1.2999343>
- Grimaud L, Mazouffre S (2017) Conducting wall Hall thrusters in magnetically shielded and standard configurations. *J. Appl. Phys.* 122(3):011101–011122. <https://doi.org/10.1063/1.4995285>
- Grimaud L, Mazouffre S, Boniface C (2018) Performance comparison between standard and magnetically shielded 200 W Hall thrusters with BN-SiO₂ and graphite channel walls. *Vacuum* 155:514–523
- Hargus WA Jr, Cappelli MA (2002) Interior and exterior laser-induced fluorescence and plasma measurements within a Hall thruster. *J. Propul. Power* 18:160–168. <https://doi.org/10.2514/2.5912>
- Hargus WA, Pote B (2002) Examination of a Hall thruster start transient. AIAA. <https://doi.org/10.2514/6.2002-3956>
- Hobbs GD, Wesson JA (1967) Heat flow through a langmuir sheath in the presence of electron emission. *Plasma Phys.* 9(1):85–87. <https://doi.org/10.1088/0032-1028/9/1/410>
- Hofer RR, Gallimore AD (2006) High-specific impulse Hall thrusters, part 2: efficiency analysis. *J. Propul. Power* 22(6):732–740. <https://doi.org/10.2514/1.15954>
- Hofer RR, Goebel DM, Mikellides IG, Katz I (2014) Magnetically shielded of a laboratory Hall thruster. II. Experiments. *J. Appl. Phys.* 115(4):043304. <https://doi.org/10.1063/1.4862314>
- I. Katz, I.G. Mikellides, R.R. Hofer, Channel wall plasma thermal loads in Hall thrusters with magnetically shielded. AIAA 2011-6082 (2011). <https://doi.org/10.2514/6.2011-6082>
- I.G. Mikellides, A.L. Ortega, Assessment of pole erosion in a magnetically shielded Hall thruster. AIAA 2014-3897 (2014) <https://doi.org/10.2514/6.2014-3897>
- I.G. Mikellides, I. Katz, R.R. Hofer, Design of a laboratory Hall thruster with magnetically shielded channel walls, phase I: numerical simulations. AIAA 2011-5809 (2011). <https://doi.org/10.2514/6.2011-5809>
- I.G. Mikellides, R.R. Hofer, I. Katz, D.M. Goebel (2013b) The effectiveness of magnetically shielded in high-Isp Hall thrusters. AIAA 2013-3885 (2013). <https://doi.org/10.2514/6.2013-3885>
- Jacobson D, Manzella D (2003) 50 kW Class Krypton hall thruster performance. AIAA. <https://doi.org/10.2514/6.2003-4550>
- J.E. Polk, R. Lobbia, A. Barriault, P. Guerrero, I. Mikellides, A. L. Ortega, Inner front pole cover erosion in the 12.5 kW HERMeS Hall thruster over a range of operating conditions. IEPC-2017-409 (2017)
- Jiang T, Jin Z, Yang J, Qiao G (2009) Investigation on the preparation and machinability of the B₄C/BN nanocomposites by hot-pressing process. *J. Mater. Process. Technol.* 209(1):561–571. <https://doi.org/10.1016/j.jmatprotec>
- Jiang YW, Tang HB, Ren JX, Li M, Cao JB (2018) Magnetic mirror effect in a cylindrical Hall thruster. *J. Phys. D Appl. Phys.* 51:035201. <https://doi.org/10.1088/1361-6463>
- J.M. Haas, R.R. Hofer, D.L. Brown, B.M. Reid, A.D. Gallimore, Design of a 6-kW Hall thruster for high thrust/power investigation. In: 54th JANNAF Propulsion Meeting, pp. 14–17 (2007)
- J.T. Yim, M. Keidar, I.D. Boyd, An investigation of factors involved in Hall thruster wall erosion modeling. AIAA 2006-4657 (2006). <https://doi.org/10.2514/6.2006-4657>
- K. Grysz, A. Mathers, B. Welander, V. Khayms, Demonstration of 10,400 hours of operation on 4.5 kW qualification model Hall thruster. AIAA 2010-6698 (2010). <https://doi.org/10.2514/6.2010-6698>
- K. Matyash, R. Schneider, 3D simulation of the rotating spoke in a Hall thruster. IEPC 2013-307 (2013)
- Kaganovich ID, Raitses Y, Sydorenko D, Smolyakov A (2007) Kinetic effects in a Hall thruster discharge. *Phys. Plasma* 14(5):057104. <https://doi.org/10.1063/1.2709865>
- Karadag B, Cho S, Funaki I (2018a) Thrust performance, propellant ionization, and thruster erosion of an external discharge plasma thruster. *J. Appl. Phys.* 123(15):153302. <https://doi.org/10.1063/1.5023829>
- Karadag B, Cho S, Funaki I, Hamada Y, Komurasaki K (2018b) External discharge plasma thruster. *J. Propul. Power* 34(4):1093–1096. <https://doi.org/10.2514/1.B36900>
- Katz I, Mikellides IG (2011) Neutral gas free molecular flow algorithm including ionization and walls for use in plasma simulations. *J. Comput. Phys.* 230(4):1454–1464. <https://doi.org/10.1016/j.jcp.2010.11.013>

- Keidar M, Boyd ID (2001) Plasma flow and plasma–wall transition in Hall thruster channel. *Phys. Plasma* 8:5315–5322. <https://doi.org/10.1063/1.1421370>
- Keidar M, Boyd ID, Beilis II (2004) Modeling of a high-power thruster with anode layer. *Phys. Plasma* 11:1715. <https://doi.org/10.1063/1.1668642>
- Kim V (1998) Main physical features and processes determining the performance of stationary plasma thrusters. *J. Propul. Power* 14(5):736–743. <https://doi.org/10.2514/2.5335>
- Kim H, Lim Y, Choe W, Park S, Seon J (2015) Effect of magnetic field configuration on the multiply charged ion and plume characteristics in Hall thruster plasmas. *Appl. Phys. Lett.* 106:154103. <https://doi.org/10.1063/1.4918654>
- Kim H, Choe W, Lim Y, Lee S, Park S (2017) Magnetic field configurations on thruster performance in accordance with ion beam characteristics in cylindrical Hall thruster plasmas. *Appl. Phys. Lett.* 110:114101. <https://doi.org/10.1063/1.4978532>
- Kishi N (2017) Management analysis for the space industry. *Space Policy* 39–40:1–6. <https://doi.org/10.1016/j.spacepol.2017.03.006>
- Koizumi H, Komurasaki K, Arakawa Y (2008) Numerical prediction of wall erosion on a Hall thruster. *Vacuum* 83:67–71. <https://doi.org/10.1016/j.vacuum.2008.03.096>
- L. Grimaud, J. Vaudolon, S. Mazouffre, Design and characterization of a 200 W Hall thruster in magnetically shielded configuration. AIAA 2016-4832 (2016). <https://doi.org/10.2514/6.2016-4832>
- Lee J, Seo M, Seon J, Lee HJ, Choe W (2011) Performance characteristics according to the channel length and magnetic fields of cylindrical Hall thrusters. *Appl. Phys. Lett.* 99:131505. <https://doi.org/10.1063/1.3643435>
- Levchenko I, Beilis II, Keidar M (2016) Nanoscaled metamaterial as an advanced heat pump and cooling media. *Adv. Mater. Technol.* <https://doi.org/10.1002/admt.201600008>
- Levchenko I, Bazaka K, Keidar M, Xu S, Fang J (2017) Hierarchical multicomponent inorganic metamaterials: intrinsically driven self-assembly at the nanoscale. *Adv. Mater.* <https://doi.org/10.1002/adma.201702226>
- Levchenko I, Bazaka K, Baranov O, Mohan Sankaran R, Nomine A, Belmonte T, Xu S (2018a) Lighting under water: diverse reactive environments and evidence of synergistic effects for material treatment and activation. *Appl. Phys. Rev.* 5(2):021103. <https://doi.org/10.1063/1.5024865>
- Levchenko I, Bazaka K, Mazouffre S, Xu SY (2018b) Prospects and physical mechanisms for photonic space propulsion. *Nat. Photon.* 2:649. <https://doi.org/10.1038/s41566-018-0280-7>
- Levchenko I, Bazaka K, Belmonte T, Keidar M, Xu SY (2018c) Advanced materials for next-generation spacecraft. *Adv. Mater.* 30:1802201. <https://doi.org/10.1002/adma.201802201>
- Levchenko I, Bazaka K, Ding YJ, Raitses Y, Mazouffre S, Henning T, Klar PJ, Shinohara S, Schein J, Garrigues L, Kim M, Lev D, Taccogna F, Boswell RW, Charles C, Koizumi H, Shen Y, Scharlemann C, Keidar M, Xu SY (2018d) Space micropropulsion systems for Cubesats and small satellites: From proximate targets to furthermost frontiers. *Appl. Phys. Rev.* 5:011104. <https://doi.org/10.1063/1.5007734>
- Levchenko I, Keidar M, Cantrell J, Wu Y, Kuninaka H, Bazaka K, Xu S (2018e) Explore space using swarms of tiny satellites. *Nature* 562:185–187. <https://doi.org/10.1038/d41586-018-06957-2>
- Levchenko I, Xu S, Teel G, Mariotti D, Walker M, Keidar M et al (2018f) Recent progress and perspectives of space electric propulsion systems based on smart nanomaterials. *Nat. Commun.* 9(1):879. <https://doi.org/10.1038/s41467-017-02269-7>
- Levchenko I, Xu S, Mazouffre S, Keidar M, Bazaka K (2018g) Mars colonization: beyond getting there. *Glob. Challeng.* 2:1800062. <https://doi.org/10.1002/gch2.201800062>
- Li H, Xia GJ, Mao W, Liu JW, Ding YJ, Yu DR, Wang XG (2018) Experimental and numerical investigation of a Hall thruster with a chamfered channel wall. *Chin. Phys. B* 27(10):105209. <https://doi.org/10.1088/1674-1056/27/10/105209>
- Li WB, Li H, Ding YJ, Wei LQ, Gao Q, Yan SL, Meng TH, Zhu ZM (2019) Study on electrons conduction paths in Hall thruster ignition processes with the cathode located inside and outside the magnetic separatrix. *Acta Astron.* 155:153–159. <https://doi.org/10.1016/j.actaastro.2018.11.027>
- Linnell JA, Gallimore AD (2006) Efficiency analysis of a Hall thruster operating with Krypton and Xenon. *J. Propul. Power* 22(6):1402–1412. <https://doi.org/10.2514/1.19613>
- M. Nakles, W. Hargas, J. Delgado, R. Corey, A performance and plume comparison of Xenon and Krypton propellant on the SPT-100. AIAA 2012-4116 (2012). <https://doi.org/10.2514/6.2012-4116>
- Martinez-Sanchez M, Pollard JE (1998) Spacecraft electric propulsion—an overview. *J. Propul. Power* 4:688–699. <https://doi.org/10.2514/2.5331>

- Mazouffre S (2016) Electric propulsion for satellites and spacecraft: established technologies and novel approaches. *Plasma Sour. Sci. Technol.* 25(3):033002. <https://doi.org/10.1088/0963-0252/25/3/033002>
- Mazouffre S, Vaudolon J, Largeau G, Hénaux C, Rossi A, Harribey D (2014a) Visual evidence of magnetically shielded with the PPS-Flex Hall thruster. *IEEE T. Plasma Sci.* 42(10):2668–2669. <https://doi.org/10.1109/TPS.2014.2331180>
- Mazouffre S, Tsikata S, Vaudolon J (2014b) Development and experimental characterization of a Wall-less Hall thruster. *J. Appl. Phys.* 116:243302. <https://doi.org/10.1063/1.4904965>
- Mazouffre S, Bourgeois G, Vaudolon J, Garrigues L, Hénaux C, Harribey D, Vilamot R, Rossi A, Zurbach S, Méhauté DL (2015) Development and testing of Hall thruster with flexible magnetic field configuration. *J. Propul. Power* 31(4):1167–1174. <https://doi.org/10.2514/1.B35417>
- Meng Y, Mao HK, Eng PJ, Trainor TP, Newville M, Hu MY, Kao CC, Shu JF, Hausermann D, Hemley RJ (2014) The formation of sp^3 bonding in compressed BN. *Nat. Mater.* 3(2):111–114. <https://doi.org/10.1038/nmat3060>
- Mikellides IG, Katz I (2012) Numerical simulations of Hall-effect plasma accelerators on a magnetic-field-aligned mesh. *Phys. Rev. E* 86(4):046703. <https://doi.org/10.1103/PhysRevE.86.046703>
- Mikellides IG, Katz I, Hofer RR, Goebel DM, Grys KD, Mathers A (2011) Magnetically shielded of the channel walls in a Hall plasma accelerator. *Phys. Plasma*. 18(3):033501. <https://doi.org/10.1063/1.3551583>
- Mikellides IG, Katz I, Hofer RR, Goebel DM (2013a) Magnetically shielded of walls from the unmagnetized ion beam in a Hall thruster. *Appl. Phys. Lett.* 102(2):023509. <https://doi.org/10.1063/1.4776192>
- Mikellides IG, Katz I, Hofer RR (2014) Magnetically shielded of a laboratory Hall thruster. I. Theory and validation. *J. Appl. Phys.* 115(4):203. <https://doi.org/10.1063/1.4862313>
- Morozov AI, Savelyev VV (2001) Fundamentals of stationary plasma thruster theory. *Rev. Plasma Phys.* 21:203–391
- Oluwafemi FA, De La Torre A, Afolayan EM, Olalekan-Ajai BM, Dhital B, Mora-Almanza JG, Potrivitu G, Creech J, Rivolta A (2018) Space food and nutrition in a long term manned mission. *Adv. Astron. Sci. Technol.* 1:1–21. <https://doi.org/10.1007/s42423-018-0016-2>
- Parker JB, Raitses Y, Fisch NJ (2010) Transition in electron transport in a cylindrical Hall thruster. *Appl. Phys. Lett.* 97:091501. <https://doi.org/10.1063/1.3486164>
- Petro EM, Sedwick RJ (2017) Survey of moderate-power electric propulsion systems. *J. Spacecraft Rockets* 54(3):529–541. <https://doi.org/10.2514/1.A33647>
- Potrivitu G, Joussot R, Mazouffre S (2018) Anode position influence on discharge modes of a LaB6 cathode in diode configuration. *Vacuum* 151:122–132. <https://doi.org/10.1016/j.vacuum.2018.02.010>
- P.Y. Peterson, A.D. Gallimore, J.M. Hass, Experimental investigation of a Hall thruster internal magnetic field topography. IEPC 2001-030 (2001)
- P.Y. Peterson, D.H. Manzella, Investigation of the erosion characteristics of a laboratory Hall thruster. AIAA 2003-5005 (2003). <https://doi.org/10.2514/6.2003-5005>
- R. Shastry, A.D. Gallimore, R.R. Hofer, Experimental characterization of the near-wall plasma in a 6-kW Hall thruster and comparison to simulation. AIAA 2011-5589 (2011). <https://doi.org/10.2514/6.2011-5589>
- Raitses Y, Fisch NJ (2001) Parametric investigations of a nonconventional Hall thruster. *Phys. Plasma* 8:2579. <https://doi.org/10.1063/1.1355318>
- Raitses Y, Dorf LA, Litvak AA, Fisch NJ (2000) Plume reduction in segmented electrode Hall thruster. *J. Appl. Phys.* 88:1263. <https://doi.org/10.1063/1.373813>
- Raitses Y, Staack D, Keidar M, Fisch NJ (2005) Electron-wall interaction in Hall thrusters. *Phys. Plasma* 12:1–9. <https://doi.org/10.1063/1.1891747>
- Raitses Y, Smirnov A, Fisch NJ (2007) Enhanced performance of CHTs. *Appl. Phys. Lett.* 90:221502. <https://doi.org/10.1063/1.2741413>
- Raitses Y, Smirnov A, Fisch NJ (2009) Effects of enhanced cathode electron emission on Hall thruster operation. *Phys. Plasma* 16:057106. <https://doi.org/10.1063/1.3131282>
- Raitses Y, Merino E, Fisch NJ (2010) Cylindrical Hall thrusters with permanent magnets. *J. Appl. Phys.* 108:093307. <https://doi.org/10.1063/1.3499694>
- Roy S, Pandey BP (2002) Plasma-wall interaction inside a Hall thruster. *J. Plasma Phys.* 68:305–319. <https://doi.org/10.1017/S0022377802002027>
- R.R. Hofer, B.A. Jorns, J.E. Polk, I.G. Mikellides, Wear test of a magnetically shielded Hall thruster at 3000 seconds specific impulse. IEPC 2013-033 (2013)

- R.R. Hofer, D.M. Goebel, I.G. Mikellides, I. Katz, Design of a laboratory Hall thruster with magnetically shielded channel walls, phase II: experiments. AIAA 2012-3788 (2012). <https://doi.org/10.2514/6.2012-3788>
- R.R. Hofer, High-specific impulse operation of the BPT-4000 Hall Thruster for NASA science mission. AIAA 2010-6623 (2010). <https://doi.org/10.2514/6.2010-6623>
- R.R. Hofer, Magnetically-conformed, variable area discharge chamber for hall thruster, and method, US Patent 8,407,979 (2013)
- R.R. Hofer, S.E. Cusson, R.B. Lobbia, A.D. Gallimore, The H9 magnetically shielded Hall thruster. IEPC 2017-232 (2017)
- R.W. Conversano, R.B. Lobbia, K.C. Tilley, D.M. Goebel, S.W. Reilly, Development and initial performance testing of a low-power magnetically shielded Hall thruster with an internally-mounted hollow cathode. IEPC 2017-64 (2017)
- S. Barral, K. Makowski, Z. Peradzyński, N. Gascon, M. Dudeck, Wall material effects in stationary plasma thrusters. II. Near-wall and in-wall conductivity. Phys. Plasma **10**, 4137 (2003). <https://doi.org/10.1063/1.1611881>
- S. Mazouffre, F. Dubois, L. Albareda, D. Pagnon, M. Touzeau, M. Dudeck, Plasma induced erosion phenomena in a Hall thruster. In: International conference on recent advances in space technologies, RAST '03. Proceedings of 69-74 (2003) <https://doi.org/10.1109/rast.2003.1303393>
- S. Mazouffre, S. Tsikata, J. Vaudolon, Development and characterization of a Wall-less Hall thruster. AIAA 2014-3513 (2014). <https://doi.org/10.2514/6.2014-3513>
- S. Roy, B.P. Pandey, Modeling the effect of plasma–wall interaction in a Hall thruster. AIAA 2003-493 (2003). <https://doi.org/10.2514/6.2003-493>
- S. Y. Cheng, Modeling of Hall thruster lifetime and erosion mechanisms. Ph.D Thesis, Massachusetts Institute of Technology. pp. 79–100 (2007)
- S.E. Cusson, R.R. Hofer, R.B. Lobbia, B.A. Jorns, A.D. Gallimore, Performance of the H9 magnetically shielded Hall thrusters. IEPC 2017-239 (2017)
- Seah MP (2005) An accurate semi-empirical equation for sputtering yields, II: for Neon, Argon and Xenon ions. Nucl. Instrum. Methods B 229:348–358. <https://doi.org/10.1016/j.nimb.2004.12.129>
- Seiler H (1983) Secondary electron emission in the scanning electron microscope. J. Appl. Phys. 54:R1. <https://doi.org/10.1063/1.332840>
- Seo M, Lee J, Seon J, Lee HJ, Choe W (2013a) Effect of the annular region on the performance of a cylindrical Hall plasma thruster. Phys. Plasma 20:023507. <https://doi.org/10.1063/1.4793741>
- Seo M, Lee J, Seon J, Lee HJ, Choe W (2013b) Radial scale effect on the performance of low-power cylindrical Hall plasma thrusters. Appl. Phys. Lett. 103:133501. <https://doi.org/10.1063/1.4820774>
- Shi Y, Raitses Y, Diallo A (2018) Controlling azimuthal spoke modes in a CHT using a segmented anode. Plasma Sources Sci. Technol. 27:104006. <https://doi.org/10.1088/1361-6595>
- Smirnov A, Raitses Y, Fisch NJ (2002) Parametric investigation of miniaturized cylindrical and annular Hall thrusters. J. Appl. Phys. 92:5673. <https://doi.org/10.1063/1.1515106>
- Smirnov A, Raitses Y, Fisch NJ (2004) Plasma measurements in a 100 W CHT. J. Appl. Phys. 95:2283. <https://doi.org/10.1063/1.1642734>
- Szocik K, Lysenko-Ryba K, Banas S, Mazur S (2016) Political and legal challenges in a Mars colony. Space Policy 38:27–29. <https://doi.org/10.1016/j.spacepol.2016.05.012>
- Thomas S, Tyson CB, Steven BB, Gregory BF (2017) Thompson, influence of surface roughness on secondary electron emission from graphite. J. Vac. Sci. Technol., A 35:041404. <https://doi.org/10.1116/1.4986629>
- Tian Z, Duan XM, Yang ZH, Ye SQ, Jia DC, Zhou Y (2016) Microstructure and erosion resistance of in situ SiAlON reinforced BN-SiO₂ composite ceramics. J. Wuhan Univ. Technol. 31(2):315–320. <https://doi.org/10.1007/s11595-016-1369-9>
- Vaudolon J, Mazouffre S, Hénaux C, Harribey D, Rossi A (2015) Optimization of a Wall-less Hall thruster. Appl. Phys. Lett. 107:174103. <https://doi.org/10.1063/1.4932196>
- Yamamura Y, Tawara H (1996) Energy dependence of ion-induced sputtering yields from monoatomic solids at normal incidence. Atom. Data Nucl. Data 62:149–253. <https://doi.org/10.1006/adnd.1996.0005>
- Zhang GJ, Yang JF, Ando M, Ohji T (2002) Nonoxide-boron nitride composites: in situ synthesis, microstructure and properties. J. Eur. Ceram. Soc. 22:2551–2554
- Zhou Y, Duan XM, Jia DC, Yang ZH, Meng QC, Yu Y, Yu DR, Ding YJ (2011) Mechanical properties and plasma erosion resistance of ZrO_{2p}(3Y)/BN-SiO₂ ceramic composites under different

- sintering temperature. IOP Conf. Ser. Mater. Sci. Eng. 18:202003. <https://doi.org/10.1088/1757-899x/18/20/202003>
- Zhurin VV, Kaufman HR, Robinson RS (1999) Physics of closed drift thrusters. *Plasma Source Sci. Technol.* 8:R1–R20. <https://doi.org/10.1088/0963-0252/8/1/021>
- Zypries B (2017) Space, the public, and politics. *Space Policy* 41:73–74. <https://doi.org/10.1016/j.spacepol.2017.01.005>

Publisher's Note Springer Nature remains neutral with regard to jurisdictional claims in published maps and institutional affiliations.